An uncertainty budget for the precursor Watt balance for South Africa

Thapelo Given Mametja

(MMTTHA003)

A thesis submitted to the University of Cape Town in fulfilment

of the degree of Master of Science (Physics)

Department of Physics

Faculty of Science

University of Cape Town

February 2019

Declarations

I Thapelo Given Mametja hereby declare that:

- I am presenting this dissertation in full fulfilment of the requirements for my degree;

- I know the meaning of plagiarism and declare that all of the work in the dissertation (or thesis), save for that which is properly acknowledged, is my own; and

- I hereby grant the University of Cape Town free licence to reproduce for the purpose of research either the whole or any portion of the contents in any manner whatsoever of the dissertation.

Acknowledgement

Firstly I would like to thank the living god for the good health and wellbeing throughout my years of study that were necessary to complete this thesis.

My sincere thanks to:

My supervisor Prof. Andy Buffler for the continuous support and guidance throughout the course of study. I could not have imagined having a better supervisor and advisor for my MSc. study. The insightful comments and challenging questions made me to be more creative and have more knowledge of the work I was doing;

My co-supervisor Dr. Aletta Karsten for the proper guidance and always making sure that I get all the resources required for my study. Both my supervisors consistently allowed this work to be my own but steered me in the right direction whenever they thought I needed it;

Ms. Jill Patel for helping me with the application and registration processes throughout the years of my study, no words can summarise the role she played;

The National Metrology institute of South Africa (NMISA) and the National Research Foundation (NRF) for the financial support. NMISA for introducing me to the metrology field and giving me the opportunity to participate in a major and exciting project that contributes to the revision of the International system of units;

My fellow colleagues at NMISA from different fields of study, I am gratefully indebted to their valuable comments, discussions, criticisms and assistance on this work. My lab mates Henk Potgieter, Marang Mutloatse, Vumile Tyalimpi and Sven du Clue for their opinions, brilliant suggestions and for always being available for me when I needed some assistance in the lab.

Last but not the least, I would like to express my very profound gratitude to my family: my parents, uncle, brother and sisters for their unfailing support, advices and encouraging words throughout my years of study.

To all I say thank you, this achievement would have not been possible without you.

Abstract

The 26th General Conference on Weights and Measures (CGPM) held on the 16th November 2018 has adopted the revision of the International system of units (SI) to be based on the fundamental physical constants. The changes will be implemented on World Metrology day, 20th May 2019. Currently, the kilogram is the only base unit that is still based on an artefact, a platinum-Iridium alloy cylinder, known as the International Prototype of the Kilogram (IPK). Worldwide, all mass measurements are traceable to the IPK. It has been proven that there is a drift between the IPK and the other prototypes (IPK copies) at an average rate of 50 μg per century, which indicates that the primary mass reference standard is lacking long-term stability. After the revision of the SI, a fixed value of Planck's constant will be used to realise a unit of mass (kilogram).

The so-called Kibble balance has shown capability to provide a link between the macroscopic mass m and Planck's constant h within a few parts in 10^8. A Kibble balance is an electromechanical mass measuring instrument that measures the mass of a test object through the strength of electric quantities. The National Metrology Institute of South Africa (NMISA) and the University of Cape Town (UCT) Physics Department, have embarked on a joint project to construct the first Kibble balance in South Africa and most probably on the African continent. In this study, prototypes have been constructed from Lego blocks, 3D printing and modifying an old equal-arm balance. From the comparison between calibrated mass pieces traceable to the IPK and precursor Kibble balance results, it has been shown that the method is feasible.

Any measurement performed and expressed as a number without been accompanied by any statement of uncertainty, is incomplete. All uncertainty measurements evaluations and expressions should be done according to the ISO-recommended framework, the so-called "Guide to the Expression of Uncertainty in Measurement", or ISO-GUM. An ISO-GUM method has been applied to give a full uncertainty assessment on all the major sources of uncertainty incorporated within the precursor Kibble balance. The final prototype based on a modified equal-arm balance showed capabilities of measuring gram level masses with ≤ 0.5 % relative uncertainty. The traceability of the mass measurements performed with the precursor Kibble balance to various primary reference standards has been established.

Table of contents

List of Figures

List of Tables

List of Abbreviations

BIPM	- International Bureau of Weights and Measures
CAD	- Computer Aided Drawing
CCM	- Consultative Committee for Mass and Related Quantities
CGPM	- General Conference on Weights and Measures
CGS	- Council for Geoscience
CIPM	- International Committee for Weights & Measures
CIPM-MRA	- International Committee for Weights & Measures Mutual Recognition Agreement
CMCs	- Calibration and Measurement Capabilities
CODATA	- Committee on Data for Science and Technology of the International Council for Science
DAQ	- Data Acquisition Card
DTI	- Department of Trade and Industry
IAC	- International Avogadro Coordination
IFCC	- International Federation of Clinical Chemistry
IPK	- International Prototype Kilogram
ISO	- International Standardization Organization
IUPAC	- International Union of Pure and Applied Chemistry
IUPAP	- International Union of Pure and Applied Physics
JVS	- Josephson Voltage Standard
NIST	- National Institute of Standards and Technology
NMIs	- National Metrology Institutes

NMISA - National Metrology Institute of South Africa

NPL - National Physical Laboratory

NRCS - National Regulator for Compulsory Specifications

PTB - National Metrology Institute of Germany

SABS - South African Bureau of Standards

SANAS - South African National Accreditation System

SI - International System of Units

UCT - University of Cape Town

UTC - Coordinated universal time

VIM - Vocabulary in Metrology

WB - Kibble Balance

XRCD - X-ray-crystal density method

List of Symbols

e	- Elementary charge
h	- Planck's constant
c	- Speed of light
R_∞	- Rydberg constant
m	- mass
m_{IPK}	- mass of the International Prototype of the kilogram
T_{TPW}	- Triple point of water
$M(^{12}\mathrm{C})$	- Molar mass of carbon-12

1. Introduction

1.1 Measurements overview

The scientific study, practice, understanding and interpretation of measurements is known as metrology. This interdisciplinary scientific area plays a significant role in what we do and experience in our everyday lives, spanning interests from science (physics, engineering, chemistry etc.) and innovation (high-technology manufacturing), through trade and industry to the quality of life (health and safety). This field of study is concerned with how measurements are realised and applied to ensure stability, comparability and coherency in measurement to satisfy the needs of the society.

Although it was not common universally, the use of reference standards for measurements goes long back during the ancient times where human body parts and physical objects were used. This differed according to nations which made the international trade of goods and services complex. Now through national metrology institutes (NMIs), the international agreed measurement reference standards play a vital role in making trade amongst various nations easier due to a common adhered measurement language.

Measurements are described by units which have definitions, realisations and representatives. Experiments performed in national laboratories whose results match the definitions are used to achieve the realisation of reference units. These representatives are the measurement reference standards kept at national laboratories which have been universally accepted for measurements traceability. Measurement standard and traceability are defined according to Vocabulary in Metrology (VIM) [1] as follows:

- **Measurement standard** - a realisation of the definition of a given quantity, with stated quantity value and associated measurement uncertainty, used as a reference; and

- **Traceability** - the property of a measurement result whereby the result can be related to a reference through a documented unbroken chain of calibrations, each contributing to the measurement uncertainty, respectively. Traceability refers to how measurement results are related to the national or international reference standard through an unbroken chain of quality accredited comparisons and procedures. Traceability forms a foundation for controlled measurements of high quality and accuracy.

Figure 1.1 shows a general relationship between the measurement traceability, calibrations and how the uncertainties vary along the traceability chain. Calibration refers to a process of establishing, under specified conditions, a relation between the measurement quantity value together with its known certified uncertainty given by the measurement reference standard and the corresponding output/indication with the uncertainty associated given by a measuring instrument or a system [1]. Calibration can be seen as the verification of the test equipment to a reference standard, which is established by comparing the measurement values from the test equipment to those from the reference standard with known accuracies. Calibrations form a basis for traceability, ensures consistency and provide quality in measurements. It is a form of disseminating the measurement value from the realisation to the next measurement standard up to the end use of the measurement unit.

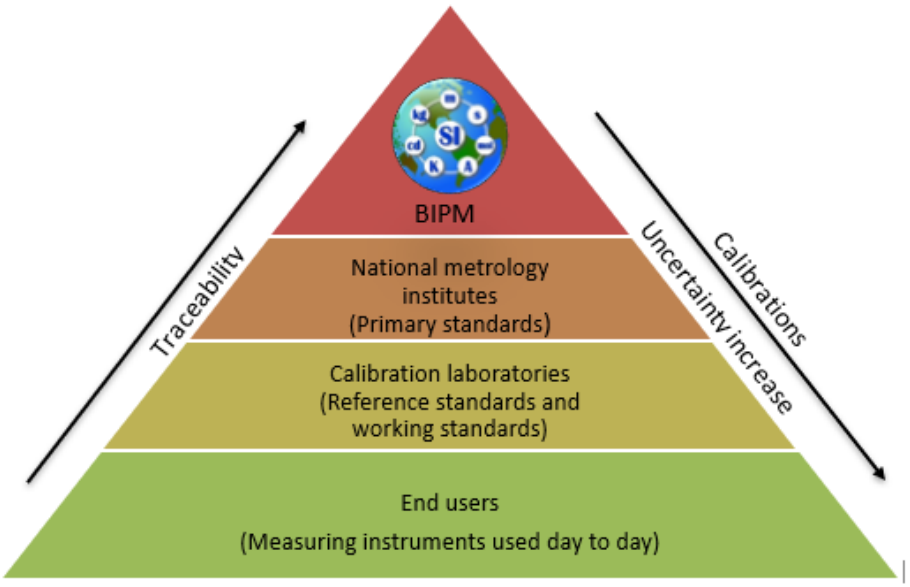

Figure 1.1: An illustration of the relationship between measurement traceability, calibrations and uncertainty variations.

The international standards are recognised globally and have been agreed to serve as the primary realisation of the measurement units. The international standards are used to calibrate the national standards held by different nations but for a common purpose. These national standards are periodically compared to each other in a form of international key comparisons to ensure consistency in measurements amongst nations. The international key comparisons give confidence to the state and users that the measurements done within the country are internationally comparable and accepted. The use of measurement reference standards allows comparison in measurements done in various places at various times.

On the 20th of May 1875, seventeen nations signed the Metre Convention [2] with the purpose of providing a basis for international collaboration on the science of measurement and creating a global coherent measurement system that supports the scientific discovery and the development of the metric system [3], [4]. The Metre Convention is an international treaty that allows nations to act in common accord on units of measurements and related matters.

The signing of the Metre Convention led to the creation of an international measurement governing body responsible for measurement related matters known as the International Bureau of Weights and Measures (BIPM), located in France. As of the 07th August 2018, the BIPM has 60-member states and 42-associates acting together on scientific measurements and measurements reference standards related matters [5]. The BIPM is now the hub for all metrology institutes with regards to measurement comparisons, traceability and references. In summary, the mandate of the BIPM is to ensure global uniformity on measurement and their link or traceability to the international system of units (SI). The global responsibility for measurement standardisation is held by the four internationally recognised bodies, which are the International Bureau of Weights and Measures (BIPM), the International Standardization Organization (ISO), the International Organisation of Legal Metrology (OIML) and the International Laboratory Accreditation Cooperation (ILAC) [6].

South Africa adhered to this treaty in 1964 and became the 40th signatory of the Convention [7]. This allows South Africa to participate in all matters related to the international measurement system of units, to apply it nationally and ultimately to support the competitiveness of the South African industry and allow fair trade. The Measuring Units and National Measuring Standard Act of South Africa (Act No.18 of 2006: Measurement Units and Measurement Standards Act, 2006) [8] delegates the responsibility of the maintenance and the traceability dissemination of the South African National Measuring Standards to National Metrology Institute of South Africa (NMISA). This function is performed through the support and sponsorship of the Department of Trade and Industry (DTI).

Figure 1.2 shows the interrelationship between various governing bodies and reference standards throughout the globe giving more insight on the Republic of South Africa's national measurement structure. There is a variety of organisations other than the ones shown in the measurement assurance system in Figure 1.2 that help to relate measurements done in all parts of the world. The definitions of the measurements defining units and the way that these units are realised are modified from time to time as technology and measurement techniques evolve. This is done to allow more accurate realisations, thereby tightening the stability of measurement reference structure, and to cater for the need for high accuracy measurements.

The measurement system also underpins all standards and regulations in a system steering towards "measured once, accepted everywhere". NMISA, together with other national entities such as South African National Accreditation System (SANAS) [9], South African Bureau of Standards (SABS)[10] and the National Regulator for Compulsory Specifications (NRCS) [11] are part of the Technical infrastructure reporting to the DTI [12]. These institutes are the building blocks of the national quality infrastructure. They work together to ensure that the measurement system of the country protects its citizens, the environment and promotes industrial development, commerce and trade.

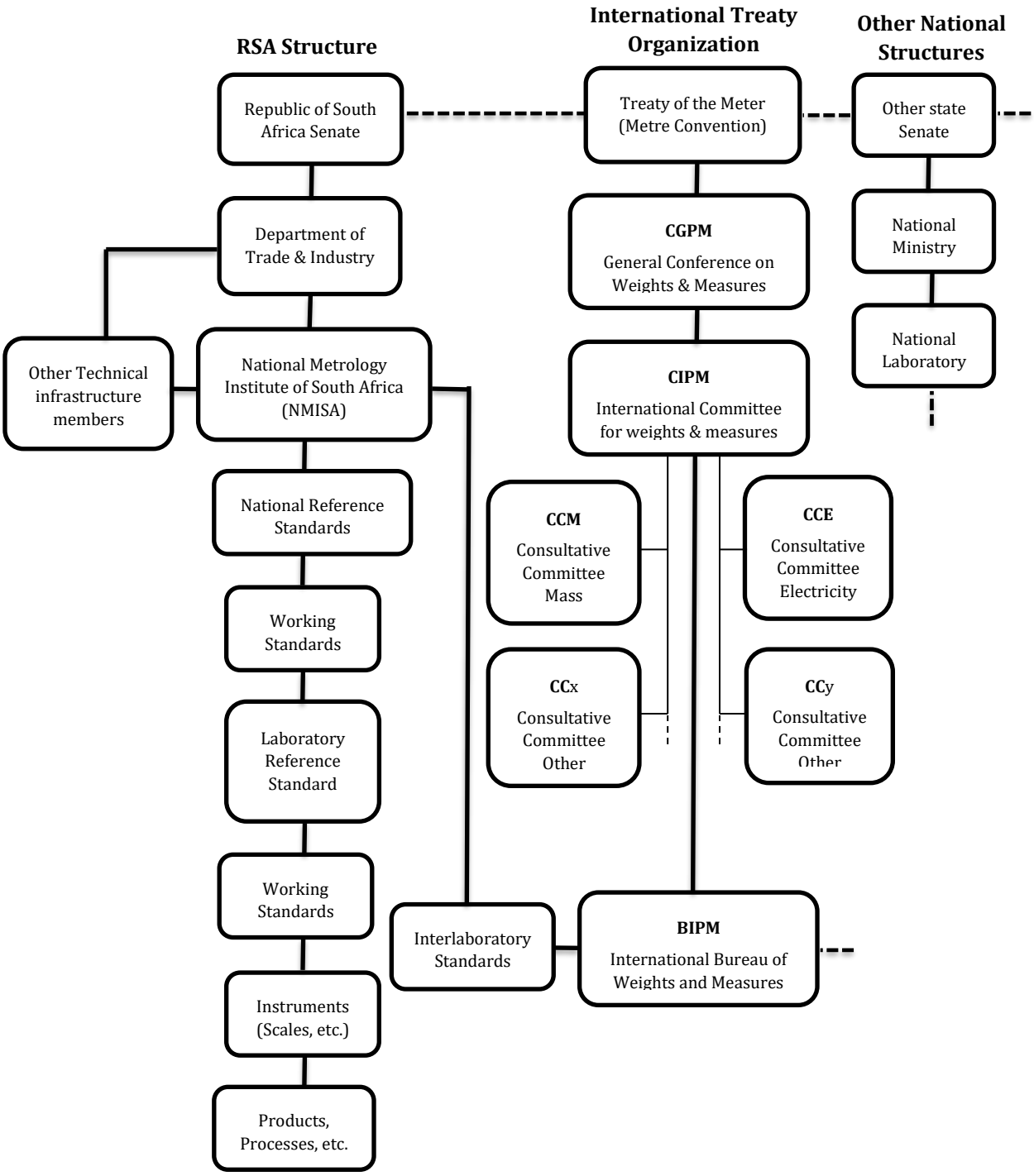

Figure 1.2: The measurement quality assurance system of South Africa.

1.2 The International System of Units

The International System of Units (SI) officially established in 1960 by the 11th General Conference on Weights and Measures (CGPM), is a system which evolves and changes due to new knowledge arising and technology advancement, dealing with practical needs thereby being in correspondence with the world's high demand for quality measurements. The first step towards the establishment of the present SI goes back to the invention of the decimal metric system in 1799. This was during the French Revolution where the Archives de la République in Paris received two platinum artefacts reference standards representing the kilogram and the metre [13].

By the mid-1800s, the measurement system comprised of three base units, that is the kilogram, metre and second named the MKS system. In 1946 during the 9th CGPM, the ampere was officially adopted as a base unit for electric current measurement. The candela and kelvin were officially adopted by the 10th CGPM as measurement base units in 1954. When the SI was introduced, it only comprised of six base units. The mole was introduced later into the system as a new base unit growing the SI system to seven base units. The SI is now comprised of the kilogram, the metre, the second, the kelvin, the ampere, the mole and the candela [14]. All other measurement units were obtained or derived from these seven base units and they are categorised as SI-derived units. For example, the unit for electric potential and potential difference, the volt (V), it is derived from four (the kilogram (kg), the metre (m), the second (s) and the ampere (A)) of these base units as follows:

$$\text{volt} = \text{kg}\,\text{m}^2\,\text{s}^{-3}\,\text{A}^{-1}. \tag{1.1}$$

Since the establishment of the SI, many projects have been initiated with the aim of realising the base units with smaller uncertainties, improving the precision and accuracy of the measurements. The 26th meeting of the CGPM that took place in November 2018 has adopted the revision of the SI [15]. The base units will now be based on fundamental physical constants. The changes will be in implemented from the 20th May 2019 onwards. The fundamental constants of nature are considered to be unchanging in time and space, which makes them

well-suited to provide a basis for the measurement system. The definitions of other base units such the metre and the second are already based on the fundamental constants (i.e. the speed of light, c_0 and the hyperfine transition frequency of the caesium 133 atom, $\Delta\nu(^{133}\mathrm{Cs})_{\mathrm{hfs}}$).

Definitions of four base units will be revised (i.e. the kilogram, the ampere, the mole and the kelvin), which is a remarkable thing to happen since the establishment of the SI as this require much more international collaborations from various fields of science. The proposed changes to the SI submitted to the CGPM at its 24th and 25th meeting are clearly explained in [13], [16], illustrating the evolution of the SI and the transition to the new SI. A satisfactory and sufficient progress has been made on the requirements for the revision of the SI. The recommended fixed numerical values of the new defining have been arranged by the Task Group on the Fundamental Constants (TGFC) of the CODATA to the CGPM for its 26th meeting and are presented as the 2017 CODATA adjusted values in [17]. These values were derived from various experimental results all over the world. Section 1.2.1 and 1.2.2 below give a summary of the current international system of units and the proposed international system after the revision respectively.

1.2.1 **The present International System of Units (SI)**

This section provides a historical summary of the current definitions of the SI base units and how they evolved with time. Table 1 shows the current base units forming the international system of units. It should be noted that the definitions are in the quotation marks as they are taken directly from section 2.1.1 of the SI brochure published by BIPM [18] and NIST [14]. More information on these SI base units can be found in these brochures.

Table 1.1: Current SI base quantities, base units and symbols

Base quantity	Base Unit	Symbol
Length	metre	m
Mass	kilogram	kg
Time	second	s
Electric current	ampere	A
Thermodynamic temperature	kelvin	K
Amount of a substance	mole	mol
Luminous intensity	candela	cd

Metre (unit of the length)

The first official definition of the metre based on an alloy of a platinum-iridium bar was sanctioned in 1889 by the 1st CGPM [19]. This was replaced during the 11th CGPM meeting (1960) by a definition based on the krypton-86 radiation's wavelength [20]. This was realised using an interferometer system with a travelling microscope, where the optical path difference was measured from the fringes counted. This was later redefined in 1983 during the 17th GCPM [21]with the following current definition of the metre:

"The length of the path travelled by light in vacuum during a time interval of 1/299 792 458 of a second".

The number 299 792 458 is the distance in metres that a light covers in a second in a vacuum, which is denoted by a symbol c_0. At NMISA, this is practically realised using an iodine stabilised He-Ne Laser [22]. A frequency f of this laser light is measured with a relative uncertainty of 2 x 10^{-11} [23]. It follows that the metre is determined by converting this frequency to wavelength λ, through the relation $\lambda = \frac{c_0}{f}$.

Kilogram (unit of mass)

The current official definition of the unit of mass was adopted together with that of the metre during the 1st CGPM [19]. This definition is based on the mass of the International Prototype Kilogram (IPK), an artefact made up of an alloy of platinum (Pt)-iridium (Ir) (90% Pt – 10% Ir) with both the height and diameter of about 39 mm. The IPK was sanctioned in 1889, kept under specified conditions in a vault at the BIPM and declared to be considered the unit of mass exactly 1 kilogram, m (IPK) = 1 kg with zero uncertainty. The following definition was again confirmed at the 3rd CGPM to clear the misuse of the term "Weight" [18]:

"The unit of mass; it is equal to the mass of the international prototype of the kilogram".

Copies of the IPK were made and distributed to the nations that were part of the treaty at that time as national prototypes and periodically compared with the IPK [24]. The national prototypes have uncertainties values assigned to them but the IPK has zero uncertainty since it is the kilogram by definition.

Second (unit of time)

The second known as the unit of time interval was once realised as the mean solar day division equating to 1/86 400. The studies made about the earth's rotation showed some anomalies which made this an unsuitable definition [14]. The 11th CGPM in 1960 [25] adopted a more precise definition based on the 1900 tropical year from the space experts. But prior to this, there was already an experimental work which showed high reproducibility at high accuracy level. The work was about the atomic standard of time based on the transition of an atom between two energy levels. After much consideration of this experimental work, it was then in 1967/68 during the 13th CGPM that the current following got adopted [14]:

"The duration of 9 192 631 770 periods of the radiation corresponding to the transition between the two hyperfine levels of the ground state of the caesium 133 atom".

The definition is valid at a temperature of 0 K where the caesium atom is at rest, and this was confirmed by the CIMP at its meeting in 1997. It follows that:

$$\Delta v(^{133}\mathrm{Cs})_{\mathrm{hfs}} = 9\ 192\ 631\ 770\ \mathrm{Hz}; \tag{1.2}$$

$$\mathrm{Hz} = \frac{\Delta v(^{133}\mathrm{Cs})_{\mathrm{hfs}}}{9\ 192\ 631\ 770}; \tag{1.3}$$

where $\mathrm{Hz} = \mathrm{second\ (s)}^{-1}$.

So, with some rearrangements, we get:

$$\mathrm{second\ (s)} = \frac{\Delta v(^{133}\mathrm{Cs})_{\mathrm{hfs}}}{9\ 192\ 631\ 770}; \tag{1.4}$$

which is the magnitude of a second.

Ampere (unit of electric current)

The unit of the electric current, the ampere was introduced in 1893 during the International Electric Congress and adopted in 1908 by the International conference together with the ohm, the unit for resistance measurements. The ampere was officially adopted in 1948 by the 9th CGPM as the base unit for electric current measurements. This followed the definition proposed by the CIPM in 1946[14]:

"The constant current which, if maintained in two straight parallel conductors of infinite length, of a negligible circular cross-section, and placed 1 metre apart in vacuum, would produce between these conductors a force equal to 2 x 10^{-7} newton per metre of length".

The realisation of the ampere is practically maintained using the volt and the ohm linked via the ohm's law. The volt and the ohm are linked to the Josephson junction voltage and the quantum Hall resistance using the 1990 fixed values of the Josephson and Von Klitzing constants ($K_{\mathrm{J}-90}$ and $R_{\mathrm{K}-90}$) respectively.

Kelvin (unit of thermodynamic temperature)

The kelvin is the SI unit for thermodynamic temperature measurement. In 1954, the 10th CGPM defined the unit of thermodynamic temperature by selecting the triple point of water (TPW) assigned the temperature of 273.16 K and this was considered as the fundamental fixed point defining the unit. The name Kelvin was officially adopted in 1967/68 during the 13th CGPM and defined as follows[14], [26]:

"The fraction 1/273.16 of the thermodynamic temperature of the triple point of water".

It follows that the triple point of water's thermodynamic temperature is exactly defined as 273.16 kelvin, T_{TPW} = 273.16 K.

Mole (unit of amount of a substance)

The unit of amount of substance, the mole was introduced as last base unit in the International System of units following the discovery of chemistry's fundamental laws. It is used to quantify the number of chemical elements in a sample. Phrases like "gram-atom" and" gram-molecule" were then used to describe the amounts of compounds or chemical elements which were in-fact relative masses linked to the atomic weights and molecular weights respectively. The atomic weights were referred to the weight of oxygen known and agreed to be 16. But there was a conflict because chemists attributed the atomic weight 16 to a mixture of isotopes, which they described as an element of oxygen that occurs naturally; while physicists attributed the value to one of the oxygen's isotopes after doing a mass spectroscopy separation. Finally, this was ended when the International Union of Pure and Applied Chemistry (IUPAC) and the International Union of Pure and Applied Physics (IUPAP) reached an agreement 1959/60 [14], [18], [27]. After that, it was agreed by both parties to attribute the number 12 as the atomic weight of the carbon isotope, which is officially known as relative atomic mass $A_r(^{12}C)$. The mole was then cleared to be:

"The amount of substance of a system which contains as many elementary entities as there are atoms in 0.012 kilograms of carbon 12; its symbol is "mol".

"When the mole is used, the elementary entities must be specified and may be atoms, molecules, ions, electrons, other particles, or specified groups of such particles".

This definition was adopted by the 14th CGPM in 1971 following the proposals from the IUPAP and the IUPAC. The mole is also related to the IPK because one mole of a specific atom (or molecule) has a mass (in grams) equal to the atomic mass of the atom (or molecule). This definition is also linked to the universal fundamental constant known as the Avogadro's constant (denoted by N_A). This constant establishes the relation between the number of entities in any sample to the amount of substance of that sample. In general, one mole of any substance contains Avogadro's number or 6.022 x 10^{23} of molecules or atoms of that substance.

Candela (unit of luminous intensity)

The candela is the measurement unit for luminous intensity. The unit describes the measurements done in radiometry and photometry. The first standards to measure "candle power" were, not surprisingly, actual candles. This was in the 1860s and usually consisted of candles made from sperm whale fat such as the British Parliamentary candle (c1860) which was discontinued due to poor reproducibility. Thereafter came the introduction of gas lamps that were more stable and reproducible, this involved burning of chemicals such as amyl acetate. This was later replaced by the electric lamps such as the International candle in the 1990s [28].

In 1937 the International candle was redefined as the luminous intensity of a blackbody at the freezing point of liquid platinum with a value of 58,9 International candles per square centimetre. This was adopted by the CIPM in 1946. The new unit was named the *candela* by the 9th CGPM in 1948 and it is defined as 1 lumen per steradian. In 1967 the 13th CGPM altered the definition to correct possible ambiguities. The corrected definition lasted for few years eventually discarded because it was difficult to realise in practice. In 1977 the CIPM recommended that the candela be in terms of a certain amount of power, it was then in 1979 that the CGPM adopted a definition relating photometric and radiometric quantities as follows[14], [29]:

"The candela is the luminous intensity, in a given direction, of a source that emits monochromatic radiation of frequency 540 × 10^{12} hertz and that has a radiant intensity in that direction of 1/683 Kibble per steradian".

1.2.2 **The revised International System of Units (SI)**

The high demand rate of quality measurement due to technology advancement, our improved knowledge on the fundamental physical constants of nature and the desire for a highly stable measurement reference system has led to the revision of the international system of units [13]. The main motive behind this revision is to reinforce the foundation of the measurement system. The proposals for revising the SI can be obtained in the 2011 and 2014 CGPM resolutions, where also a detailed smooth transition process from the old to the new SI is outlined. The revision was about updating the definition of four of the seven base units, that is the ampere, the kilogram, the kelvin and the mole. Other units such as the unit of time and length have been updated based on the fixed numerical values which brought about new inventions and technologies such as Global Positioning System (GPS). The revised international system units that is based on seven fixed fundamental constants is described by the draft of the ninth SI Brochure [30] adopted by the 26th CGPM (November 2018) as the system of units in which:

- the unperturbed ground state hyperfine transition frequency of the caesium 133 atom $\Delta\nu_{\mathrm{cs}}$ is 9 192 631 770 Hz;
- the speed of light in vacuum c is 299 792 458 m s^{-1};
- the Planck's constant h is 6.626 070 15 × 10^{-34} J s;
- the elementary charge e is 1.602 176 634 × 10^{-19} C;
- the Boltzmann constant k is 1.380 649 × 10^{-23} J K^{-1};
- the Avogadro constant N_{A} is 6.022 140 76 × 10^{23} mol^{-1}; and
- the luminous efficacy of monochromatic radiation of frequency 540 × 10^{12} Hz, K_{cd}, is 683 lm/W.

These changes will only be effective from the 20th May 2019, which is known world-wide as the World Metrology day. The units of these fundamental physical constants are expressed in simplified derived units which are related to the second (s), metre (m), kilogram (kg), ampere (A), kelvin (K), mole (mol) and candela (cd) as shown in the last column of Table 1.2. These constants are somehow linked to each other, except for the case of caesium frequency and the Avogadro's constant as shown in Figure 1.3. The revised definitions of the base units based on the new seven defining constants of the SI are tabulated in Table 1.3.

Table 1.2: The seven adopted defining constants of the revised SI, their corresponding numerical values, symbols and units.

Defining Constant	Symbol	Numerical Value	Unit
Hyperfine splitting of caesium	$\Delta\nu(^{133}\mathrm{Cs})_{\mathrm{hfs}}$	9 192 631 770	$\mathrm{Hz} = \mathrm{s}^{-1}$
Speed of light in vacuum	c	299 792 458	$\mathrm{m\ s}^{-1}$
Planck's constant	h	$6.626\,070\,15 \times 10^{-34}$	$\mathrm{J\ s} = \mathrm{kg\ m}^2\ \mathrm{s}^{-1}$
Elementary charge	e	$1.602\,176\,634 \times 10^{-19}$	$\mathrm{C} = \mathrm{A\ s}$
Boltzmann constant	K_B	$1.380\,649 \times 10^{-23}$	$\mathrm{J\ K}^{-1} = \mathrm{kg\ m}^2\ \mathrm{s}^{-2}\ \mathrm{K}^{-1}$
Avogadro constant	N_{A}	$6.022\,140\,76 \times 10^{23}$	mol^{-1}
Luminous efficacy	K_{cd}	683	$\mathrm{lm\ W}^{-1} = \mathrm{cd\ sr\ kg}^{-1}\ \mathrm{m}^{-2}\ \mathrm{s}^{3}$

These fundamental constants were carefully chosen based on practicality, accessibility, reproducibility and other scientific beneficial reasons.

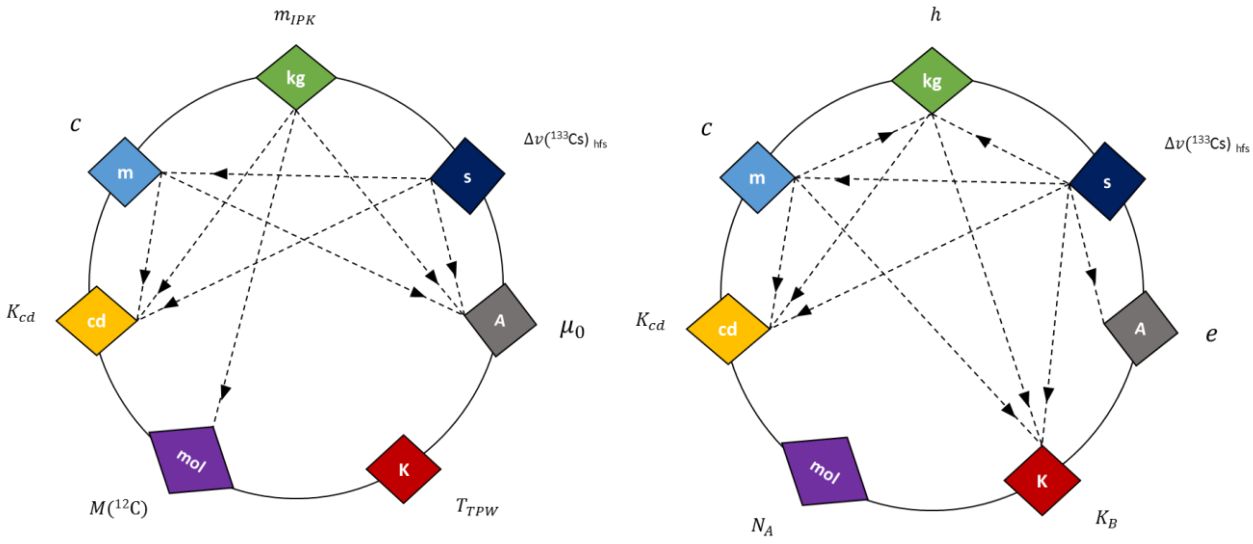

Figure 1.3: The link amongst the old international system of units (SI) (*on the left*) and the link amongst the adopted international system of units (SI) (*on the right*) with their new defining fundamental constants.

Table 1.3: The revised SI units definitions [31].

Quantity	SI unit
time	The second, symbol s, is the SI unit of time. It is defined by taking the fixed numerical value of the caesium frequency $\Delta\nu_{\mathrm{Cs}}$, the unperturbed ground-state hyperfine transition frequency of the caesium 133 atom, to be 9 192 631 770 when expressed in the unit Hz, which is equal to s^{-1}.
length	The metre, symbol m, is the SI unit of length. It is defined by taking the fixed numerical value of the speed of light in vacuum c to be 299 792 458 when expressed in the unit m s^{-1} , where the second is defined in terms of the caesium frequency $\Delta\nu_{\mathrm{Cs}}$.
mass	The kilogram, symbol kg, is the SI unit of mass. It is defined by taking the fixed numerical value of the Planck's constant h to be $6.626\ 070\ 15\ \times 10^{-34}$ when expressed in the unit J s, which is equal to kg m^2 s^{-1} , where the metre and the second are defined in terms of c and $\Delta\nu_{\mathrm{Cs}}$.
electric current	The ampere, symbol A, is the SI unit of electric current. It is defined by taking the fixed numerical value of the elementary charge e to be $1.602\ 176\ 634 \times 10^{-19}$ when expressed in the unit C, which is equal to A s, where the second is defined in terms of $\Delta\nu_{\mathrm{Cs}}$.
thermodynamic temperature	The kelvin, symbol K, is the SI unit of thermodynamic temperature. It is defined by taking the fixed numerical value of the Boltzmann constant k to be $1.380\ 649 \times 10^{-23}$ when expressed in the unit J K^{-1}, which is equal to kg m^2 s^{-2} K^{-1}, where the kilogram, metre and second are defined in terms of h, c and $\Delta\nu_{\mathrm{Cs}}$.
amount of substance	The mole, symbol mol, is the SI unit of amount of substance. One mole contains exactly $6.022\ 140\ 76 \times 10^{23}$ elementary entities. This number is the fixed numerical value of the Avogadro constant, N_{A}, when expressed in the unit mol^{-1} and is called the Avogadro number. The amount of substance, symbol n, of a system is a measure of the number of specified elementary entities. An elementary entity may be an atom, a molecule, an ion, an electron, any other particle or specified group of particles.
luminous intensity	The candela, symbol cd, is the SI unit of luminous intensity in a given direction. It is defined by taking the fixed numerical value of the luminous efficacy of monochromatic radiation of frequency 540×10^{12} Hz, K_{cd}, to be 683 when expressed in the unit lm W^{-1}, which is equal to cd sr W^{-1}, or cd sr kg^{-1} m^{-2} s^3 , where the kilogram, metre and second are defined in terms of h, c and $\Delta\nu_{\mathrm{Cs}}$.

1.2.3 **Implications of the revised SI**

After the implementation of the new SI, measurements will be referenced or traceable to the to a set of fixed values of the defining constants: $\Delta v(^{133}\mathrm{Cs})_{\mathrm{hfs}}$, $c, h, e, k, N_{\mathrm{A}}$ and K_{cd}, summarised in Table 1.2. However, for continuity and ensuring a smooth transition, the values are expressed in terms of the present traditional units: s, m, kg, A, K, mol and cd. This way there will be no confusion to the society and also this shows a continuity from the beginning of the measurement system were artefacts were used to define measurements. Although this is considered a new way of doing things, some of the units will still look the same as they have been based on the fundamental physical constants all along.

The revision will bring great advantages such as in the case of the SI unit of mass, the replacement of the IPK artefact with the Planck's constant h. This will get rid of the base unit's debatable lack of long-term stability and primary reference standard's accessibility for the NMIs. The mass measurements will no longer be confined to a particular standard were a direct comparison is needed for countries to obtain traceability to the SI. NMIs can now have a primary realisation of the unit of mass and disseminate the traceability in their respective countries. Consistency will be ensured by means of international key comparisons just like it is with other measurements standards such as standards for length measurements [16]. Another potential benefit is that a realisation of the unit of mass at values smaller than 1 kg will be possible, which is of significant impact to the pharmaceutical industry.

Values such as that of m_{IPK}, T_{TPW} and $M(^{12}\mathrm{C})$ will not change but relative uncertainties of order 1×10^{-8}, 3.7×10^{-7} and 1.0×10^{-8} will be added respectively [13], [17]. The change will also impact greatly the electrical metrology field since their measurements are presently traceable to the 1990 CIPM adopted conventional values of Josephson constant, K_{J-90} and Von Klitzing constant, R_{K-90}. These constants are based on the discovery of the Josephson effect and the quantum hall effect defined by the Planck's constant h and the elementary charge e (see chapter 3). Having the two constants fixed will bring about an insignificant change to the electrical units dissemination, but the change will be very small of order 1×10^{-7} for voltage measurements and 2×10^{-8} for resistance measurements [13], [16].

1.3 The kilogram definition

1.3.1 How is mass currently referenced

In the present SI, the unit of mass known as the kilogram (kg), amongst all the International System (SI) base units is the last to be defined by an artefact [32]. It is defined as being the same as the mass of the International Prototype Kilogram (IPK) cast in 1879 by Johnson-Matthey. This artefact is made up of an alloy of platinum-iridium (90 % platinum and 10 % iridium) with both the diameter and height of about 39 mm, housed at the International Bureau for weights and measures (BIPM) in France, near Paris, see Figure 1.4. This alloy material was chosen based on the properties such as its hardness, resistivity to wearing etc. The IPK can only be accessed with the permission provided by the CIPM [24].

Figure 1.4: The International prototype of the kilogram (IPK) stored at the BIPM in France, near Paris, secured by three glass bells [33].

The International Prototype of the Kilogram (IPK) has served and still serves as the definition of the kilogram in the international system of units since 1889. It was adopted during the first General Conference on Weights and Measures (CGPM) as the mass unit definition. The IPK succeeded the kilogram of the archives (KA) sanctioned in 1799 based on the definition that "the kilogram is the mass of a litre of distilled water at 4 ˚C", which was the temperature at which water is most dense [34]. For continuity purposes, the mass of the IPK was set to be in correspondence with that of the KA. When the IPK was sanctioned the so-called official copies and other copies were made from. These other copies were distributed to various nations that were members of the Metre Convention and they are now known as the "National prototypes", kept at national laboratories. Figure 1.5 shows South Africa's copy (no.56) received in 1965 after signing the Metre Convention, kept in a vault at NMISA in Pretoria. This prototype is periodically taken to BIPM (10 years interval) for calibration.

Figure 1.5: South Africa's copy (no. 56) of the International Prototype of the Kilogram (IPK), stored at the NMISA in Pretoria South Africa. It was recalibrated in 2015 with 4×10^{-9} relative uncertainty.

Figure 1.6 shows the current mass measurements metrological traceability chain, illustrating how mass measurements performed in South Africa are traceable to the international reference standard for the unit of mass. The quantity value of the unit of mass is disseminated by making comparisons with the IPK using accredited procedures and instruments. The dissemination is in a form of a hierarchical system formed by various traceability chains to different nations. The first rank of the dissemination and comparison is with the six official copies of the IPK. From these official copies, only two were the first duplicates of the IPK that were made, and other were added along the way. They are kept together with the IPK under same conditions. From the official copies follows the calibration of the national prototypes, e.g. copy no.56 for South Africa.

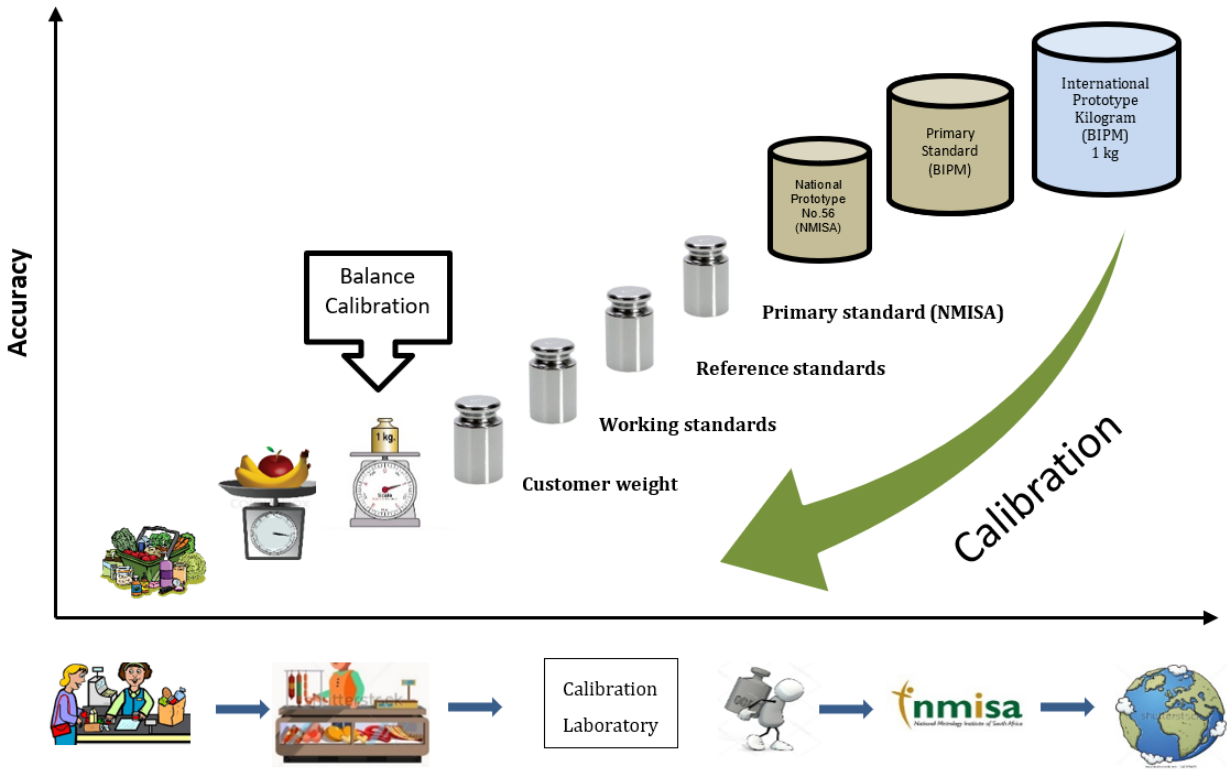

Figure 1.6: Metrological traceability chain in terms of mass calibration, showing how mass measurements are traceable to the international reference standard which in this case is the International Prototype of the Kilogram (IPK).

The calibration of the national prototypes yields a combined standard uncertainty of few parts in 10^9 relative uncertainty determined using the ISO recommended framework [24]. These national prototypes are kept by the state's national laboratory responsible for maintaining the standards. The relative uncertainty of these standards increases going down the hierarchy. This is due to standard uncertainties from external factors introduced during calibration processes and in addition from the stability of the standard under calibration (often referred to as a unit or device under test stability).

1.3.2 **Motivation for the new kilogram definition**

For more than a century, the system of using the IPK as the definition of the mass unit has ensured uniform mass measurements globally quite well. It has served its purposes (i.e. commercial, technical and scientific), until when it was realised that due to contaminations and other unknown factors, there is a drift between the IPK and its official copies at an average rate of 50 µg per century, this data is illustrated in Figure 1.7 [32]. This projected an indication that the primary mass reference standard is unstable.

The drift rate was reported after carrying out comparisons between the IPK and its official copies through a periodic verification process done in the years 1889; 1946 and 1991, this process is explained in more detail in [24]. The official copies are reported with respect to the IPK. The $y = 0$ axis line on Figure 1.7 represents the IPK, it doesn't change because there's no other standard above the IPK that it can be compared to.

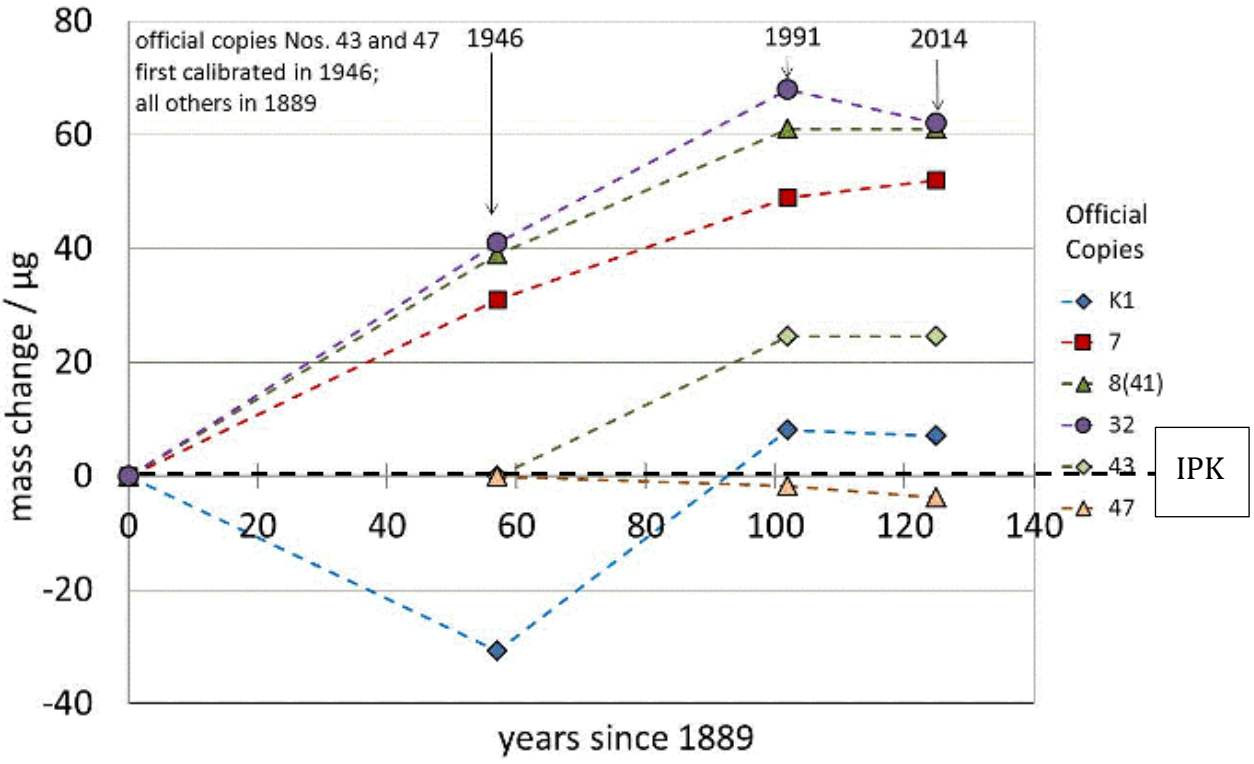

Figure 1.7: Mass changes of the official copies with respect to the International Prototype of the kilogram (IPK) [35].

Because of this instability in the mass unit reference standard, other base units such as the candela, mole, and ampere are being affected since their definitions in the current measurement system depend on the kilogram, see Figure 1.1. After the last verification of the official copies to the IPK in 1991, the 20th CGPM in resolution 5 [36] recommended that national laboratories should develop new experiments or realisation to replace the IPK. Following this recommendation, National Metrology Institutes (NMIs) took a global effort of developing methods defining the unit of mass (the kilogram) through experiments that can provide a link between the macroscopic mass and physical fundamental constant nature.

Many experiments were developed relating mass unit with the Planck's constant. Two experimental approaches demonstrated promising results with high measurement capabilities. These approaches are, the X-ray crystal density (XRCD) method (counting the number of atoms in a sphere of silicon and determining the Avogadro's constant N_A) [37], [38] and the Kibble balance (determining and fixing the value of Planck's constant h) [39].

Kibble balances have been and are still being developed by many metrology institutes such as NIST, NPL and NRC, as the metrological instruments that will in future provide the primary realisation of the unit of mass based on the fixed Planck's constant. The Consultative Committee for Mass and Related Quantities (CCM) mass metrology experts have been taking part in the effort of redefining the kilogram definition. The CCM has recommended and put forward the technical conditions that should be met before the redefinition of the unit of mass could occur. These conditions are clearly explained in the report [40] by the CCM to the BIPM from its 14th meeting and this publication [41], [42].

Following is a summary of the conditions:

- Have at least three independent experimental Planck's constant measurements, considering the results from both the Kibble balance method and the x-ray crystal density (XRCD) method. The relative standard uncertainty of all these results should be lower than 5 parts in 10^8;
- At least one of the results from the independent experiments should have relative standard uncertainty lower than 2 parts in 10^8;
- The fundamental constants (i.e. Planck's constant and Avogadro's constant) values provided by these various experiments should be consistent and always at the 95% confidence level; and
- The traceability of the prototypes to the IPK should be confirmed.

These conditions were met by the Kibble balance experiments from NMIs such as NRC and NIST, and the x-ray crystal density (XRCD) project from the International Avogadro Coordination. The published results data were gathered by the CODATA task group submitted to the 26th CGPM and adopted for the revision of the kilogram definition [15].

1.4 Research question

National Metrology Institute of South Africa (NMISA) is the leading metrology institute on the African continent, maintaining the measurement reference standards and disseminating traceability to other African metrology institutes and the industry with very high accuracy. NMISA aids the industry with measurement solutions that are comparable internationally with other countries. In order for these measurements to be comparable internationally, they should be of the same standard in terms of realisation to that of the other countries.

NMISA decided to invest in the Kibble balance method to realise mass in the future. The Kibble balance is a metrological instrument that can be used to determine the magnitude of an object in kilograms from the strength of current, voltage, gravity and velocity. This instrument has shown the capabilities of providing a link between the macroscopic mass and a fundamental constant of nature with a relative uncertainty of few parts in 10^8.

NMISA and the University of Cape Town (physics Department) have embarked on a joint project to construct the Kibble balance for South Africa, possibly the first on the African continent. Internationally, the system is being developed in collaboration with the National Physical Laboratory (NPL) in the UK. Upon completion, the Kibble balance will replace the current artefact primary reference standard (copy no.56) for South Africa. The Kibble balance will allow the kilogram to be realised in South Africa without the need to check its value regularly against an artefact kilogram (IPK) in Paris.

The aim of this study is to construct a prototype instrument that can practically demonstrate the theory of the Kibble balance in preparation for the final system. The final system will be more accurate and be used as a primary reference standard for mass measurements. In metrology any measurement performed and expressed as a number without been accompanied by any statement of uncertainty, is incomplete. The measurement accuracy of the Kibble balance depends on the measurement accuracy of each component in it. From the prototype, a full uncertainty budget will be designed and evaluated according to the ISO-recommended framework for the expression of measurement uncertainty, the so-called "Guide to the Expression of Uncertainty in Measurement", or ISO-GUM [43].

The evaluation will help in identifying components in the Kibble balance that need to be improved in order to lower the overall uncertainty of the measurements to meet the level required of order 10^{-8}. Another aim of this work is to design a measurement traceability link between measurement performed with the prototype to the primary reference standards.

1.5 Objectives of the study

The objectives of this study are:

- Highlight the background and the forthcoming revision of the International System of Units (SI);
- Construction of a prototype that can practically demonstrate the existing theory of the Kibble balance;
- Perform mass measurements with the prototype and compare the results with the measurements from the mass laboratory calibration results traceable to the current mass reference standard, the International Prototype of the Kilogram (IPK);
- Determine Planck's constant from known mass standards traceable to the current mass reference standard, the IPK;
- Design an uncertainty budget using an ISO-recommended framework for the prototype Kibble balance; and
- Design a measurement traceability chain for the measurement performed with the prototype Kibble balance.

2. Proposed methods for the revised kilogram

2.1 Introduction

The quest for redefining or realising the unit of mass with a link to fundamental constant has led to development of many experiments, with the accuracy and other metrological requirements being the limiting factors. Out of the methods that were developed, the Kibble balance (fixing the Planck's constant h) and X-ray crystal density method (fixing the Avogadro's constant N_{A}) emerged with a promising future. According to the recent studies [44]–[46] and the data in [17] that was submitted for the revision of the kilogram, these two methods have managed to fulfil the requirements or demands made by the CCM (see sub-sections 2.2 and 2.3). The definition of the Rydberg constant aids with providing a link between the Planck's constant and Avogadro's constant through the following equation:

$$N_{\mathrm{A}}h = \frac{A_r(e)c\alpha^2}{2R_\infty}M_u \tag{2.1}$$

where,

$A_r(e)$ is the relative atomic mass of the electron known with 4.2×10^{-10} relative uncertainty,

c is the speed of light (zero uncertainty),

M_u is the molar mass (zero uncertainty),

α is the fine structure constant known with 2.3×10^{-10} relative uncertainty,

R_∞ is the Rydberg constant known with 5.9×10^{-12} relative uncertainty.

The values of these constants together with their relative standard uncertainties can be found from the latest CODATA recommended values document [47]. From Eq (2.1), the product of the two constants shows that it is crucial to determine both constants very accurately because the Planck's constant h can be deduced from the Avogadro's constant N_{A} and vice versa. This is advantageous because it provides alternative methods to determine the constants and the two methods can be easily compared. The CODATA constants values make it possible for the

product of Avogadro and Planck's constants ($N_A h$) to be known with a very small relative uncertainty, i.e.:

$$\frac{u(N_A h)}{N_A h} = 4.5 \times 10^{-10}. \tag{2.2}$$

No matter which practical realisation method gets chosen by the NMIs as the primary realisation of the kilogram definition, the results will be comparable. The realisation can be with either the XRCD or the Kibble balance experiment since both constants are related to each other with very small uncertainty. In this chapter, both methods are discussed with more information on the reproducible Kibble balance method which is the main focus of this study.

2.2 The x-ray crystal density method

The x-ray crystal density method (XRCD) [38] is a method of determining the Avogadrodro's constant (N_A) from counting the number of atoms in a sphere of a single silicon-crystal (^{28}Si). Figure 2.1 shows an image of the single-crystal silicon (^{28}Si) sphere donated to NMISA by the National Metrology Institute of Germany (PTB) in August 2017. This method is considered as an indirect approach for determining the accurate measurement of the Planck's constant h through the relation described by Eq. (2.1). The silicon sphere was chosen because of its outstanding properties such as the high stability of the surface oxide layer and the small thermal expansion coefficient [48].

The complexity of the XRCD method led to the development of a coordination known as the International Avogadro Coordination (IAC). The coordination started in 2004 with the collaboration between various metrology intitutes. The institutes forming part of the IAC are: the BIPM (France),the PTB (Germany), the INRIM (Italy), the NMIA (Australia) and the NMIJ (Japan). In this collaboration, the institutes have varrying contributions according to their capabilities.

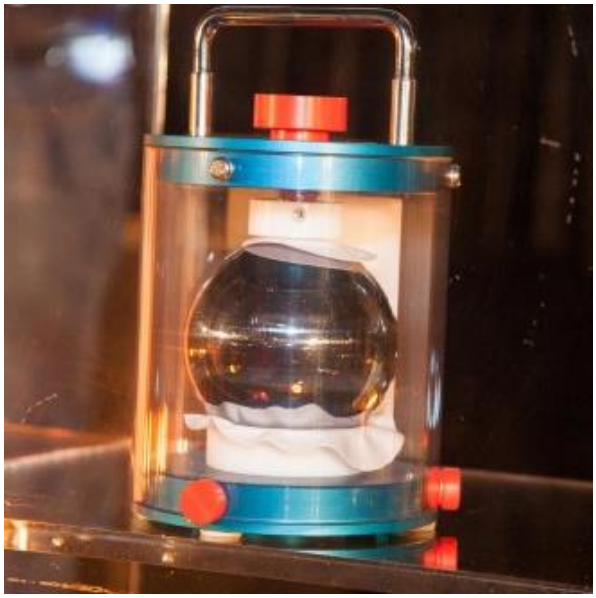

Figure 2.1: NMISA's single-crystal silicon (^{28}Si) sphere on loan from the PTB.

The determination of Avogadro's constant N_A using the XRCD method is given by the following equation [38]:

$$N_{\mathrm{A}} = \frac{nM}{\rho a^3} \tag{2.3}$$

where $n = 8$ is the amount of atoms in a unit cell, M is molar mass, ρ is the density and a is the lattice parameter. These componets need to be measured at a very high accuracy with capable equipment, as a result different methods were applied to measure these components individually by institutes in the IAC collaboration where the results were later compared and a value of N_A was calculated from highly accurate results. The first measurement result of Avogadro's constant $(N_A) = 6.022\ 140\ 82(18) \times 10^{23}\ \mathrm{mol}^{-1}$ was published in 2011 with a relative uncertainty of 3.0×10^{-8} [38]. More work was done to reduce the large contributing uncertanties and a measurement result of $N_A = 6.022\ 140\ 76(12) \times 10^{-23}\ \mathrm{mol}^{-1}$ was published in 2015 with a relative uncertainty of 2.0×10^{-8} [49]. The latest value submited to the CGPM for the revision of the mass unit definition was published in 2017 of $N_{\mathrm{A}} = 6.022\ 140\ 526(70) \times 10^{-23}\ \mathrm{mol}^{-1}$ with a relative uncertainty 1.2×10^{-8} [46].

2.3 The Kibble balance

2.3.1 Background

A Kibble balance initially contrived by Bryan P. Kibble (1938-2016) from the National Physical Laboratory (NPL) as Watt balance, is an experimental electromechanical weight measuring instrument that measures the mass of a test object through the strength of an electric current and a voltage [39]. The renaming of the instrument was recommended by the It appears to be like the equal arm balance mechanically but unlike the equal arm balance where the weight of the unknown (test object) is compared to the weight of the known mass i.e. gravitational force against gravitational force (see Figure 2.2), the Kibble balance instrument balances the gravitational force of the test object by the electromagnetic force resulting from the current-carrying coil immersed in a magnetic field.

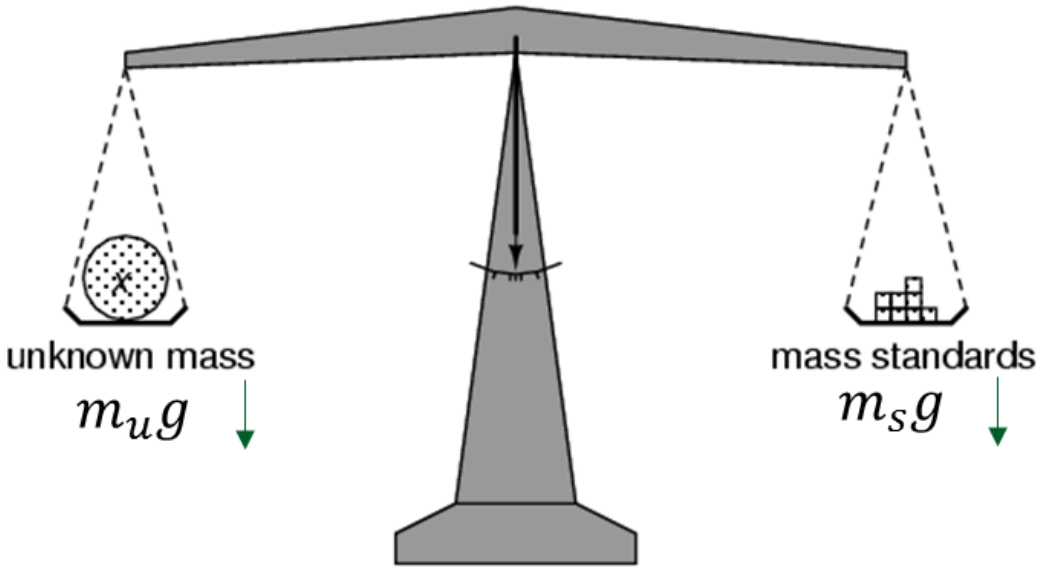

Figure 2.2: Operation of a passive equal-arm balance.

The discovery of the Josephson effect in 1962 [50] by Brian D. Josephson together with the quantum Hall effect (QHE) by Klaus von Klitzing in 1980 [51] has allowed a provision of the highly stable low uncertainty practical standards of the volt (V) and electrical resistance ohm

(Ω), respectively [52]. It has been adopted since 1990 during the 19th CGPM general conference meeting that the practical realisation of the electrical quantities be linked to the quantum standards through the conventional constants known as the Josephson constant, K_{J-90}, and the von Klitzing constant, R_{K-90}. These conventional constants are based on the Josephson effect and the quantum Hall effect, respectively.

National laboratories and other accredited calibration laboratories now use these quantum effects to calibrate the voltage and resistance standards through quantum electrical devices. The conjunction of these quantum effects allows the electrical quantities (i.e. voltage, resistance and current) to be measured in terms of the elementary charge e, Planck's constant h and the frequency f at a very high accuracy (refer to subsections 3.2.2 to 3.2.4). Kibble balance uses a combination of the two quantum effects to its advantage for the determination of the voltage and current strength at satisfactory low uncertainties. The Kibble balance uses them to provide a link between the macroscopic mass and the fundamental constant h.

2.3.2 **Kibble balance operation principle**

Kibble balance operates in two measuring modes, indirectly comparing the mechanical power and electrical power which are both measured in the units of watts, hence the origin of the name "*Watt balance*" [53]. These modes are usually executed separately, but the BIPM Kibble balance [54] operates uniquely by executing this modes simultaneously. The main reason for such design was to reduce the systematic effects that may arise due to time-varying magnetic flux density when moving from one mode to another and also to reduce the effects that may be caused by the coil misalignments [48].

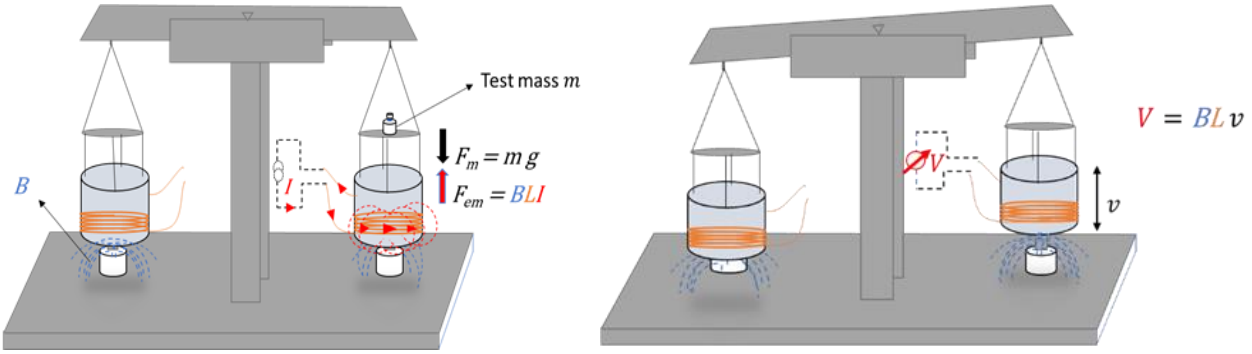

(a) (b)

Figure 2.3: The interacting modes of a Kibble balance. (a) The Force mode: where an appropriate current I is used to attain an equilibrium state between the weight mg of the test mass and the electromagnetic force BLI. (b) The velocity mode: where voltage V is induced when a coil is moved through the magnetic field at a constant velocity v.

The modes of operation involved in a Kibble balance are force mode and the velocity mode. Both modes are based on Lorentz forces and laws of induction. In the **force mode**, the gravitational force on a standard test mass m (or the weight $m \cdot g$) is exactly balanced by the electromagnetic force F_{el} generated by a DC current I carrying coil of wire length L immersed in a magnetic field with flux density B (represented by blue dash lines in Figure 2.3). The magnetic field is generated by two permanent magnets placed in a repulsion orientation. The electromagnetic force generated is given by:

$$F_{el} = (BL)_{frc} I \tag{2.4}$$

where $(BL)_{frc}$ is the product of magnetic field B and length L of the wire in the force mode. When these forces are at equilibrium it can be written that:

$$mg = (BL)_{frc} I. \tag{2.5}$$

From Eq. (2.5), it can be deduced that the mass measurements can be done by force mode operation only, but the difficulties arise when trying to get the accurate measurement of B and L. It is then imperative to introduce the second mode of operation known as the velocity or dynamic mode. In the **velocity mode**, the same coil from the force mode is moved at a velocity v along the vertical axis through the same magnetic field B. According to the Faraday's law of induction, when a wire (conductor) is moved in a magnetic flux region, a voltage V will be induced at the terminals of the wire. The magnitude of the induced voltage is given by:

$$V = (BL)_v v \tag{2.6}$$

where $(BL)_v$ denotes the product of magnetic field B and length L of the wire measured in the velocity mode. The velocity v accounts for the rate at which the wire cuts the magnetic flux. These two modes are summarized in Figure 2.3. Now, provided that the alignments, length L, magnetic field B and other properties of the coil remains the same in both operation modes, then Eq. (2.5) and (2.6) can be combined thereby eliminating the geometrical factor BL and the new equation becomes:

$$VI = mgv. \tag{2.7}$$

Now the two modes can relate the electrical power VI and the mechanical power mgv. The name "*Kibble balance"* comes from Eq. (2.7) because during the operation a mechanical power mgv is balanced by an electrical power VI and both are measured in the units of Kibbles. It is significant to note that these powers are virtual since VI and mgv are measured in separate modes, the velocity mode and force mode respectively. Rearranging Eq. (2.7), it follows that:

$$m = \frac{VI}{gv}. \tag{2.8}$$

This is the general equation for mass measurement using the Kibble balance. Direct high-precision measurement of current (I) is difficult to achieve to a satisfactory level of uncertainty. Instead of measuring current directly, the magnitude of the current I is then determined through Ohm's law. This is done by taking a measurement of the voltage drop V_R across a quantum hall resistance standard calibrated resistor R when current I is driven through the resistor. The Ohm's law is given by:

$$I = \frac{V_R}{R}. \tag{2.9}$$

Substituting Eq. (2.9) in (2.7), the equation becomes

$$V\frac{V_R}{R} = mgv. \tag{2.10}$$

2.3.3 **The link between macroscopic m and Planck's constant h**

In practice, the resistance measurements are realised by a primary reference standard known as the Quantum Hall Resistance Standard (QHRS) based on the Quantum Hall Effect defined by:

$$R = \frac{1}{i}\frac{h}{e^2}. \tag{2.11}$$

Both the induced voltage (V) and the voltage drop (V_R) measurements are to the primary reference standard known as a Josephson Voltage Standard (JVS) based on the Josephson effect given by:

$$V = \frac{nhf}{2e}. \tag{2.12}$$

Now substituting both quantum effects (i.e. (2.11) and (2.12)) for R, V and V_R in Eq. (2.10), the equation becomes:

$$Cff' \frac{h}{2e} \frac{h}{2e} \frac{e^2}{h} = mgv, \text{and} \tag{2.13}$$

$$C \frac{ff'h}{4} = mgv \tag{2.14}$$

where $C = \frac{nn'}{i}$ is the calibration constant indicating the number of junctions used in the Josephson array, f & f' are the microwave frequencies of the voltage measurements. Before the redefinition of the kilogram in 2018 the aim was to determine and fix the value of the Planck's constant h using mass m traceable to the IPK. This process serves as a continuity from the current mass reference system. This is given by a rearrangement of Eq. (2.14):

$$h = \frac{4}{Cff'} mgv. \tag{2.15}$$

After the redefinition the following equation will be used to realise the unit of mass from the prior fixed value of h:

$$m = \frac{Cff'}{4} \frac{h}{gv}. \tag{2.16}$$

2.3.4 **Existing Kibble balances**

Since the proposal of the Kibble balance in 1975 at the National Physical Laboratory (NPL), several Kibble balances have been built around the world by national laboratories. These national laboratories include the International Bureau of Weights and Measures (BIPM) [54], the Laboratoire National de Métrologie et d'Essais (LNE) [55], the Federal Institute of Metrology (METAS)[56], [57], the National Institute of Metrology (NIM) [58], the National Institute of Standards and Technology (NIST) [44], [59], the National Research Council (NRC) [45]. These Kibble balances follow the same principle; mostly they vary in the details of their designs such as the overall size of the balance, type of magnets used, mass mechanisms, coil movement mechanisms and other details. Other countries such as the Korea Research Institute of Standards and Science (KRISS) [60], National Metrology Institute of South Africa (NMISA), etc have started on the development of these instruments. Table 2.1 gives a summary of the published existing Kibble balances, where the laboratories are located and their measurement capabilities in terms of relative uncertainties. Figure 2.4 shows pictures of some of the existing Kibble balances. It should be noted that the NPL result was published based on the results taken before the NPL Kibble balance was transferred to NRC.

Table 2.1: Summary of the existing Kibble balances.

National Metrology Institute	**Country**	**Measurement capability (relative uncertainty)**
1. National Physical Laboratory (NPL)	United Kingdom, UK	2.0×10^{-7}
2. International Bureau of Weights and Measures (BIPM)	France	3.0×10^{-6}
3. National Research Council (NRC)	Canada	9.1×10^{-9}
4. National Institute of Standards and Technology (NIST)	United State of America, USA	1.3×10^{-8}
5. Laboratoire National de Métrologie et d'Essais (LNE)	France	3.1×10^{-6}
6. Federal Institute of Metrology (METAS)	Switzerland	2.9×10^{-7}
7. National Institute of Metrology (NIM)	China	1.6×10^{-6}

(a)

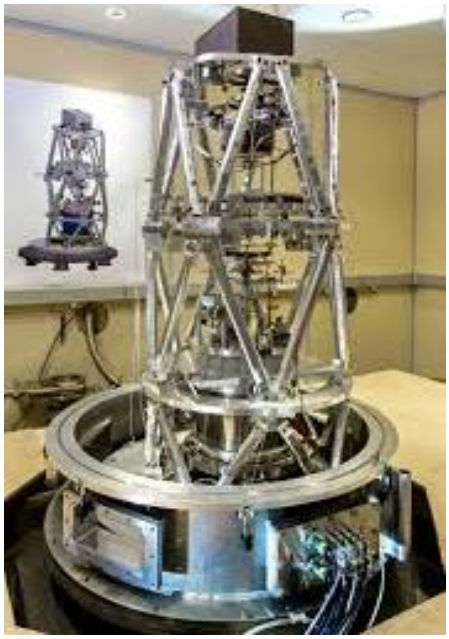

(b)

(c)

Figure 2.4: Images of some of the existing Kibble balances. (a) NIST Kibble balance, (b) BIPM Kibble balance and (c) NRC Kibble balance (former NPL Kibble balance).

3. Reference standards

3.1 Introduction

Figure 3.1 shows the general calibration hierarchy from the SI unit definition, primary reference standard to the testing equipment. Depending on the uncertainty level requirements for the measurements, an appropriate reference standard is used. NMISA is responsible for maintaining national measurement reference standards that measurements done in the South African country are traceable to and disseminates the traceability to other countries in the African continent.

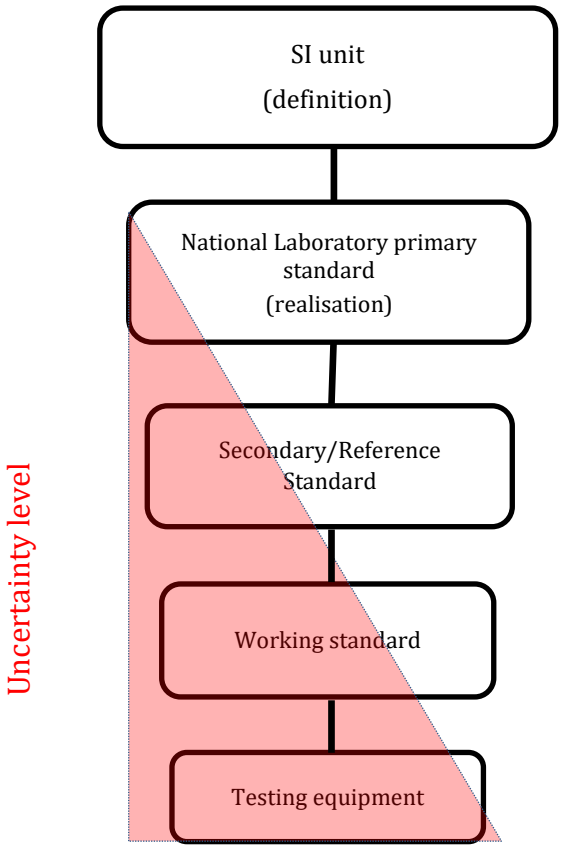

Figure 3.1: General hierarchy general calibration hierarchy from the SI unit definition, primary reference standard to the testing equipment.

Measurements results can be considered when they are defined by units, measured with an appropriate accepted equipment and through a traceable procedure. Any measurement with a defining unit should be linked to a primary measurement reference standard realising that unit, through a traceability chain. The Kibble balance is used to measure mass as one of its applications these mass measurement result contributors are traceable to various national reference standards. The standards discussed in this section are only the ones linked to the Kibble balance to the measurement results. The traceability of the Precursor Kibble balance experimental results is discussed in chapter 6.

3.2 Reference standards at NMISA linked to the Kibble balance

The reference standards discussed below are based on procedures followed by NMISA's calibration laboratories. These standards are maintained at NMISA by accredited laboratories. For the scope of this study, only the once linked to the Kibble balance are discussed. This is to give a background on the various measurements reference standards of which measurements achieved with the Kibble balance are traceable to. An exception is granted to the gravitational acceleration measurement reference standards because NMISA doesn't maintain these standards, the gravitational acceleration standards discussed below is of other NMIs and other capable institutes. The service is outsourced from outside when the NMISA laboratories need the gravitational acceleration measurements.

3.2.1 Length reference standards

The length laboratory at NMISA maintains length measurement standards and provides measurement traceability for all length measurements. The current definition of the metre adopted during the 17th CGPM meeting as defined in the SI brochure [14] allows the metre to be realised using several laser radiations. The CIPM has drawn up instructions on the practical realisation of the metre, chose the radiations to be recommended as the wavelength standards for the interferometric length measurement and several methods in which the metre should

be realised [23]. BIPM has prescribed three methods that can be used for the realisation of the metre, that is through:

a) Measuring directly the length L of the path travelled by a plane electromagnetic wave in a vacuum in a space of time t, through the relation $L = c_0 t$, where $c_0 = 299792458$ m s^{-1} is the speed of light in vacuum;
b) Determining the wavelength λ of a plane electromagnetic wave in vacuum by a direct measurement of the wave's frequency f, using the relation $\lambda = \frac{c_0}{f}$, where $c_0 = 299792458$ m. s^{-1} is the speed of light in vacuum; and
c) The use of one of the radiations on the list given by the BIPM, whose stated wavelength in vacuum and frequency can be used with an uncertainty stated.

The Krypton-86 lamp was once the primary reference standard for length measurements in the early 1900s. In 1991, the Krypton-86 lamp was replaced by the laser-based system as the national standard for length for South Africa. The most globally used radiation as the practical realisation of the metre is the He-Ne iodine-stabilized laser. From the methods listed above, NMISA is using method (b) as the practical realisation of the metre. Custom-made CSIR 3 iodine stabilised laser developed at CSIR national measurement laboratory now known as NMISA was the first laser-based system in the southern hemisphere to serve as the national standard for the metre realisation. Due to ageing of the CSIR 3, a commercial offset-locked laser-based system (Winters Model 200 iodine-stabilised offset-locked laser) shown in Figure 3.2 was procured to replace CSIR 3 and tested to confirm that it was able to operate under the recommended conditions set for a length primary standard to attain the required 2.5×10^{-11} relative uncertainty. The test results were published in [61].

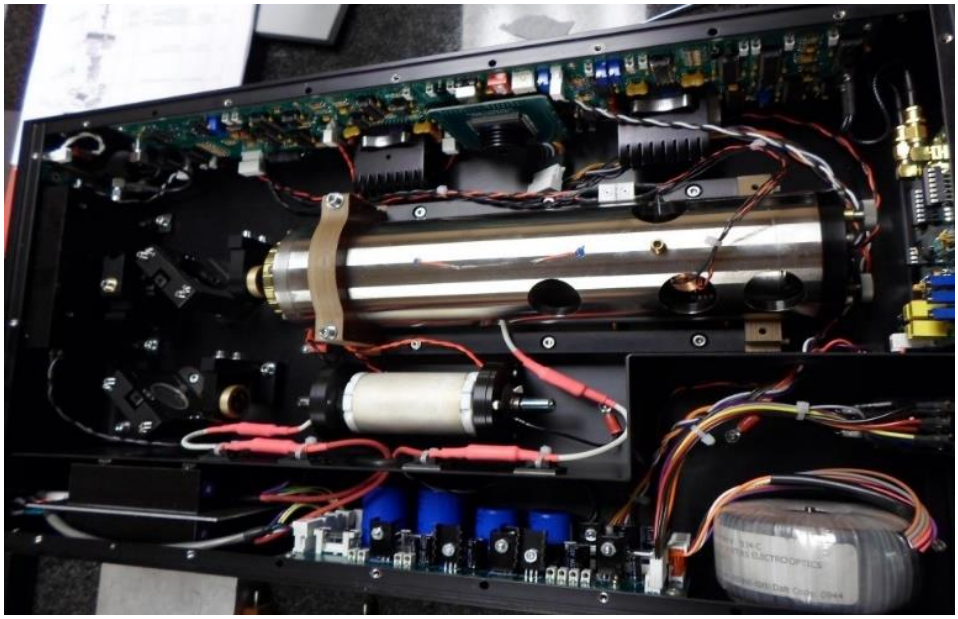

Figure 3.2: Primary reference length standard in South Africa, the He-Ne iodine stabilised laser (Winters Model 200)

Figure 3.3 shows the current length measurement traceability chain as adhered at NMISA together with the measurements capability uncertainty values achieved from each standard. The primary realisation of the metre is done using the radiation of the He-Ne laser with an internal iodine cell (Winters Model 200) stabilized using the third harmonic detection technique. The laser is characterised by the frequency value of, $f = 473\ 612\ 353\ 604$ kHz. The standard uncertainty of 12 kHz was obtained during the realisation measurements at NMISA, yielding the 2.5×10^{-11} relative uncertainty of the standard iodine laser when operated under specified conditions, as published in [23]. The frequency is converted using the fixed value of the speed of light to the wavelength through the equation:

$$\lambda = \frac{c_0}{f}. \tag{3.1}$$

The primary standard is used to calibrate the working standard (Zygo laser). This is done by measuring the beat frequency (found in the radio waves range of the spectrum) between the Winters Model 200 laser and the Zygo laser. The uncertainty increases (decrease in accuracy) to 1.2×10^{-8} $(k = 2)$ when the working standard is being calibrated due to uncertainty contributions from factors such as short-term stability of the working standard (Zygo laser), frequency counter resolution, measurement repeatability and contribution from the primary reference standard (Winters Model). The working standard is used to calibrate the Electronic Distance Metre (EDM), tapes and rulers. The uncertainty is greater than that of the working standard due to more uncertainty contribution from the alignment of the working standard, alignment of the UUT (i.e. EDM, tapes, rulers etc.), zero positioning, a volume of the laser and working standard (Zygo laser).

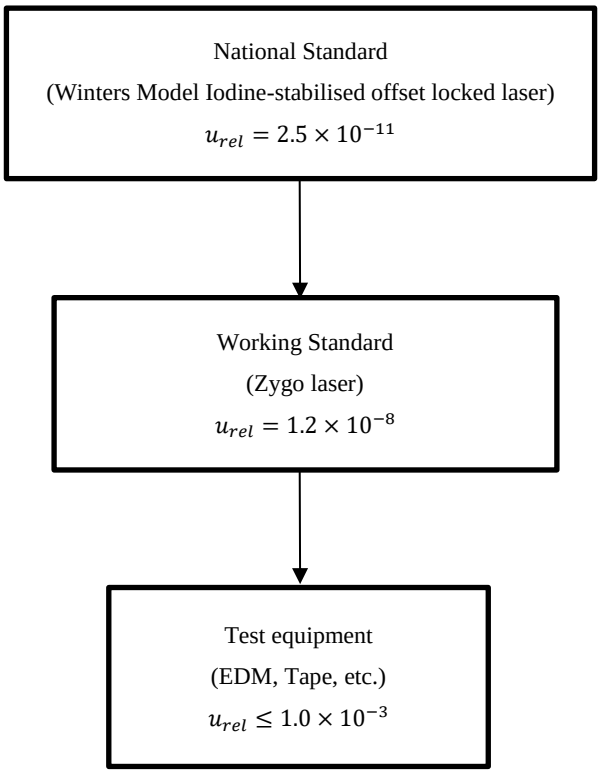

Figure 3.3: NMISA'S length measurements traceability chain.

3.2.2 **Resistance reference standards**

The ohm (Ω), derived unit for resistance measurements is realised by a quantum Hall resistance standard based on the Quantum Hall Effect phenomenon observed on sheet structure containing 2-dimensional electron gases (2DEG). When these types of structures are subjected to conditions of strong magnetic fields (typically 5 T to 14 T) and critically low temperatures, the separated Landau levels are observed because of electronic states grouping [62]. Quantized Hall resistance is then exhibited with the magnitude depending on the Planck's constant h, the elementary charge e and an integer i given by:

$$R_H = \frac{1}{i}\frac{h}{e^2} \tag{3.2}$$

where, $\frac{h}{e^2} = R_K$ is the von Klitzing constant, proven to be device independent [63] and was fixed in 1990 as the conventional value for resistance and current measurements [62]. The value of the von Klitzing constant is given by:

$$R_{K-90} = 25\,812.807\ \Omega. \tag{3.3}$$

The 2DEG structures provide a steady reference for resistance measurements linked to fundamental physical constants, h and e with a relative uncertainty of few parts in 10^{10} [62]. The realised resistance is transferred using the potentiometer or the cryogenic current comparator (CCC) bridge technique to the primary and secondary standards.

The DCLF Laboratory at NMISA maintains resistance measurement standards and disseminates the traceability to the Southern hemisphere industries. The measurements are categorized as low resistance, high resistance and ultra-high resistance. The low resistance measurements range from 10 μΩ to 10 kΩ with accredited calibration measurement

capabilities from 0.2 ppm to 7 ppm. The high resistance measurements range from 100 kΩ to 1 GΩ with accredited calibration measurement capabilities from 2 ppm to 9 ppm. The ultra-high resistance measurements range from 10 GΩ to 1 TΩ with accredited calibration measurement capabilities from 0.2 ppm to 7 ppm.

For this scope, the focus was on the low resistance measurement range. The laboratory does not provide an in-house traceability, instead two 1 Ω standard resistors (see Figure 3.4); serial numbers 1132427 and 1146606 are calibrated at the BIPM with 17×10^{-9} relative standard uncertainty. The traceability is transferred to laboratory working standards (10 μΩ to 10 kΩ) using a 6010C automatic resistance bridge low resistance bridge measuring system. These standard resistors are kept in an oil bath of constant temperature. Customer standards and resistance meters are calibrated against laboratory working standards. Figure 3.5 shows the traceability chain for the resistance measurements at NMISA.

Figure 3.4: NMISA's one-ohm reference standard resistor calibrated at the BIPM, with 17×10^{-9} relative uncertainty (*on the left*) and working standard in an oil bath of constant temperature (*on the right*).

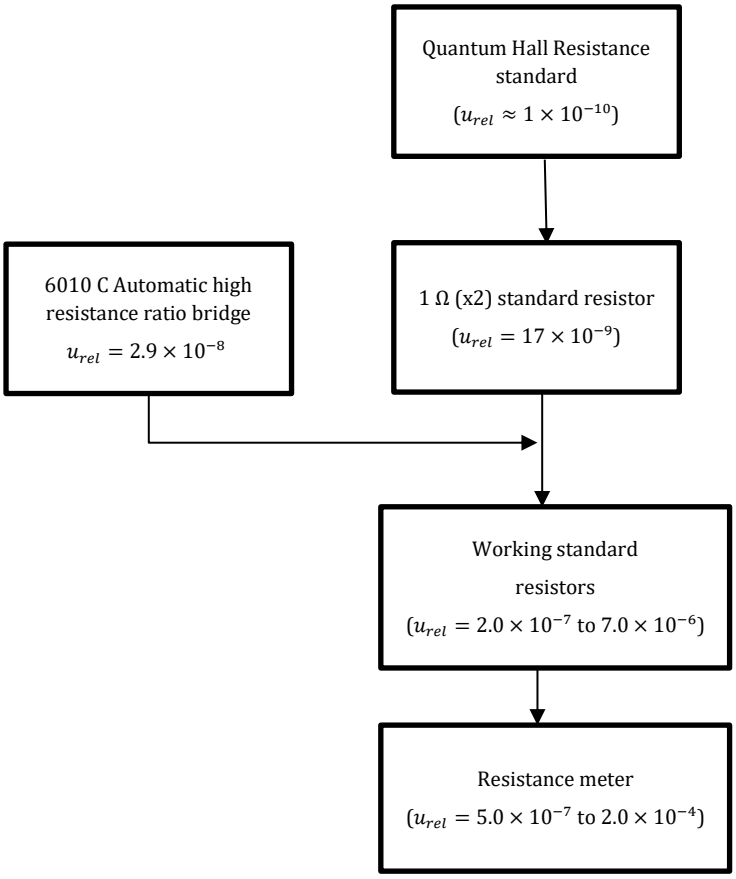

Figure 3.5: Resistance measurements traceability chain at NMISA.

3.2.3 **Voltage reference standards**

The volt (V), derived unit of voltage measurements is primarily realised using a Josephson voltage standard based on a phenomenal quantum effect known as the Josephson Effect in superconductivity. Figure 3.6 shows an image of NMISA's Josephson Voltage standard (this is the primary standard for voltage measurements in South Africa). The Josephson effect was predicted by Brian Josephson in 1962 [50]. This effect is observed when there is a junction consisting of two superconductors separated by a thin insulator (<2 nm) thereby resulting in tunnelling of electron pairs (Cooper pairs). Such a junction is now known as the Josephson junction (see Figure 3.7).

Figure 3.6: NMISA's Josephson voltage standard.

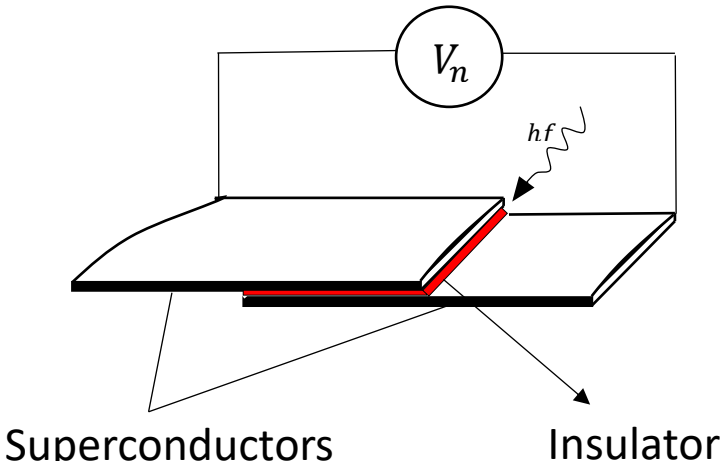

Figure 3.7: Structure of the Josephson junction.

When the microwave radiation of energy $= hf$ is applied to a Josephson junction at very low temperatures, a DC voltage V_n is produced across the junction. The value of the generated is given by:

$$V_n = \frac{nhf}{2e}. \tag{3.4}$$

Where n is the for number of junctions, e is the elementary charge, f is the frequency of the microwave radiation and h is the Planck's constant. The ratio $\frac{2e}{h}$, which is the ratio of double the elementary charge to Planck's constant is known as the Josephson constant [64]. It was proven to be material independent in 1968 by Clark [65] and was fixed in 1990 [52] to be:

$$\mathrm{K_{J-90}} = 483\ 597{,}9\ \mathrm{GHz/V}. \tag{3.5}$$

Now eq. (3.4) becomes:

$$V_n = nfK_J^{-1}. \tag{3.6}$$

A single junction can only provide few millivolts. To realise the voltage at a one-volt level, a Josephson array standard microchip (18 mm × 9 mm) consisting of thousands of these junctions is used to generate a volt with an uncertainty of order 1×10^{-9} [62]. The microchip is immersed and operated under the very low temperature of liquid helium. The voltage measurements are traceable to the JVS via the adopted conventional value of the Josephson constant K_{J-90}.

The DCLF laboratory at NMISA provides high accuracy dc and ac voltage measurements traceability. The laboratory provides an in-house derived dc voltage reference at the points 1 V, 1.018 V and 10 V with accredited calibration measurement relative uncertainty capabilities between 0.02 ppm and 0.1 ppm using a JVS system. The realised voltage is transferred to the 732A and 732B Fluke dc voltage reference working standards at points 1 V, 1.018 V and 10 V with relative uncertainties 1×10^{-7}, 1×10^{-7} and 2×10^{-8}. The uncertainty increases due to external factors introduced during the calibration process. Working standards are used together with the 752A voltage reference divider to calibrate the 5720A voltage source calibrator at points shown in Table 3.1. The 5720A calibrator is used as a voltage source to calibrate the digital voltmeters. The flow chart in Figure 3.8 illustrating the voltage measurement traceability from the primary reference standard and the uncertainty variations.

Table 3.1: 5720A Calibrator voltage points calibrated using 732A/B reference standard and the corresponding certified uncertainties.

Voltage Points	Certified relative uncertainties
100 mV	7ppm
1 v	1ppm
10V	3ppm
100V	3ppm
1000 V	3ppm

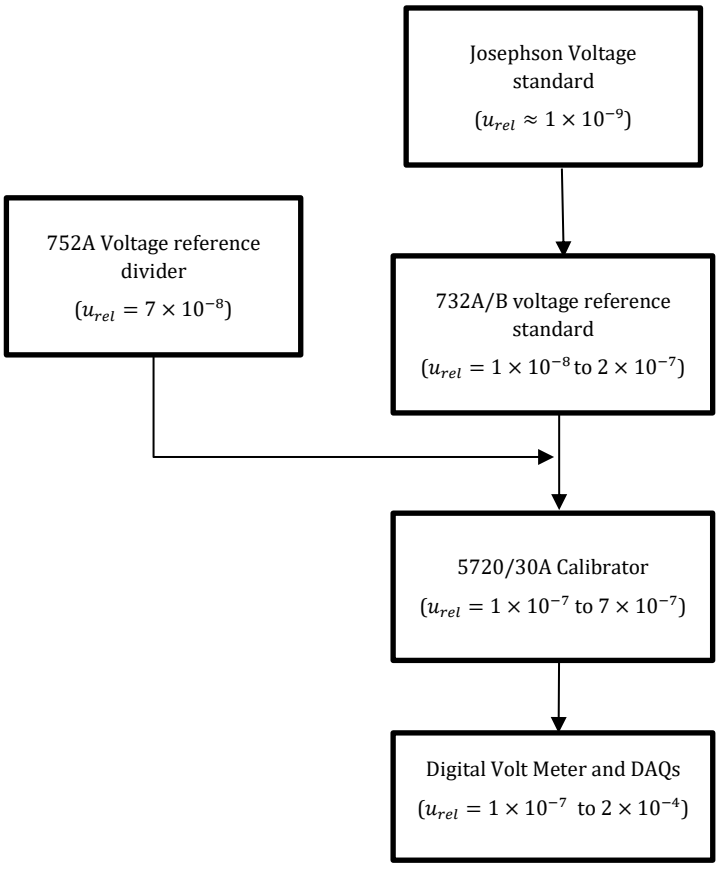

Figure 3.8: Voltage measurements traceability chain at NMISA.

3.2.4 **Current reference standards**

The ampere, the unit of current is primarily realised through Ohm's law, with the accredited traceability to the derived units of resistance and voltage. Current reference standards are traceable to the SI unit ampere defined in the SI brochure [14]. The current is realised via the volt drop method defined by Ohm's law as follows:

$$I = \frac{V}{R} \tag{3.7}$$

where V is the voltage measurement traceable to the Josephson Voltage Standard (JVS) and R is the resistance measurement traceable to the Quantum Hall Resistance Standard (QHRS). The reference standards for resistance and voltage measurements are discussed in section 3.2.2 and 3.2.3 respectively. The DCLF laboratory at NMISA maintains the reference standards and provides traceability for voltage, resistance and current at high accuracy compared to any other labs in South Africa. The traceability is offered in the range 0.1 μA and 100 A. The current points are obtained using different standard resistors traceable to the BIPM quantum hall resistance standard. These standard resistors are also known as the current shunts summarised in Table 3.2.

The voltage drop method is performed using the following equipment: standard resistors summarised in Table 3.2 traceable to the Quantum hall standard, the Wavetek 1281 digital multimeter for voltage measurement traceable to the Josephson voltage standard, power supply and 5730A/5720A multi-function Calibrator. This method is used to calibrate the current source 5730A/5720A multi-function Calibrator at the nominal points summarised in Table 3.2. Figure 3.9 shows the 5730A multifunctional calibrator. During the realisation process, the Wavetek 1281 digital multimeter is connected across the standard resistor measuring the voltage drop across.

The uncertainties of the 5730A/ 5720A multi-function Calibrator at the calibration points depends on the accuracy of the voltmeter and the standard resistors. The 5730A/ 5720A multi-function Calibrator is now used as a current source to calibrate current meters. The current meter measurements are then traceable to the voltage and resistance standards through the traceability chain show by Figure 3.10.

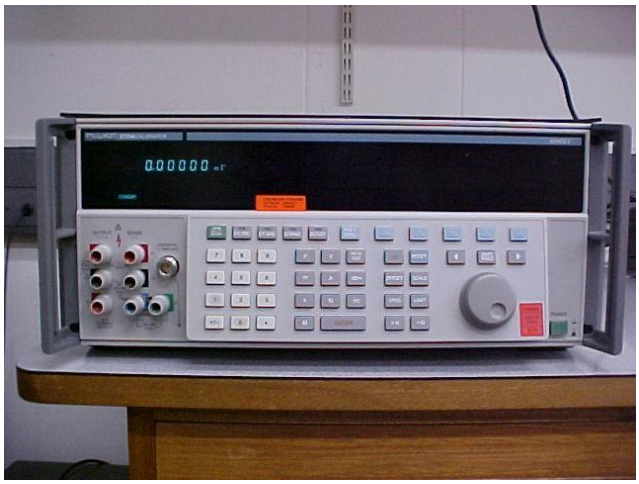

Figure 3.9: 5720 A multifunctional calibrator.

Table 3.2: Standard resistors required for the realisation of the nominal current between 0.1 μA and 100 A.

Nominal current	Nominal resistance	Model	Serial number
0.1 μA	1 MΩ	2792	00220
1 μA	100 kΩ	2792	00262
10 μA	10 kΩ	2792	00325
100 μA	10 kΩ	2792	00325
1 mA	1 kΩ	2792	00598
10 mA	10 Ω	2792	00820
100 mA	1 Ω	2792	01288
1 A	100 mΩ	2792	00696
10 A	10 mΩ	2792	00561
100 A	100 μΩ	3200/KD	126930

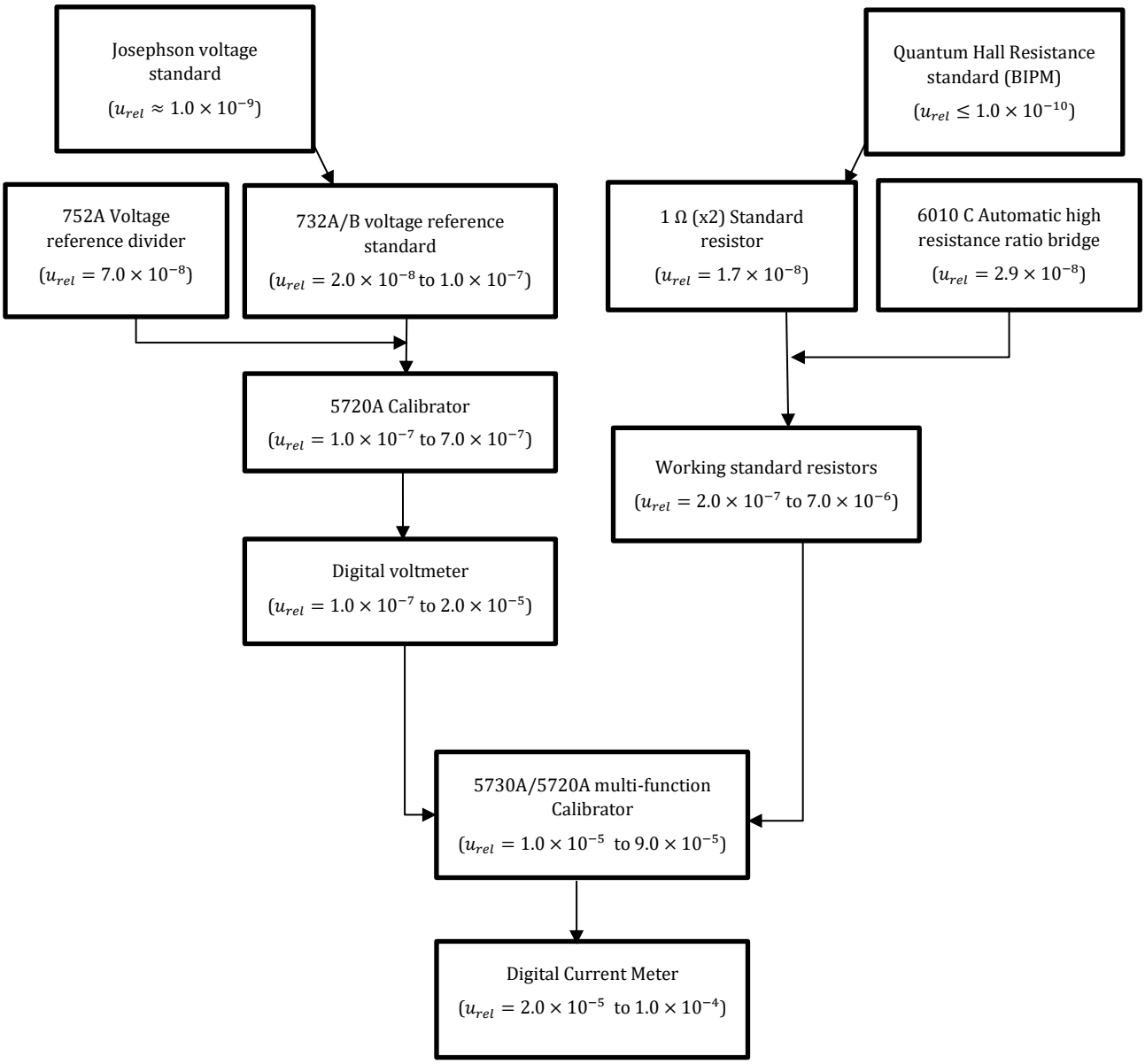

Figure 3.10: Current reference standards traceability chain at NMISA.

3.2.5 **Time and frequency reference standards**

The second (s), unit of time interval is primarily realised using the caesium clocks and oscillators based on the hyperfine transition frequency of the caesium 133 atom ($\Delta v(^{133}\mathrm{Cs})_{\mathrm{hfs}}$) between the two energy states [14]. The current definition and the realisation of the second makes it to be realised or measured with a very small uncertainty compared to all the SI units [66]. Time and Frequency laboratory at NMISA is responsible for maintaining, providing and monitoring the traceability of the reference standards for time and frequency measurements in South Africa. At NMISA, the measurement of a second can be achieved with the relative uncertainty of order 1.0×10^{-13} or less. Figure 3.11 shows the time and frequency primary reference standard at NMISA consisting of atomic clocks and oscillators.

Figure 3.11: Time and frequency primary reference standard at NMISA.

The time and frequency primary reference standards of all the NMIs are traceable to the international standard time scale known as the Coordinated Universal Time (UTC). The UTC is the adjusted version of the International Atomic Time (TAI). The UTC is adjusted by the so called leap seconds in order to correct the difference between the rotation of the earth and the SI definition of the second. To create this time scale, the BIPM collects data of the time interval and frequency from over 60 laboratories-worldwide and calculate a weighted average of the data [66]. The laboratories send the measurement data to the BIPM together with their uncertainties. The data is published in a document known as the *circular T* which can be

accessable from the BIPM website. It should be noted that the UTC and TAI are only the paper time scales, so there is no official physical version of UTC and TAI time scales. The BIPM does not generate any signal but the clocks maintained by the NMI's do. Now since the data is generated by atomic clocks maintained by the NMI's, the tracebility chain for time interval and frequency measurement should have a link to the UTC and back to the signals at the NMI.In most metrology fields, the establishment of traceability is done periodically which involves shipping or transporting standards from one area to another. However, it is different when it comes to the time and frequency metrology field where the traceability can be established in many ways in a form of signal broadcasts. For example, the traceabilty can be obtained by a direct link to the NMI through signal broadcast over the network path, radio, or telephone and again the traceability can be obtained in a form of receiving the signals monitored by the NMI.

Figure 3.12 shows the time interval and frequency measurement traceability, showing how the test equipment/measurrement instruments calibrated at NMISA are traceable to the international standard, the UTC. The data generated by the NMI atomic clocks and oscillator is often sent to the BIPM on monthly basis to feature in the *circular T* thereby updating the UTC. NMISA generates the South African real time version of the UTC known as UTC(ZA). This time scale is synchronised time versions of other countries via the Global Navigation satellite systems (GNSS), an exaple of such systems is the Global positioning system (GPS) [67]. This system is under the control of the United states Naval Observatory (USNO) and National Institute of Standards and Technology (NIST) signals, the so-called real time version of the UTC (*UTC(USNO) & UTC(NIST)*) [68]–[70]. The UTC(USNO) and UTC(NIST) agree within nanoseconds of the computed UTC by BPIM [71]. The GPS time scale is steered on monthly basis to correspond to the UTC scale from *circular T* by the controllers. The signal can be received at site from the satellite using the following GPS receiving methods: the GPS one-way, GPS disciplined oscillator and GPS common-view [72].

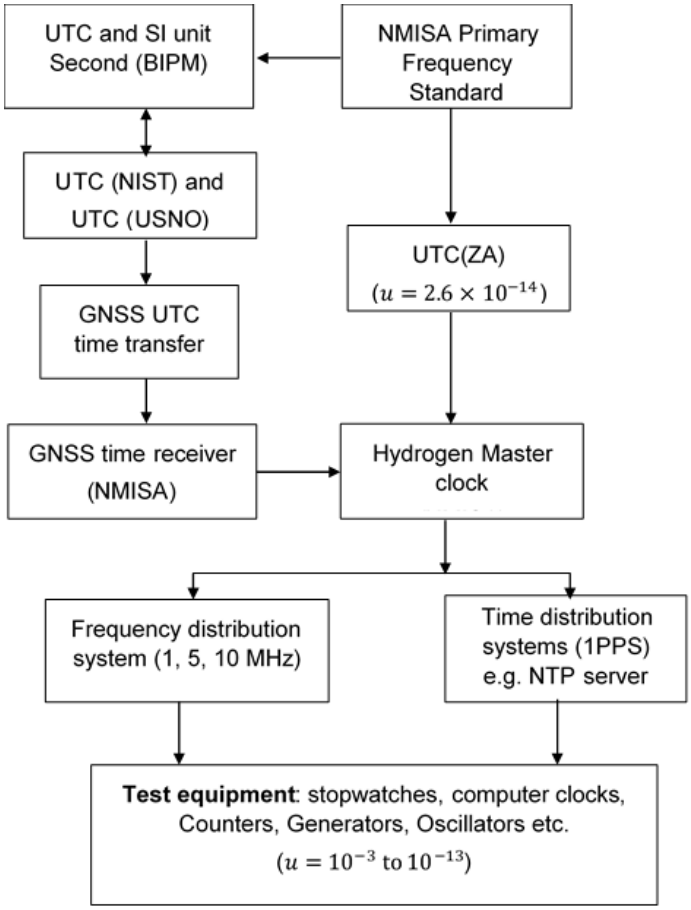

Figure 3.12: Time interval and frequency measurements traceability in South Africa.

The accuracy of the time interval measurement depends on the type of equipment and method used. Many techniques are available to establish the traceability with the uncertainties ranging between few parts in $10^3$and 10^{14}. NMISA also offer the network time services to the users through an operation of the networktime protocol (NTP) server [73]. The server is is traceable to the master clock that can be linked to the UTC(ZA). The time stamps of the devices such as computers, surveilance cameras etc.are linked to the server via the ethernet network switch with an uncertainty of order few parts in 10^3 or even less in some cases. For high accuracy measurements, it is necessary for the user to get the GNSS timing reciever (e.g GPS receiver).

3.2.6 **Gravitational acceleration reference standards**

The gravitational acceleration is known as the rate of change of the velocity of a falling object due to the force of attraction towards the centre of the earth. The gravitational acceleration measurements play a significant role in many metrology fields. The primary measurements in the fields such as the vibration, force, pressure, torque and mass measurements depends directly on the measurements of gravitational acceleration g [74]. The gravitational acceleration is measured in the units of m s^{-2}. At high accuracy level measurements of gravitational acceleration are performed with gravimeters. The gravimeters are divided into two categories i.e. absolute and relative gravimeters. An absolute gravimeter measures the local gravitational acceleration at a given location and a relative gravimeter measures a comparison in gravity between two places.

The most commonly used gravimeters operate via the free-fall method (refer to Figure 3.13), where an object (corner cube) is freely dropped in a vacuum chamber. A Michelson interferometer is used to accurately track the free-fall motion of the object. The interferometer uses the primary standard for length measurements (helium-neon (He-Ne) iodine stabilised laser) to track the free-fall motion. The motion is measured in terms of optical interference fringes. The interference fringes are generated every time the object moves half the wavelength of laser. and the occurrence of the optical fringes is accurately timed using an atomic clock traceable [75]. The gravimeter measurements are traceable to the primary reference standard for length (He-Ne laser) and time (atomic clocks), this is illustrated by Figure 3.14.

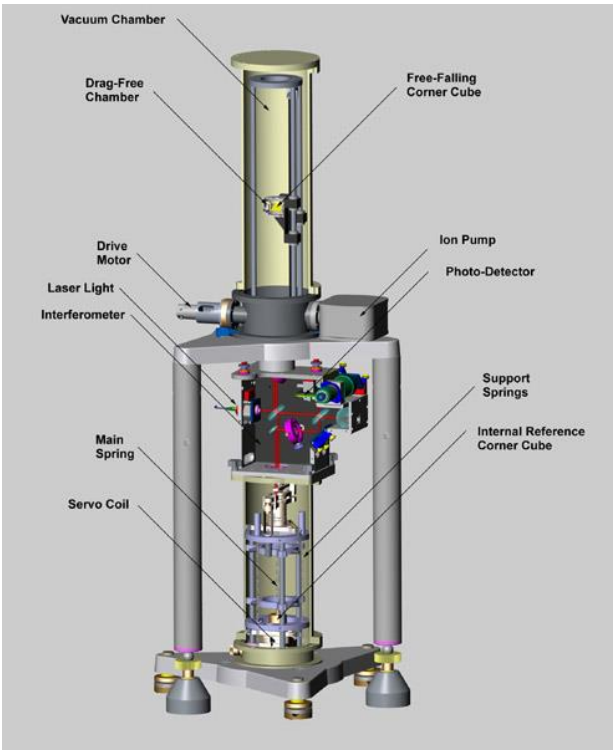

Figure 3.13: Schematic display of an absolute gravimeter [75].

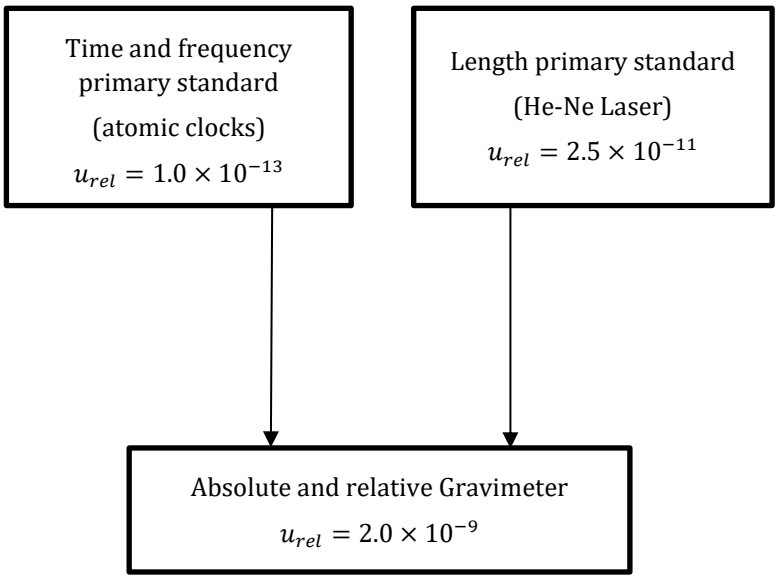

Figure 3.14: Traceability chain for gravitational acceleration g measurements performed with an absolute gravimeter.

NMISA currently does not provide the traceability for gravitational acceleration measurements. According to [74], currently there is no institute with declared calibration and measurement capabilities (CMCs) to calibrate other gravimeters, only five NMIs have declared measurement capabilities for gravitational acceleration measurements at an international level so far, where the traceability is linked directly to the SI (length and time). The NMIs are: NSC in Ukraine, FGI in Finland, INRiM in Italy, BEV in Austria and METAS in Switzerland with standard uncertainties ranging between 8.0×10^{-8} and $2.1 \times 10^{-7}\mathrm{m\,s^{-2}}$. This does not mean that measurement performed with other gravimeters are not valid as there is another standard method for performing traceable g measurements.

Currently, the gravitational acceleration measurements performed by most gravimetry institutes over the world are linked to each other via the International Gravity Standardization Network established in 1971 (IGSN71) [76] and the International Absolute Gravity Base Station Network established in 1986 (IAGBN), based on a collective of absolute g measurement from over 20000 gravimeters worldwide. These networks are shown in Figure 3.15. The measurements are performed by institutes that are members of the International Association of Geodesy (IAG). They ensure their traceability by means of a tie procedure described by Morelli et al.[76] and the standard error of the gravity values from this network is less than $10^{-6}\,\mathrm{ms^{-2}}$. The International Comparison of Absolute Gravimeters (ICAG) is responsible for the periodic comparison of the absolute gravimeters.

In South Africa, the Council for Geoscience have the capability to perform this procedure where the g mapping results at a site are tied to the main base SIL1 in Silverton that is in turn linked to the international base station (located at the National Botanical Gardens in Pretoria). The South African international gravity base station is shown in Figure 3.15, forming part of the International gravity network. The CCM and the International Association of Geodesy (IAG) are working on creating a global system for the traceability of g measurements at an uncertainty level of order $10^{-8}\,\mathrm{ms^{-2}}$ following the CIPM-MRA principles for metrology [77].

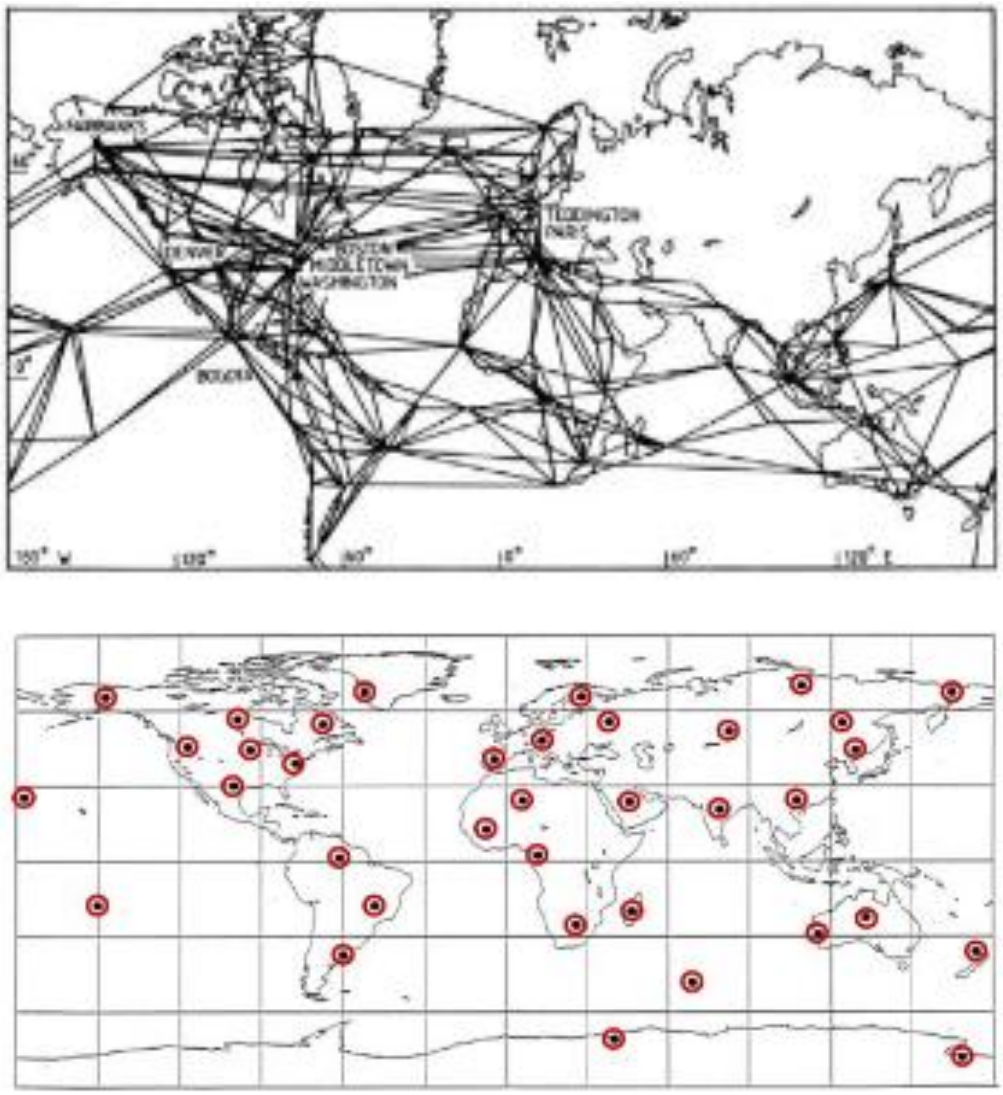

Figure 3.15: The international gravity networks. The IGSN71 (top) and IAGBN (bottom)[74].

4. NMISA's precursor Kibble balance

4.1 Introduction

This chapter gives details on how the precursor Kibble balance discussed in this study was constructed, showing the type of materials, apparatus and procedures used. The measurement methods of how the magnitude of the test mass can be obtained from electrical quantities are also discussed. Furthermore, the method of determining the Planck's constant using masses traceable to the current primary mass reference standards (the IPK) is shown and the results are presented in Chapter 5.

4.2 Sub-components description

Existing Kibble balances from different NMIs have been listed in Table 2.1, with distinctive designs. At NMISA designs that are more reproducible were chosen to measure masses at a low scale. In this study, three low-cost tabletop systems capable of measuring gram-level masses have been constructed. The work started with the construction of a replica of the NIST Lego system (built mainly from Lego blocks) illustrated by an image illustrated by the CAD drawing in Figure 4.1 [53].

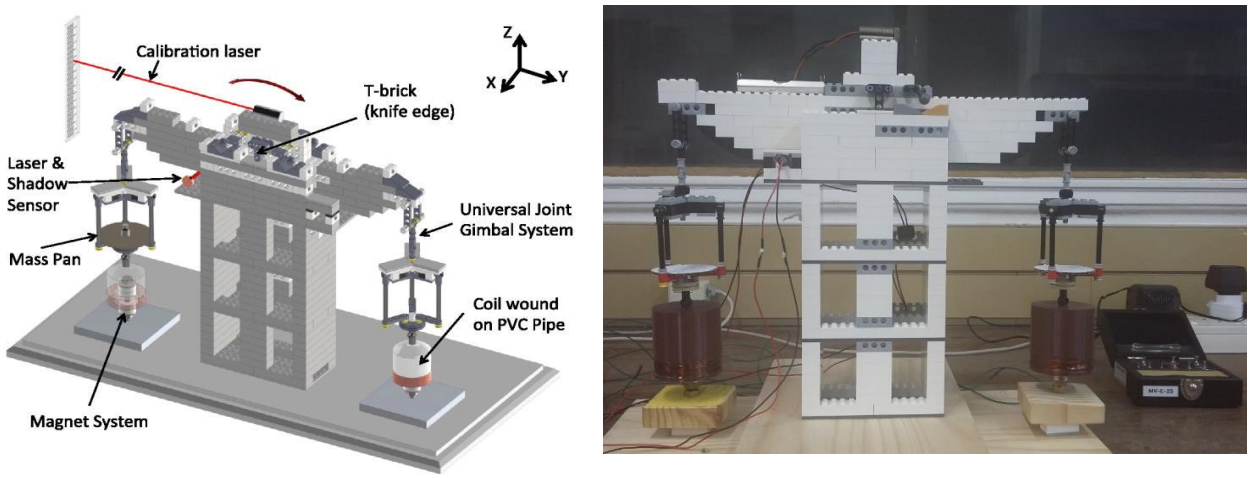

Figure 4.1: CAD sketch of the Lego Kibble balance (*on the left*) [53] and its image (*on the right*).

In the second phase (2nd prototype), a 3D-printing technique was introduced, almost all parts of the balance beam were 3D printed as shown in Figure 4.2. SolidWorks software was employed to design the CAD models of the balance and converted to 3D printable models using an Ultimaker Cura software, provided by Ultimaker [78]. Figure 4.3 shows NMISA's Ultimaker 2+ 3D printer in the process of printing out some parts of the balance.

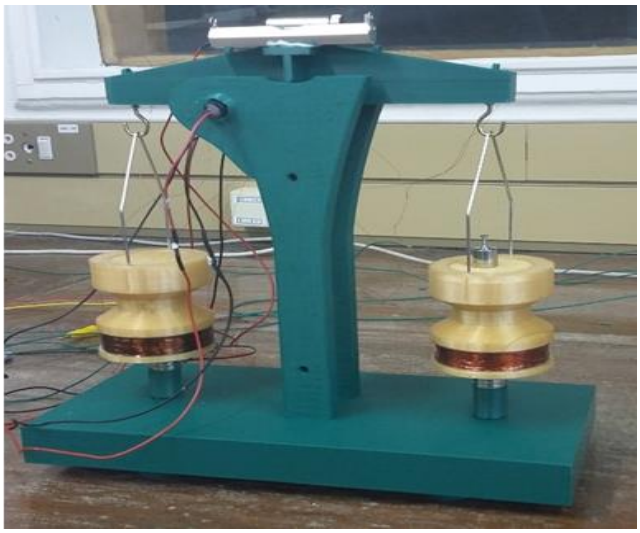

Figure 4.2: 3D printed Kibble balance.

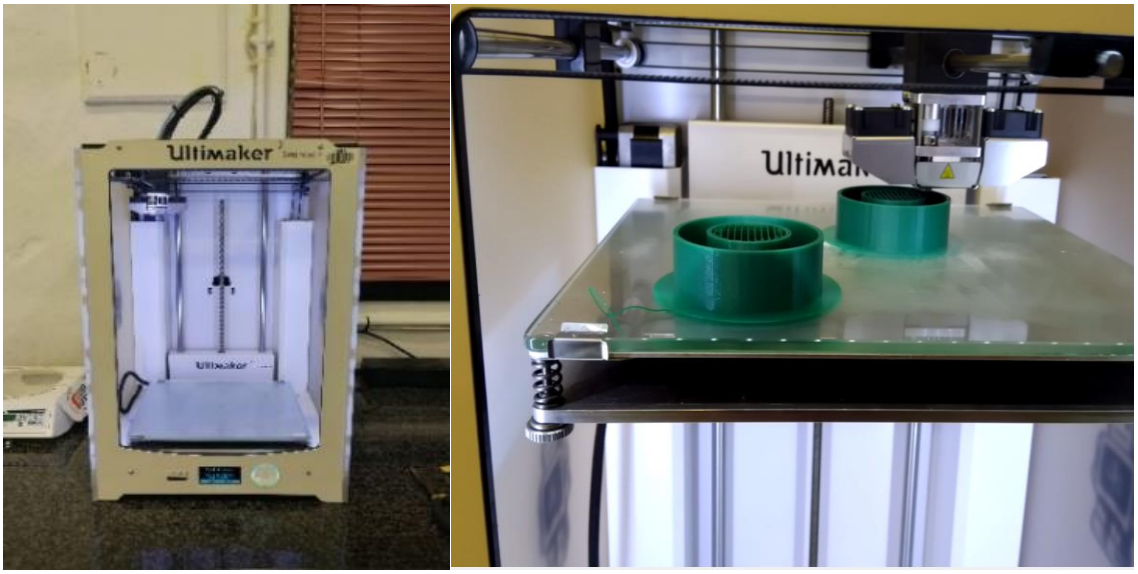

Figure 4.3: NMISA's Ultimaker 2 Extended + 3D printer on the left and printing process on the right.

It can be recognised that both systems (LEGO and 3D printed) resemble the mechanical appearance of an equal-arm balance beam. In both systems, just like it is on an equal arm balance scale, the beam is supported on the central knife edge. The knife edge of about half a centimetre diameter also serves as the pivoting point (fulcrum) of the beam.

The final prototype was constructed by modifying one of the old equal arm balances from the mass laboratory in NMISA. Figure 4.4 shows an image of 500g scale equal arm balance beam before modification and after modification. Most of the work in this study is based on this final prototype. Figure 4.5 below shows the experimental set-up of the NMISA precursor Kibble balance, more details are to follow in the subsections below.

(a) Before b) After

Figure 4.4: Final precursor Kibble balance (a) before and (b) after modifications.

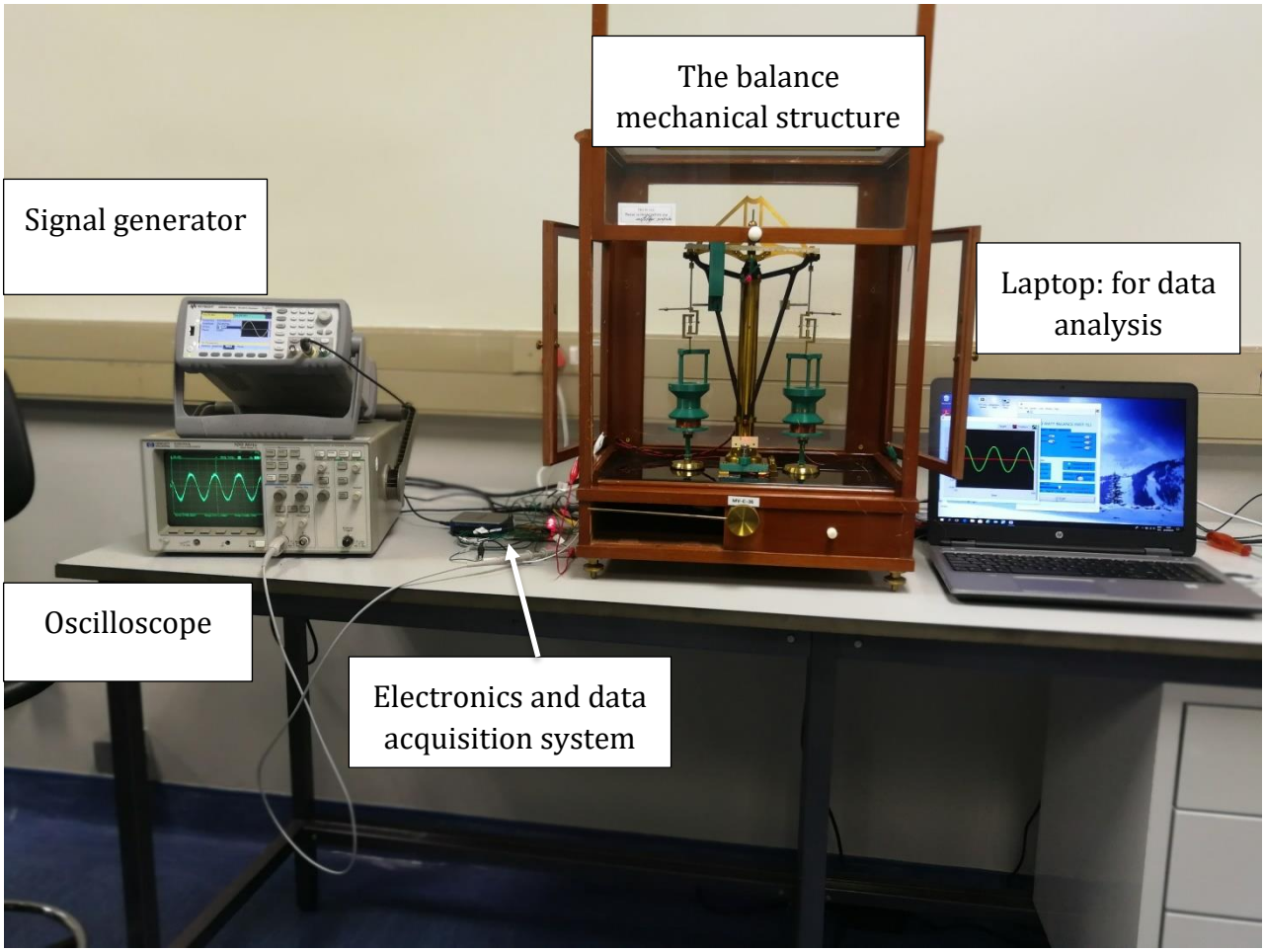

Figure 4.5: Experimental set up of the NMISA precursor Kibble balance.

4.2.1 **Mechanics**

A design of the modified equal arm beam balance has been chosen as the main prototype for this study. The balance is enclosed in a box made of wood with glass doors. The balance beam is suspended and supported at its centre by a knife edge set at a right angle relative to the supporting structure. The coil formers of relatively equal weight are suspended on each side of the beam, equidistant from the point of support (i.e. approximately 80 mm half-arm length). The beam suspending the coil formers will be balanced when it is horizontal relative to the table surface level. To ensure that the beam is horizontal, a needle pointer is attached perpendicular to the centre of the beam (fulcrum point) and pointing zero on a small scale attached at the bottom vertically in line with the fulcrum when the beam is parallel to the table surface level.

The top side of the coil serves as a weighing platform marked with a cross indicating where the test mass should be placed during the weighing process. The coil suspension rods are attached to the ends of balance beam on both sides at the top with small knife edge set. This eliminates most of the coil's horizontal movements because the main aim is to allow the coil to move in the z- direction only. The balance has a locking mechanism, which is used to lock the balance by uplifting the arms of the balance and keeping the knife edge of the pivoting position. The importance of the black glass base plate was used as a foundation to hold the balance's structure. The CAD model of the balance is shown in Figure 4.6 and supported by and an image with the main parts being magnified (labelled A-D) shown in Figure 4.7.

To monitor the movement of the balance and the coil position, laser modules (point & line lasers) and a shadow sensor were employed and mounted onto the balance structure. At the lower edge of the arm, the system consists of a line laser directed towards a shadow sensor with the ruler parallel to the arm (mount on the balance arm) partially obstructing ≈50% of the light when the balance is at zero position (see Figure 4.7A & Figure 4.8 A). When the balance tilts, the shadow sensor receives more or less light depending on the tilting direction.

Secondly, a point laser was used to serve as an optical lever, this is used to calibrate the shadow sensor voltages. With the NIST Lego Kibble balance the laser is mounted on top of the arm pointing to the ruler scale attached to the wall. For the NMISA system, the laser was not mount on top of the balance arm, as it was suspected that wires supplying power to the laser module might be introducing external forces on one side of the balance and causing resistance to the balance movement during the velocity mode (this causes irregularities in the movement). Instead, the point laser was mounted onto the base plate in line with the pivoting region, pointing vertically towards a small mirror fixed at 45° angle. The light gets reflected at 90° angle to the ruler scale attached to the wall (see Figure 4.7 B and Figure 4.8 B).

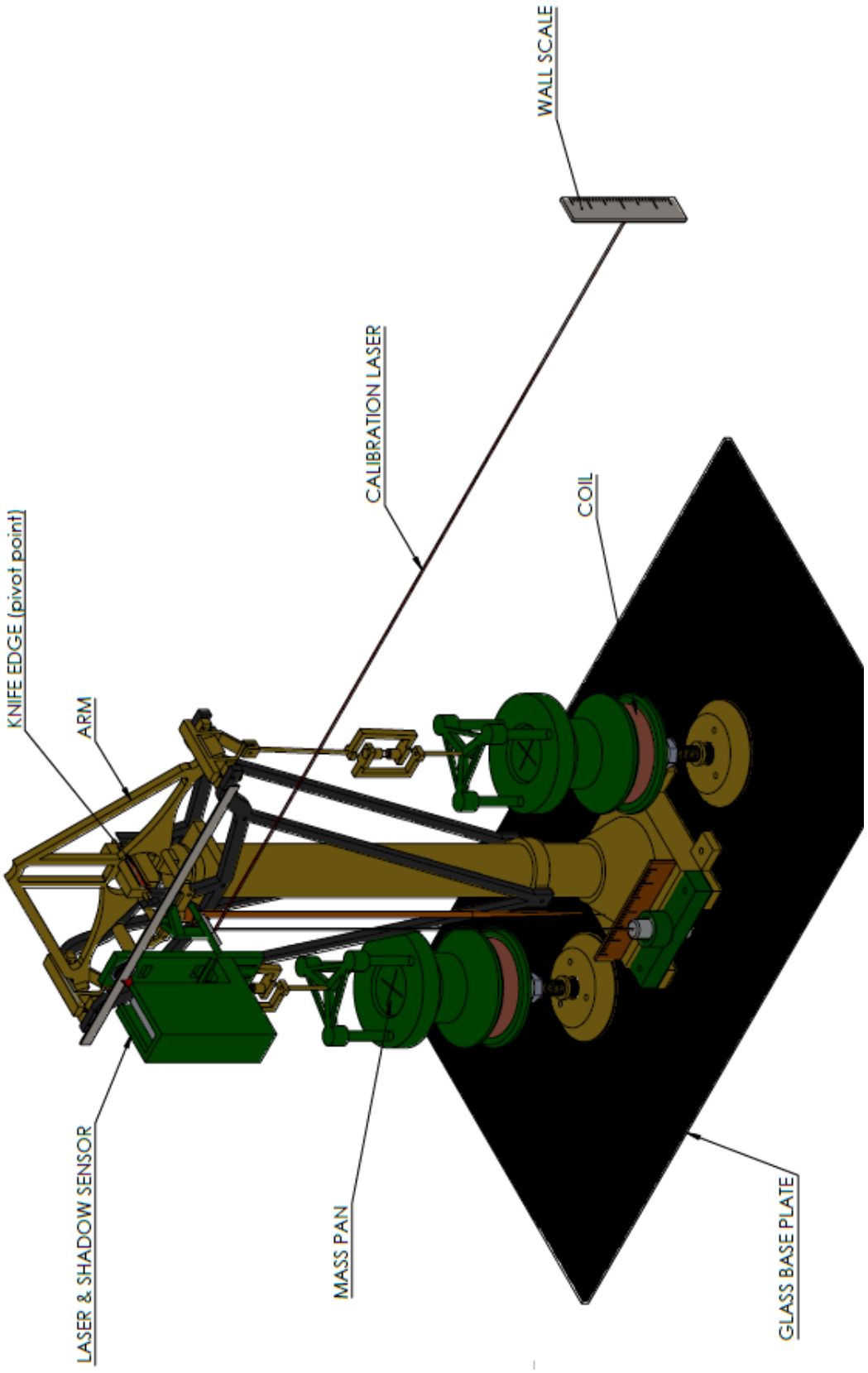

Figure 4.6: CAD model of the NMISA equal-arm Kibble balance.

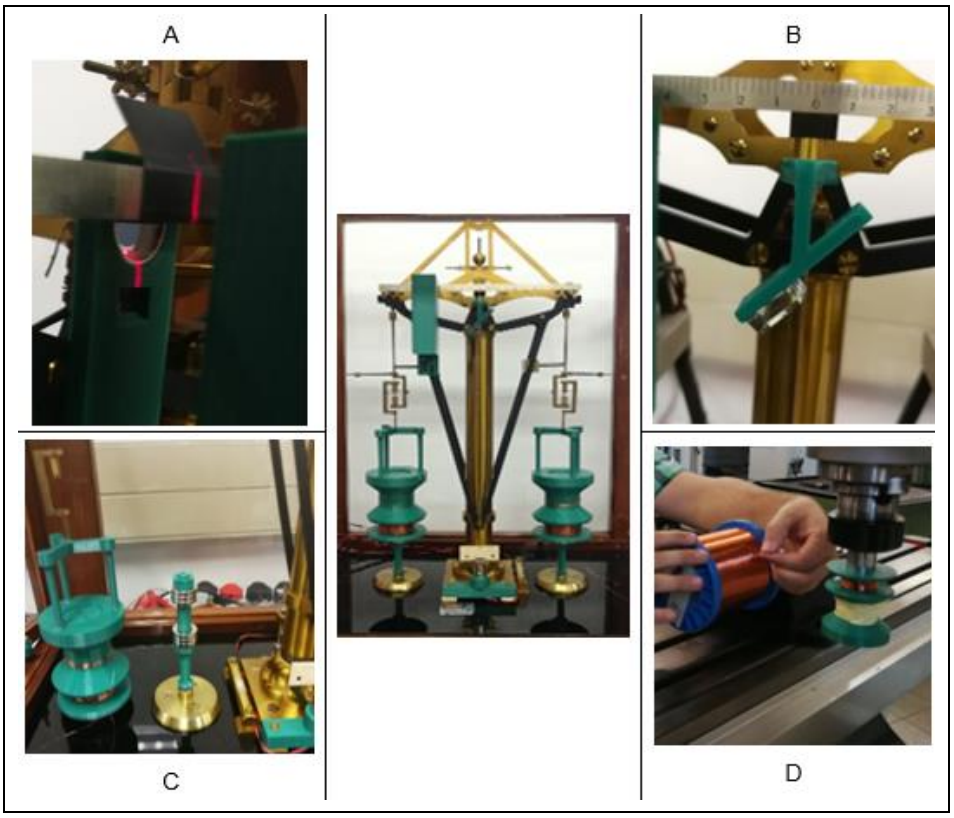

Figure 4.7: The precursor Kibble balance with main subcomponents being magnified. A. line laser & shadow sensor, B. small mirror fixed at 45° angle with respect to the balance arm, C. magnet system consisting of neodymium (N42 grade) ring magnets placed in repulsion, D. Coil winding using a speed lathe.

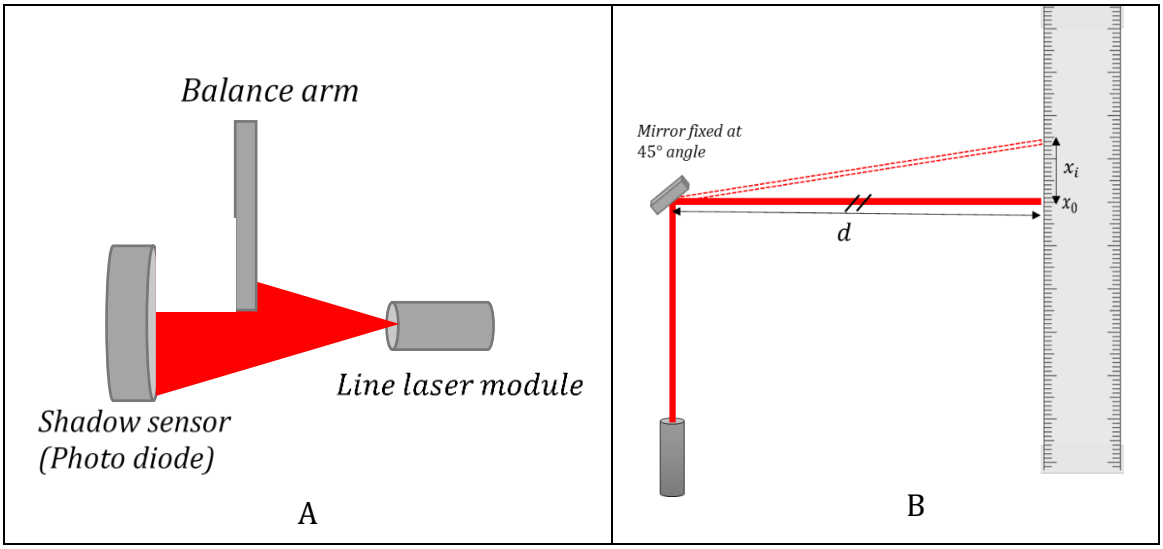

Figure 4.8: Calibration setup for monitoring coil position in the z-direction. (A) a schematic side view of Figure 4.7 A. (B) shows a schematic illustration of the use of the mirror in Figure 4.7 B.

4.2.2 **Coil and magnet assembly**

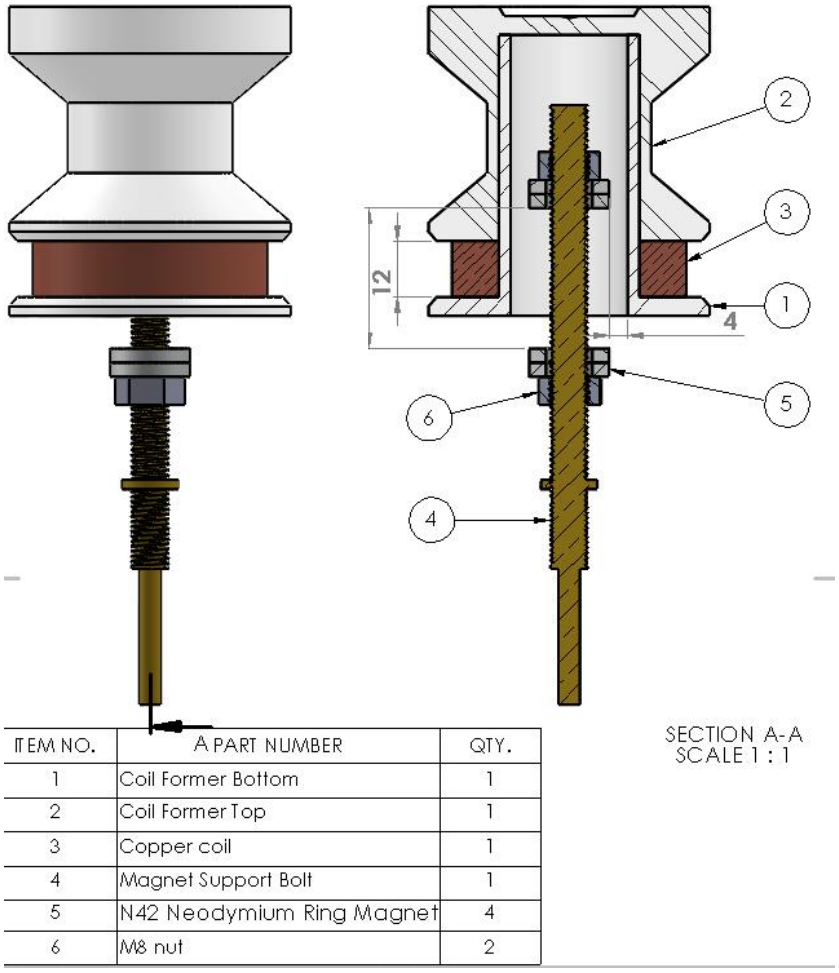

ITEM NO.	A PART NUMBER	QTY.
1	Coil Former Bottom	1
2	Coil Former Top	1
3	Copper coil	1
4	Magnet Support Bolt	1
5	N42 Neodymium Ring Magnet	4
6	M8 nut	2

Figure 4.9: CAD model of the coil and magnetic circuit assembly.

Figure 4.9 illustrates the CAD drawing of the coil and magnetic circuit assembly of the Kibble balance. The coil formers with an outer diameter of 60 mm and outer height of 80 mm were 3D printed using Ultimaker 2+ 3D printer in two parts and press-fitted. They were printed with holes (25 mm inner diameter and 75 mm inner height) that allow a threaded rod holding the magnets to fit inside. The threaded rods were fixed to a glass base plate aligned vertically in line with the suspend coil formers. About 4 mm all round clearance was left between the ring magnets and the inner walls of the coil to ensure that the ring magnets do rub against the inner walls of the coil former during velocity mode as this will affect the coil movement.

The magnetic system composed of neodymium (N42 grade) ring magnets was chosen to generate a radial uniform magnetic field. The magnets were stacked in pairs with 2 at the top and bottom. They were placed on a threaded rod orientated such that they repel each other. 3D printed nuts were mounted on both sides of the magnets, holding the magnets in place at a fixed separation distance thereby constraining the repulsive force between the magnets. Without the nuts, the top magnets would jump off the support rod. Both the nuts and support rod are having the same type of threading which makes it easier to adjust the separation distance between the magnets. The material used in the balance construction was chosen such that its non-magnetic so that the magnetic flux lines of the magnets are not disturbed.

The coil formers serve as both the weighing pan and a platform for winding the wire. A speed lathe in the mechanical workshop was used to manually wind the wire onto the formers (speed lathe set at 100 turns per minute) as shown in Figure 4.7 D. A 0.1 mm thick copper wire was used to wind about 3000 turns on each coil former. To get an approximate total number of turns, a timer was put in place and run for a duration of 30 minutes. Multiplying the timer duration by the speed lathe frequency, the total number of turns was obtained. The process was done for both coil formers, which lasted for about plus an hour provided that the wire does not break.

During the winding process, the layers of wire were frequently covered with power epoxy glue to avoid unwinding of the wire at the end. Winding more wire can increase the BL factor but also increases the resistance of the wire, this can limit the amount of current required in the force mode and also the current source has a limited supply. A resistance meter was then used to measure around the total resistance of the wire for both coils, which was found to be 650 Ω.

4.2.3 **Electronics and data acquisition**

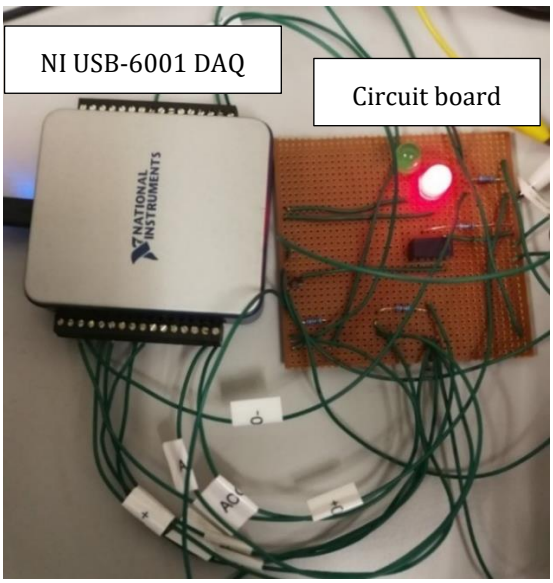

Figure 4.10: The NI USB-6001 DAQ from National instrument used to acquire data (*on the left*) and the circuit board (*on the right*) used to connect all the wires together. The name tags (in white) on the wires are for indicating the wire path. The LED lights also described as coil indicators are representatives of the coils, indicating the coil currently in use.

The low-cost NI multifunctional USB-6001 DAQ from National Instruments (see Figure 4.10) was employed for data acquisition as a replacement for the LABJACK U6 and Phidget 1002_0 used by NIST for the Lego balance described in [53]. It was used to obtain measurements from the Kibble balance, and it connects the balance with a laptop (for data analysis). The DAQ measures the induced voltage, position of the coil in volts from the photodiode and current flowing in the coils. The DAQ has about 8 single ended analogue input (AI) channels capable of measuring voltages between -10 V to +10 V (the analog input channels can also be differentiated into a configuration of four channels) and it has also two analogue output (AO) channels. The two analog output channels were used supply voltage signal to the coils when the system is operated in an automated mode using the software provided by NIST. When the balance is operated in an automated scheme, a control loop known as the proportional, integral and derivative (PID) is required to limit the magnitude of the required balancing signal. For this work, the measurement scheme was executed manually because the provided

software had a resolution of 2 digits of which was not satisfactory for this work as the balance showed capabilities of measuring beyond.

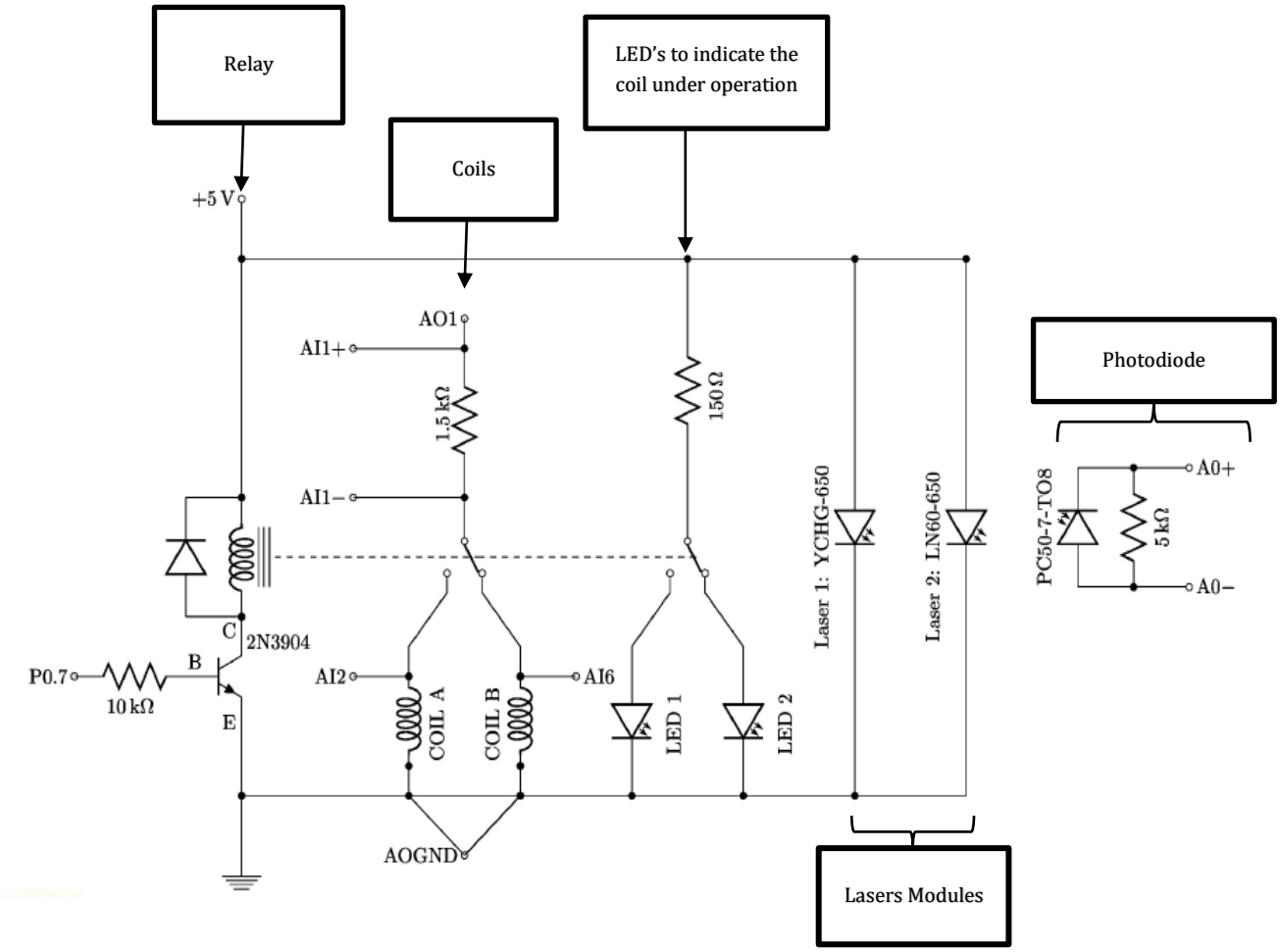

Figure 4.11: The precursor Kibble balance circuit [79].

Figure 4.11 shows the circuit connection of the Kibble balance system. The circuit on the right is for the photodiode. The photocurrent is generated by the photodiode when the laser light hit its detection surface (see Figure 4.8), where there is a current flowing through the 5 kΩ resistor. The voltage measurement is then determined using the voltage drop method. The measured voltage is proportional to the balance position (see section 4.3). The two laser modules and the two light emitting diodes (coil indicators) in Figure 4.10 are powered with 5 V. A 33600A waveform generator was connected to the AO1 channel when the system was operated manually, used to supply signal to the coils which can be manually adjusted with a knob on the front panel of the generator.

The generator has a bipolar output capable of generating voltages between -5 V and $+5$ V, with an output resolution of up to μV range. The fine output resolution is very useful when trying to put the balance beam at its exactly at original marked balancing position during the force or weighing mode. A 1.5 kΩ colour coded resistor was used to measure current flowing through the coil via the voltage drop method using voltage measurements from channel AI1 $+$ and AI1 $-$. A basic custom LabVIEW program was designed for the NI USB-6001, the program was used to gather the measurement from all the input channels into a text file with a time stamp of millisecond resolution.

4.3 Calibration of NI USB-6001 DAQ

The National Instrument USB-6001 data acquisition was used in this work for voltage measurements. The measurements include the shadow sensor readings for velocity measurements, the induced voltage and the voltage drop across a resistor for current measurements. It has been explained before that the NI USB-6001 has multiple channels capable of taking all these voltage measurements. The accuracy of the voltage measurements read by the DAQ has an influence on the final measurements performed with the balance. The NI USB-6001 has 14-bit analog to digital convertor resolution, that is $2^{14} = 16384$ parts. This implies that theoretically the DAQ has a resolution of 1 part in 16384 at 1 V scale. The NI USB-6001 DAQ has a maximum input voltage ± 10 V, it follows that the theoretical resolution of the DAQ at full range scale is given by $10/16384 = 6.1 \times 10^{-4}$ V. According to the manufacture's specification [80], the DAQ has an absolute accuracy of 6 mV typically at full scale (± 10 V range). This DAQ is a low-cost DAQ with no proper calibration data sheet provided for other voltage points.

The calibration of the NI USB-6001 was performed to get capabilities at other voltage points following the calibration procedure for multifunctional DAQs from the DCLF laboratory. The standards used for the DAQ calibration are the Fluke 5720A multifunction calibrator and Wavetek 1281 self-calibrator digital multimeter. These standards are traceable to the 732A/B Fluke reference standard that is in turn traceable to the Josephson primary voltage standard.

4.3.1 **Input channels calibration**

The Fluke 5720A multifunction calibrator was used to source voltages from 0 V to 10 V with known uncertainties from the calibration certificate of the calibrator. The output of the calibrator is connected directly to the input channel of the DAQ. This was done for all the 8 input channels at varying voltage points. The mathematical model of this calibration is given by:

$$V_{6001} = V_{5720A} \tag{4.1}$$

where V_{6001} is the voltage reading from the NI-USB 6001 DAQ and V_{5720A} is the output voltage from the 5720A multifunctional calibrator. The sources of uncertainty considered for this calibration process are: the 5720A accuracy, 5720A drift, 5720A resolution, 6001 resolution and repeatability of the DAQ readings by calculating the experimental standard deviation of the mean (ESDM) for at least five number of measurements.

4.3.2 **Output channels calibration**

For the output channels, the Wavetek 1281 self-calibrator digital multimeter was used as the calibration standard connected directly to the output channel of the DAQ. The voltages with nominal values in the range 0-10 V were sourced from the output channel of the DAQ and measured by the calibrated digital multimeter. The mathematical model of the calibration is given by:

$$V_{6001} = V_{1281} \tag{4.2}$$

where V_{6001} is the voltage sourced from the NI-USB 6001 DAQ and V_{1281} is the voltage reading displayed on the 1281 digital multimeter. The sources of uncertainty considered for this calibration process are: the 1281 accuracy, 1281 drift, 1281 resolution and repeatability of the displayed readings by calculating the ESDM for at least five number of measurements.

4.4 Shadow sensor calibration

NMISA's prototype Kibble balance operates in two modes i.e. force mode and velocity mode. Before performing any measurement with the balance, it needs to be aligned and calibrated. The calibration process is necessary to establish a relationship between the shadow sensor output voltage and the coil's z-directional displacement. This was done using the laser modules and shadow sensor illustrated in Figure 4.8 . The following steps were followed prior to the calibration phase:

- The balance was placed on a flat and level table surface at 4840 mm from the wall.
- The reflected point laser was shone upon the wall with the ruler attached (as shown in Figure 4.8 B), and distance d from the mirror (ideally the pivoting point) to the wall was measured.
- The balance beam was aligned on the support tower. The balance beam was checked that is fairly balanced and not leaned to one side without any masses on. This was done using spirit levels and the needle pointer attached perpendicular to the centre of the beam pointing the zero position when the balance is level.
- The inner holes of the suspended coil formers were aligned with the threaded rods carrying the magnets in such a way that the magnets are not touching the inner walls of the coil formers as this can cause friction and creating problems during the measurements.

After the above-described alignments, the balance was ready for calibration. In the calibration mode, the shadow sensor voltage readings (Vss_i) are calibrated with the coil's vertical positions, z_i. The zero position x_0 of the point laser was marked on the wall scale when the balance was at the horizontal position and its corresponding voltage read by the shadow sensor, Vss_0 was measured. The balance arm was then moved at various angles to distinct positions $\pm x_i$ (this was done by supplying the coil with constant dc voltages in steps). This caused the shadow sensor to read varying light intensities in terms of voltage (Vss_i) as the arm gradually obstruct the line laser light. The balance angle was determined by measuring

the position x_i on the wall scale and the distance d from the pivoting point to the wall scale as follows:

$$\theta_i = x_i/d. \tag{4.3}$$

The coil height z_i was determined by multiplying the angle by the distance from the pivoting point to the coil suspension point, known as an effective radius (r_{eff}), as follows:

$$z_i = r_{eff}\theta_i. \tag{4.4}$$

For the prototypes discussed in this study, the r_{eff} =175 mm (Lego), 135 mm (3D printed) and 80.50 mm (modified equal arm). This description is illustrated in Figure 4.8 and Figure 4.12. The calibration results are presented in section 5.1.

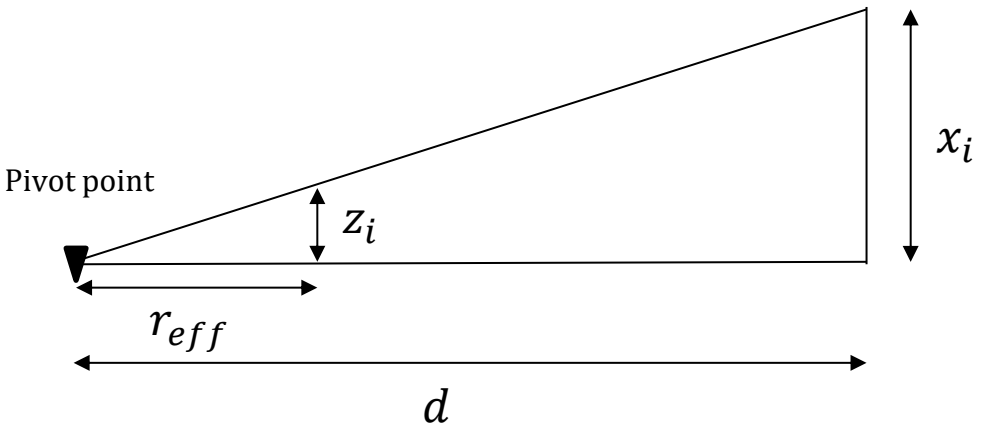

Figure 4.12: An illustration of length measurements required for the shadow sensor calibration. This is used to measure the coil's displacement.

4.5 Description of the mass measurement components

The measurement scheme is executed in two phases, the force mode and the velocity mode given by:

$$mg = BLI \text{ (force mode); and} \tag{4.5}$$

$$V = BLv \text{ (velocity mode).} \tag{4.6}$$

The measurement modes follow after the shadow sensor calibration has been completed, which also involve the alignment of the balance. The measurement modes are executed in quick succession back to back in the form of A-B-A sequence: force mode, velocity mode and force mode again. This sequence is performed such that the balance mechanic orientations changes are minimal, to minimise the time-dependent drifts that might be associated with the measurements.

According to the designs of the balance described in this study, the balance has two coils, coil A and coil B. Any of the coils can be used to perform measurements, but for consistency sake coil B is chosen as the measurement coil while coil A is used as the driver coil. The driver coil is used to drive the measurement coil in a sinusoidal motion. This is done by inserting an AC signal into the driver coil immersed in magnetic field gap and the interaction between the signal in the wire and the magnetic flux causes the coil to move in a sinusoidal motion. The velocity at which the coil is moving will induce voltage given by Eq. (4.6) in the measurement coil following Faraday's Law of Induction.

From rearranging Eq. (4.6), it follows that:

$$BL = \frac{V}{v}. \tag{4.7}$$

The measurement coil is immersed in the same magnetic field gap and has same the wire length or number of winding in both modes of operation. Based on these grounds, an assumption can be made that the BL factor is the same in both modes. This implies that the BL factor in Eq. (4.5) can be substituted with the ratio of the induced voltage over the velocity from Eq. (4.7). Making the substitution, the equation for the measurement after performing both modes is:

$$m = \frac{VI}{gv}. \tag{4.8}$$

4.5.1 **The force mode measurements**

In this mode, the measurement coil (coil B) is used to generate an electromagnetic force required to put the coil at the equilibrium/zero position. This electromagnetic force is generated by running current through a wire immersed in a magnetic field flux. The magnitude of the current was carefully adjusted manually using the function generator until the balance reaches its null position. In this phase, the electromagnetic force is generated to cancel the offset caused by the weight of the test mass. This is done by measuring the change in current required to keep the balance at the equilibrium position with the test mass on and off the weighing pan.

Figure 4.13 summarises the force mode operation, where the gravitational force exerted by a test mass is balanced out by the electromagnetic force. Initially, the balance structure mechanics is balanced such that the balance is at the null position without any mass on it. A relatively small to zero current in the micro ampere ($\pm$ μA) range is introduced to the coil in

order to eliminate the small balancing offsets due to the mechanic imbalances of the two arm sides.

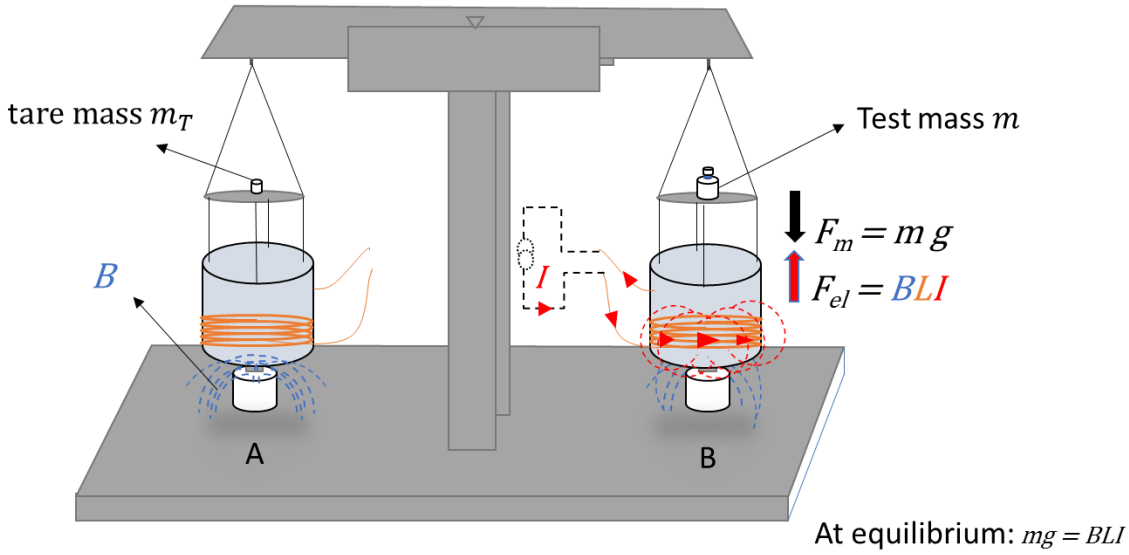

Figure 4.13: Schematic illustration of the weighing or force mode.

The mass measurements are performed in a typical sequence of mass ON and OFF, referring to loading and offloading of the test mass. A tare mass with a nominal value about half of the test mass is used to obtain approximately the same but opposite currents during the loading states. A tare mass is added on the pan of coil A and test mass is on to the measurement coil (coil B). For example, considering using a test mass of 4 g and a tare mass of 2 g. The 2 g tare mass is added above coil A and a current of approximately -1.4 mA is measured producing a downward electromagnetic force in the measurement coil, a test mass of 4 g is then added above the measurement coil and a current approximately $+1.4$ mA producing the upward electromagnetic force in the measurement coil. When the 4 g test mass is removed, a reverse current will be required to generate an opposite electromagnetic force.

The total current required to balance the 4 g test mass is equal to the difference of the two current values (i.e. $I = 2.8$ mA). This typical sequence is essential for removing the bias zero-point drift that may be due to lack of balance stability [81]. This is because at the zero position with all the masses off, the force keeping the balance steady is very low compared to when there is a mass on. In this mode the current I and the gravitational acceleration g are the only

evaluated parameters, because the BL product substituted by the ratio of the induced voltage over the velocity.

a) Test mass samples

The measurements discussed in this study were performed with stainless steel mass standards ranging from nominal values 0.2 g to 4 g. These masses were even taken to the mass laboratory at NMISA for calibration to establish a traceability to the prototype No. 56 of the kilogram (the South African national standard for mass) that is in turn traceable to the IPK (the current primary mass reference standard), the calibration certificate is shown in Appendix C. Figure 4.14 show the test masses used for the precursor Kibble balance measurements.

Figure 4.14: Stainless steel test masses used for the Kibble balance measurements.

b) Current Measurements

The voltage drop method is employed to measure current I generating the balancing electromagnetic force. A dc voltage is passed through the 1.5 kΩ colour coded resistor connected in series with the measurement coil there by resulting in a voltage drop across the resistor terminals. The current is given by ratio of the voltage drop over the resistance value of the resistor (Ohm's Law). The voltage drop is measured with the input channel of the NI USB-6001. The measured voltage values are then divided by the measured resistor value of the nominal resistor 1.5 kΩ. The resistance is measured with the HP 3458A digital multimeter. The current is manually adjusted, while the equilibrium position or zero position of the coil is

checked with a laser system. The source has the capability to deliver dc voltages between -5 V and +5 V with a microvolt output resolution.

c) Absolute gravitational acceleration measurements

Before executing measurements with the Kibble balance, the absolute gravitational acceleration g in the lab where the measurements will take place needs to be measured. This g is the local gravitational acceleration in the lab were the Kibble balance is located. The service from Council for Geosciences (CGS) was utilised in December 1999 to measure the local gravitational acceleration g were the precursor Kibble balance was constructed. Although this mapping date might appear dated, the data was compared with the recent data mapped in a laboratory in Building 5 opposite to Building 7 (see the map in Appendix A), the results are presented in Chapter 6.

The g mapping in the lab was performed using three relative gravimeters (micro-g LaCoste and Romberg gravimeters) through a tie procedure as explained by Morelli et al in [76]. The relative gravimeters were calibrated to correspond with the known difference in absolute gravity between the Pretoria and the Paarl (Cape Town) stations. The reason that three gravimeters were used is that should a tear occur to one, the other two could still be used to calculate the base value. The mapping results were tied to the national gravity base station network through the main base SIL1 at the CGS building in Silverton which is in turn linked to the international base station located at the underground seismic monitoring station at the National Botanical Gardens in Pretoria.

4.5.2 Velocity mode measurements

The velocity mode is used to determine and characterise the balance's electromagnetic properties, $(BL)_{vel}$. During this mode, a sinusoidal signal is input into coil A driving the balance in a sinusoidal motion and the output position of the measurement coil B was measured by the line laser and the shadow sensor technique described in section 4.3. The driving signal leads to the measurement coil moving vertically up and down in a sinusoidal motion at a velocity v

on a 2-3 mm range interval. This movement resulted in a voltage V being induced in the millivolts range scale at the terminals of the measurement coil.

The ratio of measured quantities induced voltage V and the velocity v gives the characteristic of the electromagnetic properties of the measurement coil, $(BL)_v$. Figure 4.15 gives a summarised schematic illustration of the velocity mode. The procedure of measuring the velocity and induced voltage measurements is described below.

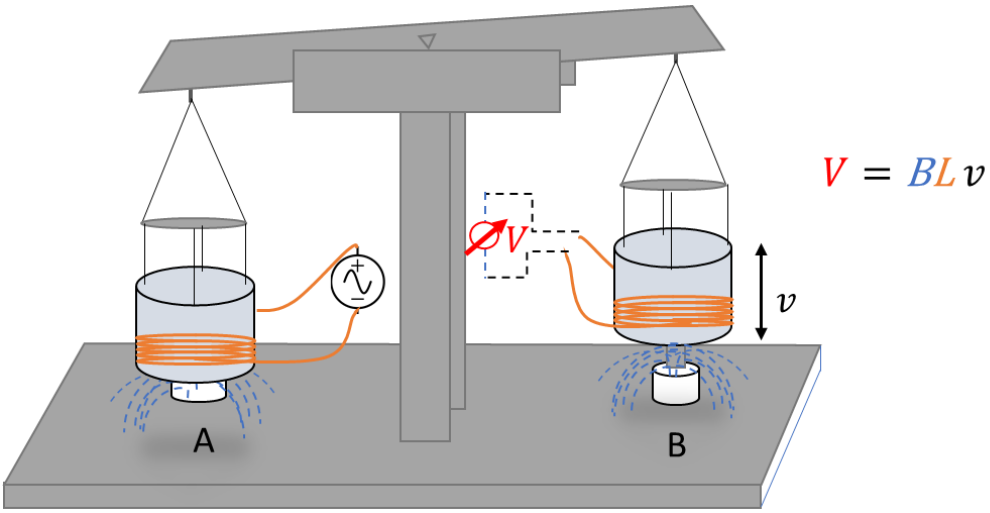

Figure 4.15: Schematic illustration of the moving or velocity mode.

a) Velocity measurements

An AC signal was sourced from the 3300A waveform generator into the driver coil (coil A). This signal resulted in the measurement coil moving up and down along the z-direction. The signal was adjusted such that the coil moves symmetrically with respect to the balancing position and also that the inner wall of measurement coil doesn't rub against the surface of the magnets. The velocity of the measurement coil is characterised by the coil's displacement and the time interval it takes to cover the displacement. The coil's displacement is measured using the shadow sensor technique, of which the output a voltage signal is proportional to the height of the coil. The data were acquired with the NI USB-6001 at a sampling rate of $\Delta t = 100$ ms. The velocity was then calculated as the numerical derivative of the sampled data from the shadow sensor output.

b) Induced voltage measurements

The voltage V is induced in the wire as a result of the rate at which the conductor (wire) cuts the magnetic flux. The induced voltage is thus dependent of the coil's velocity. The induced voltage was also measured with one of the NI USB-6001 input channels at the same sampling rate as of the velocity measurements. Now since the induced voltage depends on the velocity, the sampling rate from a computer time stamp was used to synchronise/ simultaneously record the results from the two signals to get ratio pairs of the induced voltage over the velocity. This is necessary because as the coil moves in a sinusoidal motion the velocity changes and so does the induced voltage. The signals are measured with the input channels of the NI USB-6001 data acquisition card and stored into a text file using a LabVIEW program.

4.6 Determining h from a known mass m

As stated before in section 2.3 from the general principle of the Kibble balance, when the quantum electrical standards (i.e. the quantum hall resistance standard for resistance measurements and Josephson voltage standard for voltage measurements) are used directly in the Kibble balance, the Planck's constant h can be measured accurately using a known mass m traceable to the IPK through the following formula:

$$h = \frac{4}{Cff'} mgv. \tag{4.9}$$

For the prototype discussed in this study, the quantum electrical standards were not used. Although these standards were not available to this project, the measurement of h could still be achievable due to the way the current SI system is structured and using apparatus that can perform measurements traceable to these high accuracy standards. The measurement of Planck constant h was determined from the fixed conventional values for electrical quantities,

namely Josephson constant, $K_{\mathrm{J}-90}$, and von Klitzing constant, $R_{\mathrm{K}-90}$. This was done by comparing the electrical power VI (using the conventional units) to the mechanical power mgv (using the current SI units). We have from Eq. (2.7):

$$VI = mgv \quad \Rightarrow \quad \{VI\}_{90} = \{mgv\}_{SI} \tag{4.10}$$

where the symbols $\{x\}_{90}$ and $\{x\}_{SI}$ are the respective numerical values due to the 1990 fixed conventional units and the current SI units, and x denotes their quantity values. From Eq. (4.10), it can be seen that the electrical power and the mechanical power are equal, this implies that their ratio is nominally equal to one. Therefore

$$\frac{\{mgv\}_{SI}}{\{VI\}_{90}} = 1. \tag{4.11}$$

Equation (4.11) can be re-written as:

$$1 = \frac{h}{h_{90}} \tag{4.12}$$

where h is the Planck's constant that can be determined with the Kibble balance and h_{90} is the Planck's constant obtained from the numerical values of the 1990 fixed conventional values of Josephson constant, $K_{\mathrm{J}-90}$, and von Klitzing constant, $R_{\mathrm{K}-90}$ as:

$$h_{90} = \frac{4}{K_{J-90}^2 R_{K-90}} \tag{4.13}$$

$$= 6.626\ 068\ 854\ 361 \ldots \times 10^{-34}\ \mathrm{J\ s}.$$

From the two modes of Kibble balance operation (i.e. force mode and velocity) we have

$$(BL)_{frc} = \frac{mg}{I} \text{ and } (BL)_v = \frac{V}{v}. \tag{4.14}$$

Substituting Eq. (4.12) and (4.14) into Eq. (4.11), we get that the ratio of the Planck constant measured using the Kibble balance, h and the Planck constant value due to the 1990 fixed convectional values h_{90} is equal to the ratio of the measurable values of BL factor in the force and velocity modes as:

$$\frac{h}{h_{90}} = \frac{(BL)_{frc}}{(BL)_v}; \text{and} \tag{4.15}$$

$$h = h_{90}\frac{(BL)_{frc}}{(BL)_v}. \tag{4.16}$$

The $(BL)_{frc}$ is a function of mass m, current I and the local gravitational acceleration g, were the mass m is the known mass m with an established traceability to the IPK. The $(BL)_v$ measurement is given by the ratio of the induced voltage over the velocity which is performed similarly to the method when measuring mass.

5. Experimental results

5.1 Shadow sensor calibration results

The calibration process was performed to establish a link between the coil height measurements (mm) from the ruler scale with the shadow sensor voltage readings (mV) following the procedure described in section 4.3. From the calibration process it was found that the coil height z_i is directly proportional to the shadow sensor voltage within a reasonable range. The coil height position was then determined as a linear function of the shadow sensor voltage as follows:

$$z_i(Vss_i) = C(Vss_i - Vss_0) \tag{5.1}$$

where z_i is the coil height of a sample number i depending on the shadow sensor voltage Vss_i, Vss_0 is the shadow sensor reading at zero position which is also considered as the position where the balancing position and C is the calibration conversion factor that converts the shadow sensor voltage readings to coil height position or the other way round. The conversion factor was deduced from the best fit line of the calibration data (z_i, Vss_i) shown in Figure 5.1. The best fitted line was generated using the method of least squares fitting. The conversion factor is given by the following formula:

$$C = \frac{x_i}{Vss_i}\left(\frac{r_{eff}}{d}\right) \tag{5.2}$$

$$= 2.997 \times 10^{-2} \pm 1.6 \times 10^{-4}\ \mathrm{m\,V^{-1}}$$

where x_i represents the wall scale positions during the calibration process and Vss_i denotes the corresponding shadow sensor voltages. The data presented by Figure 5.1 were generated as follows: the balance was moved to 9 distinct positions in steps of 20 mm on the wall scale (4 points in both negative and positive directions of the marked zero or balancing position) and the corresponding shadow sensor voltages were measured. The wall scale was read with an uncertainty of 0.5 mm, shown in Figure 5.1 as the residuals between the best fit line and measurement data points.

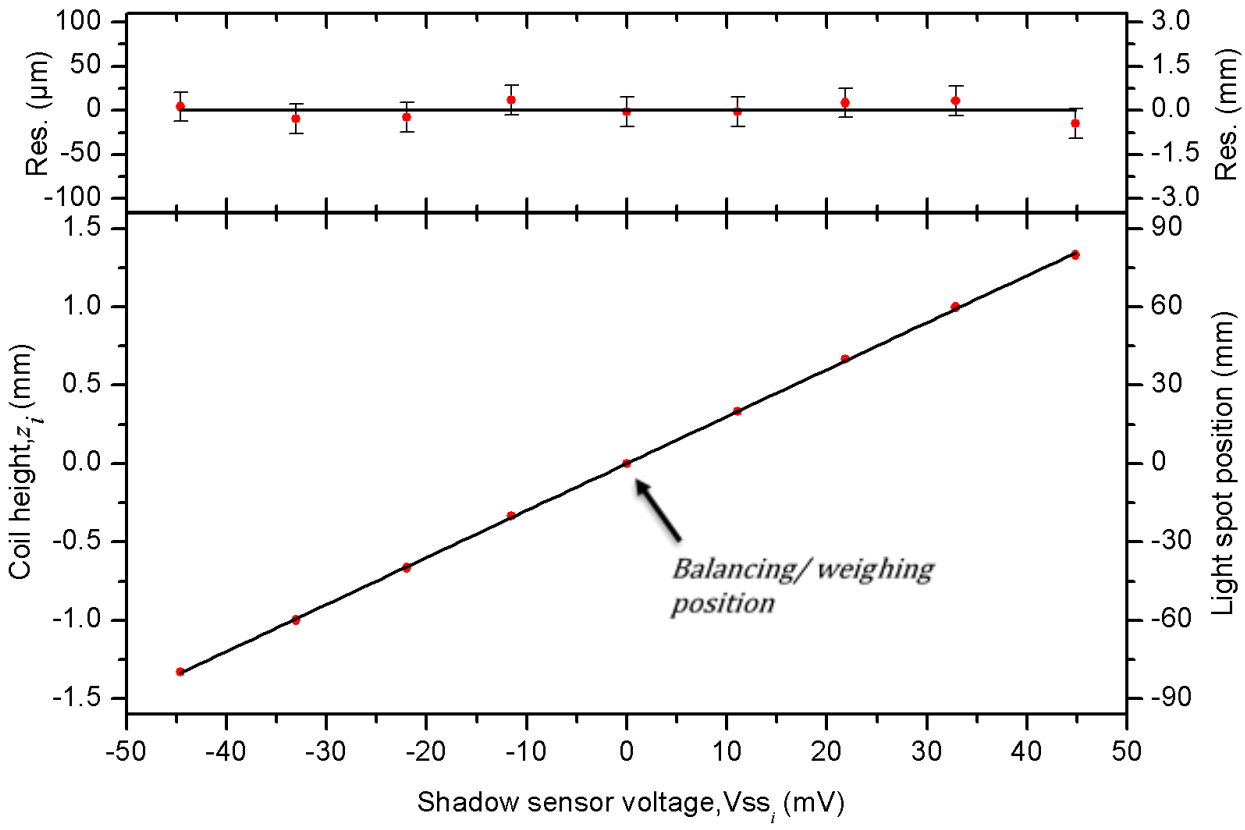

Figure 5.1: Shadow sensor calibration. The bottom graph shows a linear relationship between the light spot position on the wall, the coil height and the output shadow sensor voltage readings. The residuals between the data points and the best fit line are shown by the top graph, with the measurement uncertainty of the light spot position on the wall scale.

5.2 Sub-components result

The general equation for measuring mass using the Kibble balance is given as:

$$m = \frac{VI}{\mathrm{g}v} \tag{5.3}$$

where the test mass m measurements depends on the force mode measurements (current measurements and gravitational acceleration measurements) and the velocity mode measurements (induced voltage and velocity measurements).

5.2.1 Current measurements

The current measurements results were determined via the voltage drop method, given by the ratio of the voltage drop across a resister over the resistance value of the colour coded resistor. The resistance was measured using the 3458A digital multimeter found to be $1508.7 \pm 1.3\ \Omega$. Figure 5.2 shows a sequence of the balancing current measurements running in the coil during the weighing mode for 1-4 g test masses. Initially the balance pans are empty and the balancing current running in the coil is small, $< 1.0 \times 10^{-4}$ mA, and this is represented by the (0-0g) load state. The following sequence then follows (also see Figure 5.2):

- A tare mass about half of the test mass ($m_T \approx \frac{1}{2}m$) is added above coil A and the balance leans to the heavy side. A reverse current I_1 ($-$mA) is required in the measurement coil B to restore the balancing position and this is represented by the mass OFF (0-m_T) load state.
- The test mass m is added above the measurement coil (coil B) and a positive current I_2 ($+$mA) is run through the coil to restore the balancing position. This position is represented by the mass ON (m-m_T) load state.
- The tare mass is kept ON while a sequence of loading and offloading the test mass continues, until a satisfactory number of readings is gathered. The magnitude of the

tare mass in not included when making calculations. It represents the stable reference point.

- The current I required to restore the balance position with the mass the test mass ON is given by:

$$I = I^{ON} - I^{OFF} \tag{5.4}$$

where I^{ON} denotes the balancing current reading in the measurement coil with the test mass m ON and I^{OFF} denotes the balancing current reading in the measurement coil with the test mass OFF, only the tare mass remaining.

- About 20 current readings were taken on each load state.
- To improve accuracy and to cancel the measurement drift, additional weighings were performed, and the results were averaged.
- The plots in Figure 5.2 shows about 9 load states, we neglect the two zero load states, they are only necessary to check if finally, the balance is in the same alignment state as it was initially.
- The positive currents of the 3 mass ON load states are represented by (I_2, I_4, I_6) and the negative currents of the 4 mass OFF load states are represented by (I_1, I_3, I_5, I_7), so it follows that the total current is given by:

$$I = \frac{1}{3}(I_2 + I_4 + I_6) - \frac{1}{4}(I_1 + I_3 + I_5 + I_7). \tag{5.5}$$

- This is the total magnitude of the current I required to generate the electromagnetic force balancing out the gravitational force by the test mass m.

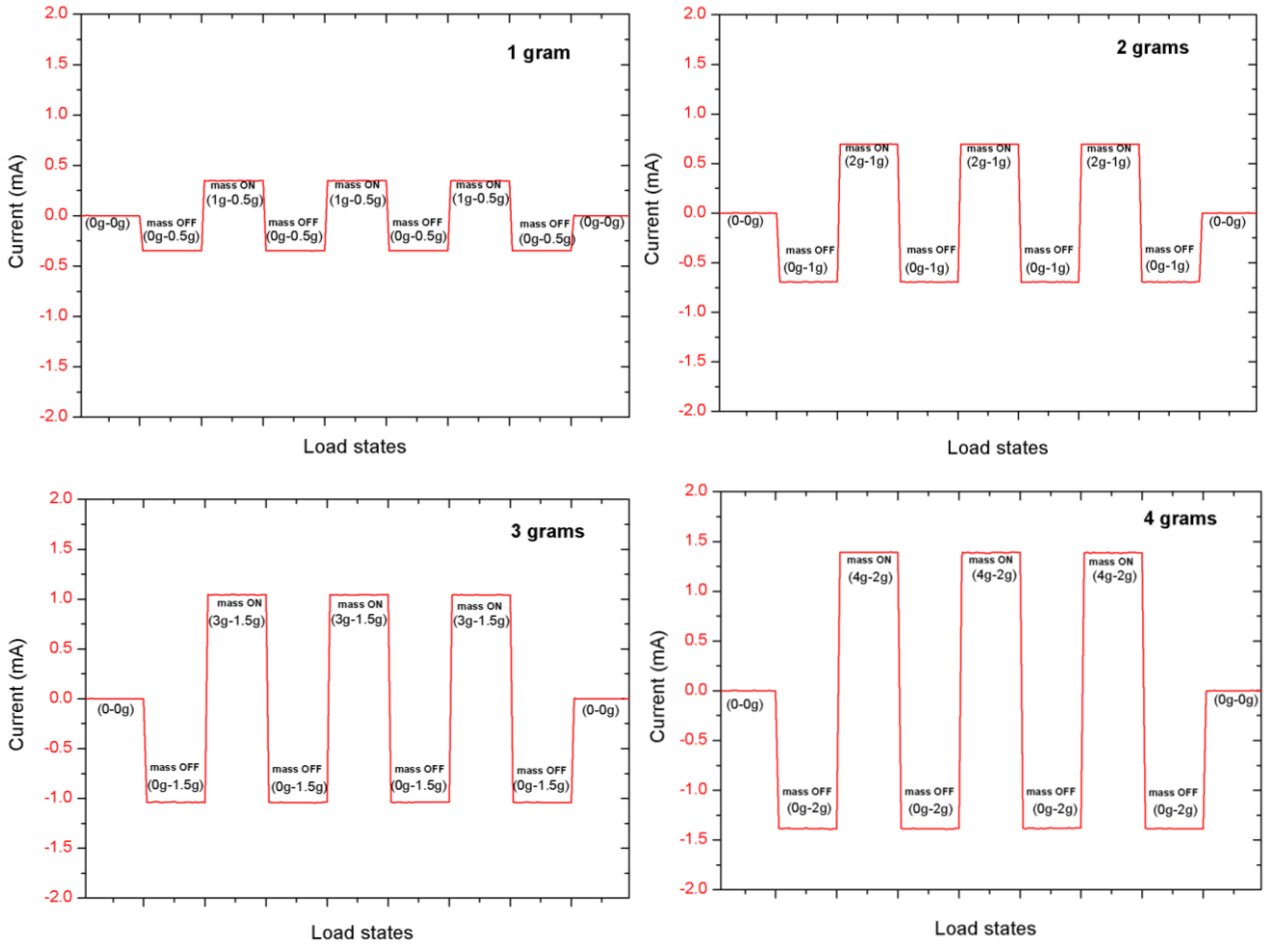

Figure 5.2: The balancing current I measurements running in the coil during the weighing sequence for 1-4 g test masses. The "mass off" denotes the reverse balancing current in the coil when the test mass is taken off and the “mass on” denotes the balancing current with the test mass on.

Figure 5.3 shows a summary of the weighing sequence for four tests masses with nominal values 1 g, 2 g, 3 g and 4 g. The sequence illustrates the loading and offloading of the test masses, with about 20 samples taken for each load state. From a comparison of all the plots, it can be observed that the higher the size of the test mass m on the weighing pan, the more current required to generate an electromagnetic force balancing the weight or gravitational force exerted by the test mass m. Table 5.1 shows the nominal values of the test masses that can be weighed with the precursor Kibble balance and the corresponding currents required to generate an appropriate balancing electromagnetic force.

The linearity of the system was investigated to quantify the accuracy of the balance throughout the capable weighing range, see Figure 5.4. The graph shows a perfect linearity. This was assessed by directly plotting the mass readings from the balance presented in Table 5.3 against the total current required to maintain balance presented in Table 5.1.

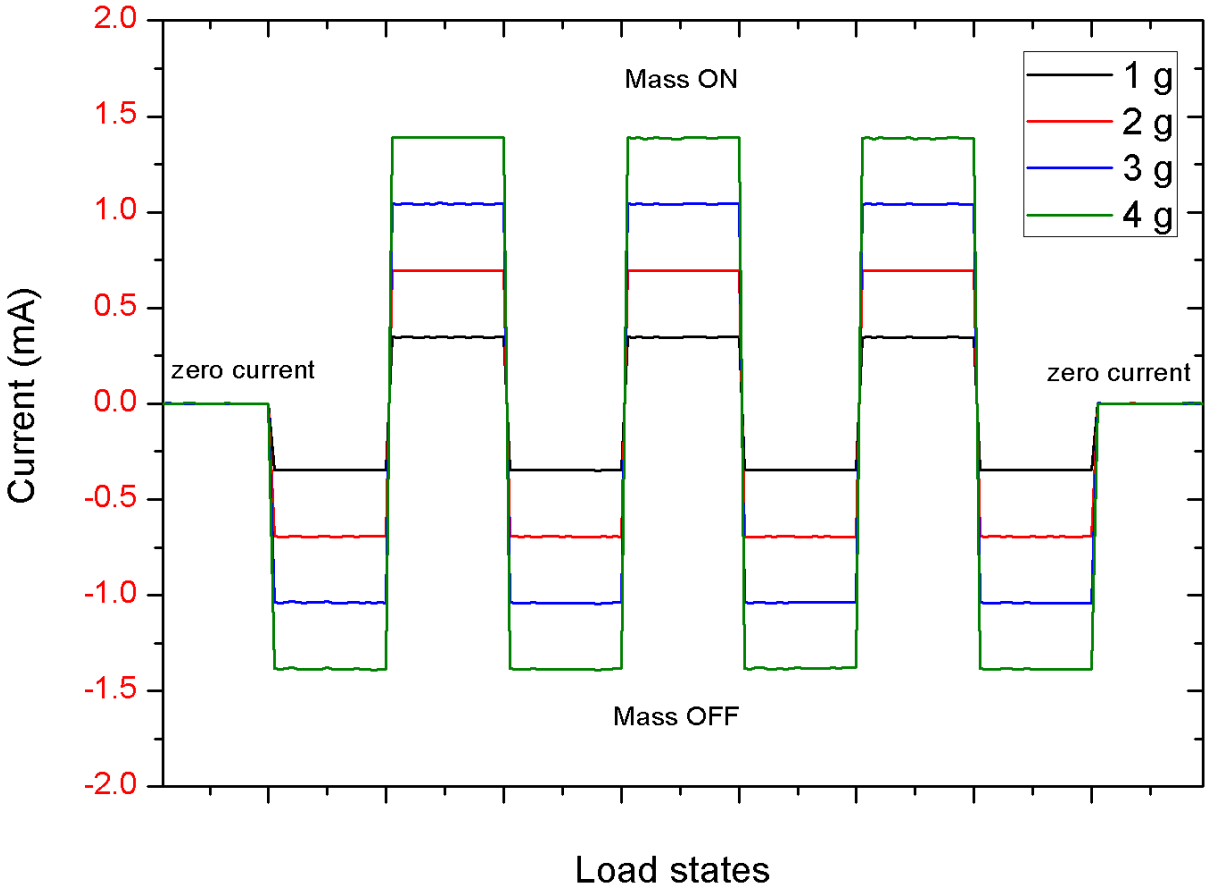

Figure 5.3: A summary of the weighing sequences for all the four test masses.

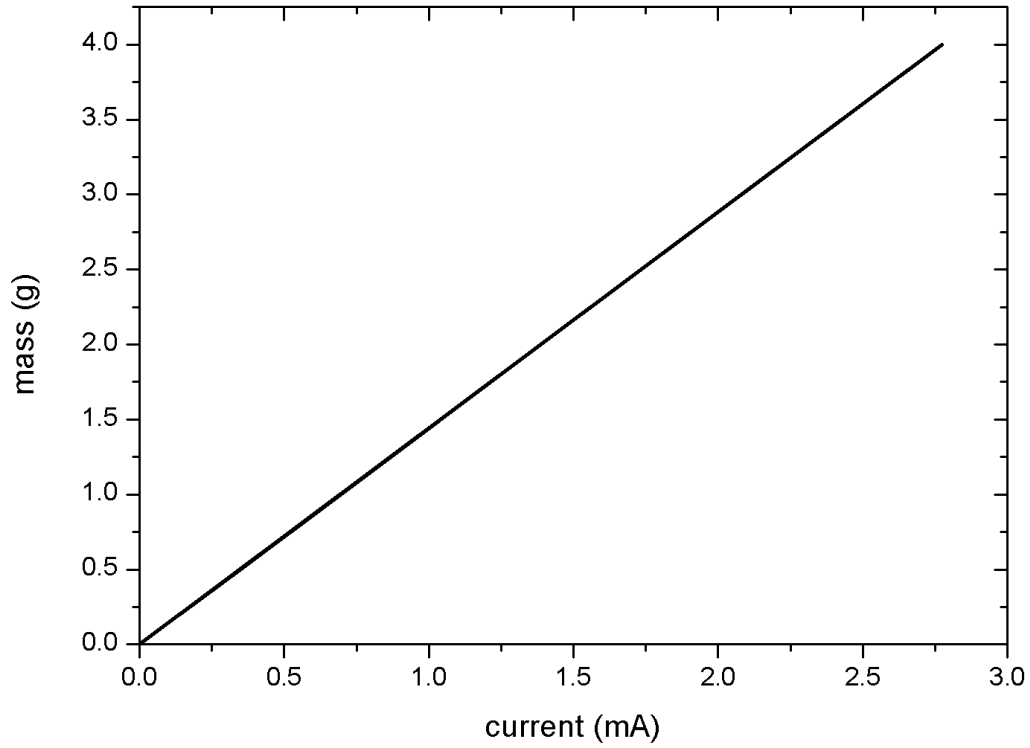

Figure 5.4: The linearity of the balance as a result of the direct proportion between the mass readings and the current used to maintain balance.

Table 5.1: Nominal values of the test masses and the current measurement values required to generate the electromagnetic force balancing the weight of the test mass.

Nominal values of the test mass, $\boldsymbol{m}$ (g)	*Current,* $\boldsymbol{I}$ (mA)		
	I^{OFF} $\frac{1}{4}(I_1 + I_3 + I_5 + I_7)$	I^{ON} $\frac{1}{3}(I_2 + I_4 + I_6)$	I $I = I^{ON} - I^{OFF}$
0.2	-0.069	0.069	$\mathbf{0.139}$
0.3	-0.104	0.104	$\mathbf{0.208}$
0.5	-0.173	0.173	$\mathbf{0.347}$
1	-0.347	0.347	$\mathbf{0.694}$
2	-0.693	0.693	$\mathbf{1.386}$
3	-1.041	1.040	$\mathbf{2.081}$
4	-1.387	1.386	$\mathbf{2.773}$

5.2.2 **Velocity and induced voltage measurements**

The measurement coil was allowed to move on a 2-3 mm interval in a sinusoidal motion. The velocity v was determined as a result of a numerical derivative of the measurement coil's position extracted from the voltage measured by the shadow sensor. The derivative was applied as follows:

$$v(i\Delta t) = \frac{z\big((i\ +1)\Delta t\big) - z((i-1)\Delta t)}{2\Delta t} \tag{5.6}$$

where $z(i\Delta t)$ is the coil position of the sample number i extracted from the shadow sensor voltage read out $V\text{ss}\,(i\Delta t)$ after some time interval Δt (sampling rate). The formula of converting the position from shadow sensor voltages to millimetre scale is given by eq. (5.1). The time interval was taken from a computer time stamp. The DAQ was sampled at Δt = 100 ms to simultaneously measure the coils position and the induced voltage measurements. A sinusoidal motion with a period of 1.7 s for about 1-1.5 mm displacement showed stable results. This movement induced voltage in the measurement coil (mV range) and the voltage was measured from the coil terminals by the NI USB-6001 DAQ.

The induced voltage and the corresponding velocity measurement were synchronised resulting in pairs of the induced voltages and velocities. It is necessary to synchronise measurements of the two parameters because the induced voltage depends on the coil velocity. The result of this synchronisation is shown by Figure 5.5, showing the measurements of the induced voltages against the velocity for one period of the sinusoidal motion. A single trajectory (1 period) is described by 17 pairs for a duration of 1.7 s. A best fitted line was generated and the slope BL_v was determined. The movement lasted for about 180 s which is about 106 up and down trajectories described by 1800 data points. The results for the duration of 180 s are shown in Figure 5.6, where a best fitted line averaging all the 106 trajectories was determined and found to be, $BL_v = 14.116\ \text{V s m}^{-1}$. Figure 5.5 shows the slope for one period and the second figure shows the average slope value from 106 periods. The repeatability uncertainty of this measurement is presented in Chapter 6.

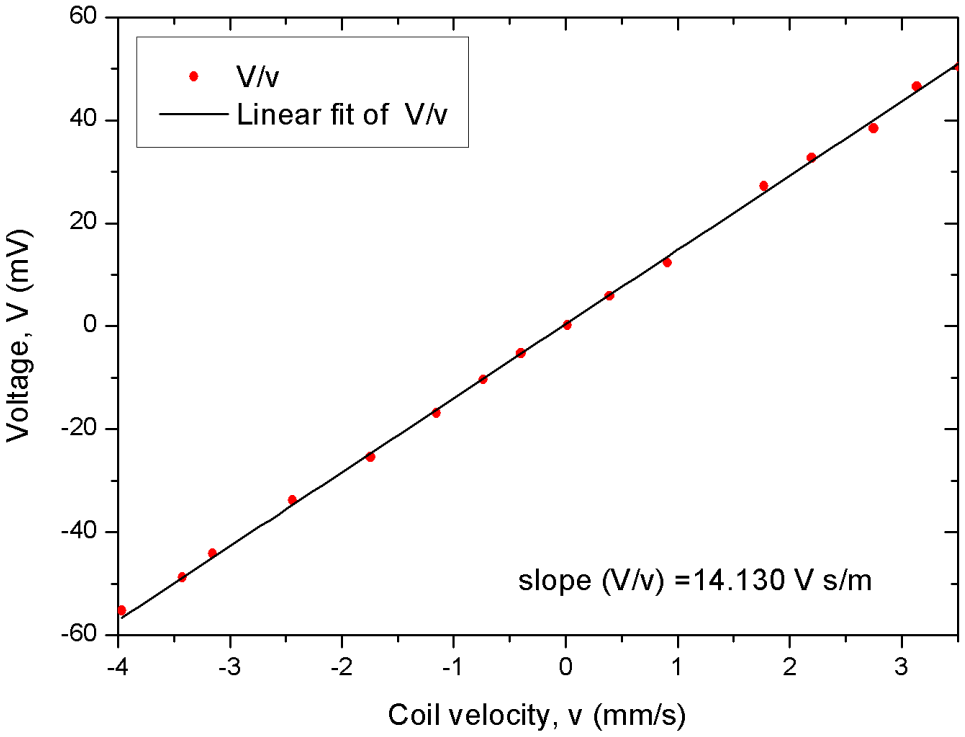

Figure 5.5: The generated voltage measurements and the corresponding velocities of the measurement coil for a period of up and down motion (1.7 s).

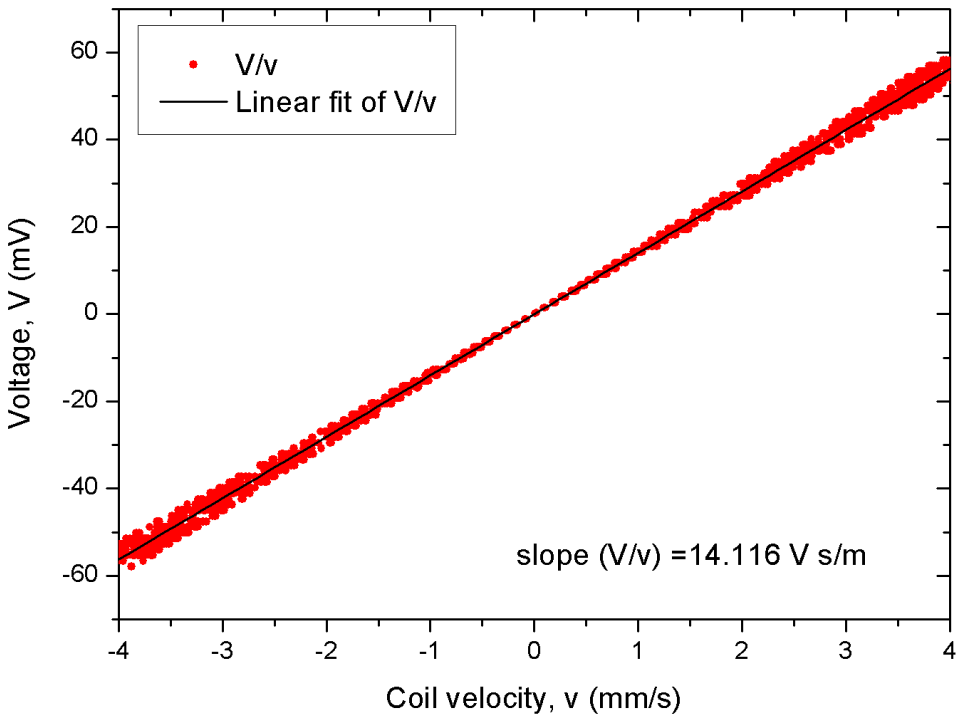

Figure 5.6: Pairs of the induced voltages and the corresponding velocities for a duration of 180 s.

Figure 5.7 shows 106 BL_v determinations from a sequence of up and down trajectories that lasted for about 180 s in total. The value of the ratio of the induced voltage over the velocity $(BL)_v$ was determined as the mean average value of these 106 data points with a relative standard deviation of about 0.12 %. Each data point denotes the slope of one period or one trajectory. The drift was expected in the $(BL)_v$ data points due to the temperature coefficient of the Neodymium NdFeB magnets which is about -1.0×10^{-3} K^{-1} and also because of the measurement coil not moving along the same path for all the trajectories.

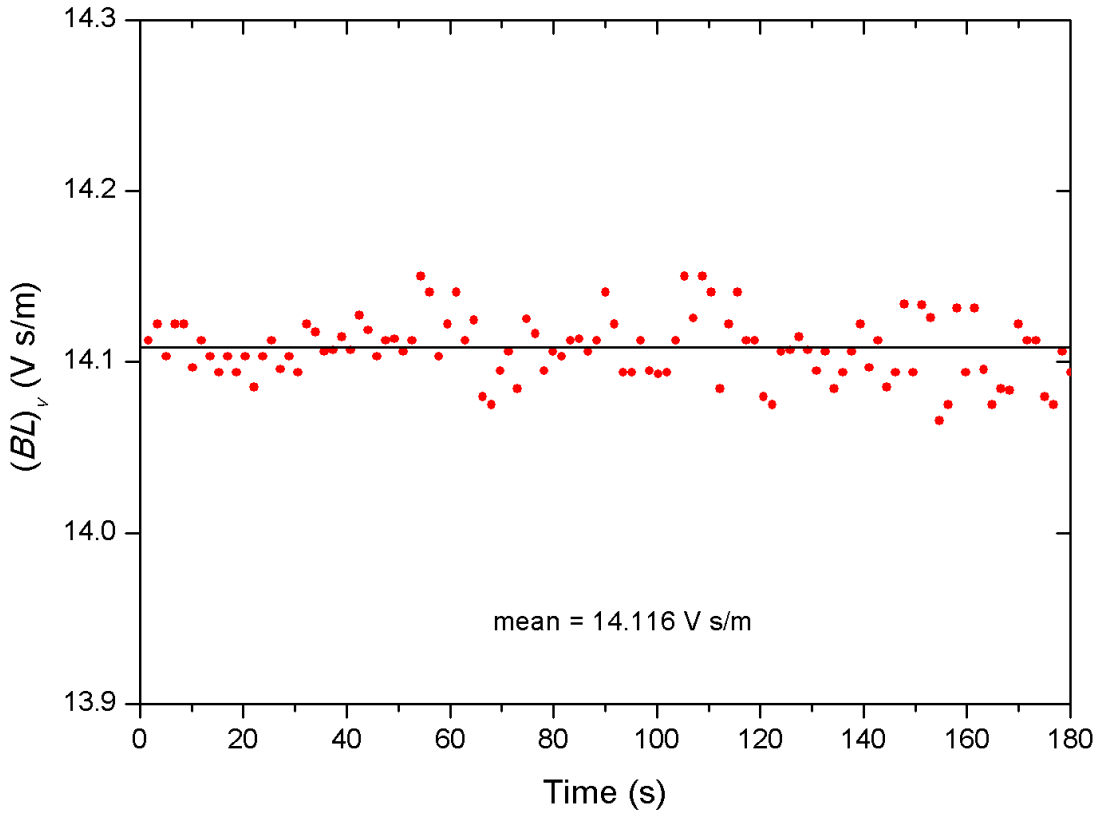

Figure 5.7: BL_v determinations for a sequence of about 106 trajectories for a total of 180 s. The horizontal line is the best fit line giving an average value of the $BL_v = V/v$.

5.2.3 **Gravitational acceleration measurements**

The gravitational acceleration g mapping was performed in the lab prior to this work, where three relative gravimeters were used to perform the mapping. As explained in section 4.5, a tie procedure was used to link the measurement at site (Kibble balance lab) with the absolute measurement at the base station. At least five readings were taken with each gravimeter at the base station SIL 1, with a time span of 15 minutes between the readings to establish a drift curve for the instruments. The same procedure was duplicated in the lab at NMISA. On return to the base station SIL 1 another set of readings were taken to establish the total drift and whether a tear had occurred.

The gravimeter readings are reduced to gravitational attraction g by correcting for the atmospheric pressure, polar motion, instrument drift and earth-tide effects. After the removal of the earth-tide effects, the drift was considered to be linear as a function of time. Since the gravimeters cannot measure absolute g but only the difference in absolute g between two localities, the difference in absolute g between SIL 1 and NMISA station is added to SIL 1 to provide absolute g (after all the corrections were applied). The measurements were performed at NMISA Building 7 CSIR campus in December 1999 [82] and again at Building 5 in February 2012 [83].

Table 5.2: The g values measured at CSIR campus Building 7 and Building 5 in the years 1999 and 2012 respectively.

g **in Building 7 (1999)**	g **in Building 5 (2012)**
9.7860985 ± 0.0000005 m s^{-2}	9.7860970 ± 0.0000005 m s^{-2}

Table 5.2 shows the two values of absolute g measured at the CSIR campus Building 5 and 7 in different years (about 12 years difference). From a comparison it was found that the two values agree within the difference of order 1.5×10^{-7}. This shows that the g value around Building 7 and building 5 has remained constant within the first 5 digits. This level of accuracy was found to be satisfactory for this precursor work.

5.3 Measurement comparisons

The magnitude test masses with nominal values ranging from 0.2 g to 4 g were measured with all the prototypes constructed for this study. The test masses were then taken to the mass laboratory at NMISA for calibration. The calibration certificate was issued and is shown in Appendix C. Table 5.3 shows a comparison between the calibration values of the test masses from a certificate and the measurement determined with all the three precursor Kibble balances.

The reported measurement uncertainties were calculated according to the ISO-recommended framework, reported at 95 % confidence level ($k = 2$) (see chapter 6 for more information). The Lego Kibble balance and the 3D printed Kibble balance reported less than 5 % relative uncertainties and the final modified equal arm Kibble balance reported ≤ 0.5 % relative uncertainty. The results from all the prototypes were found to be comparable with the results from the calibration certificate of the test masses.

Table 5.3: Comparison of the calibrated masses and the readings from all the prototypes.

Nominal Mass (g)	**Calibration value (g)**	**Lego WB (g)**	**3D printed WB (g)**	**Modified equal arm WB (g)**
0.2	0.20001 ± 0.00002	0.21 ± 0.02	0.22 ± 0.03	0.201 ± 0.001
0.5	0.50001 ± 0.00003	0.50 ± 0.03	0.51 ± 0.04	0.500 ± 0.003
1	0.99994 ± 0.00003	1.01 ± 0.03	0.99 ± 0.05	0.999 ± 0.005
2	2.00011 ± 0.00004	2.01 ± 0.05	2.00 ± 0.07	2.001 ± 0.008
3	3.00008 ± 0.00005	3.00 ± 0.05	3.01 ± 0.07	3.002 ± 0.009
4	4.00007 ± 0.00006	4.02 ± 0.07	4.00 ± 0.09	4.000 ± 0.010

5.4 Planck's constant measurements

From measurement method given in subsection 4.6, the equation for measuring the Planck constant with the Kibble balance is given as:

$$h = h_{90}\frac{(BL)_{frc}}{(BL)_v}; \tag{5.7}$$

$$(BL)_v = \frac{V}{v}; \text{and} \tag{5.8}$$

$$(BL)_{frc} = \frac{mg}{I} \tag{5.9}$$

where $h_{90} = 6.626\ 068\ 85 \ldots . \times 10^{-34}$ J s is known through the conventional constants, K_{J-90} and R_{K-90}, $(BL)_{frc}$ and $(BL)_v$ represents the unknown BL factor that can be measured from the force mode and velocity mode respectively. The $(BL)_{frc}$ is determined in the force mode using Eq. (5.9) when the true value of the test mass m is known from a calibration report. The $(BL)_v$ is given by the ratio of the induced voltage over the velocity of the measurement coil in an analogous way it was determined for mass measurements.

Theoretically, the ratio of the two BL factors should equate to 1, because the coil and magnetic properties are assumed to the same in both modes. The experimental measurements have shown that the BL value vary slightly, in which is mainly caused by the coil movement in the velocity mode measurements. During the velocity mode it is expected that the measurement coil moves exactly vertical along the z- direction and the horizontal x-y direction be 0, but the observed coil movements have shown that there some horizontal movements along the trajectory. The average value of the BL factor in both modes was found to be around 14.116 $\pm$ 0.028 Tm.

Figure 5.8 shows the Planck's constant measurements from all the prototypes, with 5 % overall data deviation for the Lego and 3D printed prototypes. The final prototype (modified equal arm Kibble balance) showed good measurement repeatability of less than 0.5 % deviation, which was due to the reduction of the offset forces produced by the rough and large-knife edge, and the instability of the balance. The Planck's constant measurements were determined using calibrated masses ($1 - 3$ grams) from the mass laboratory at NMISA traceable to the IPK mass primary standard. The red dash line represents the 2017 CODATA adjusted value of h.

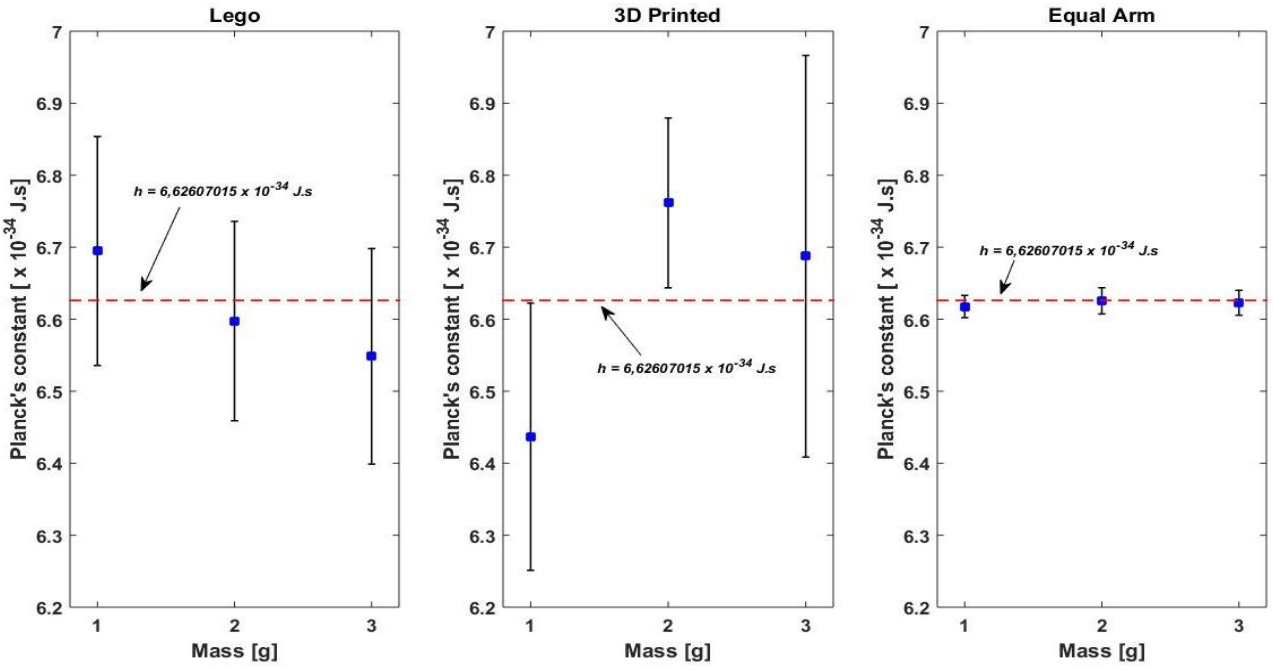

Figure 5.8: Planck's constant h measurement values determined with all the three prototypes constructed in this study. The measurements were compared with the 2017 CODATA adjusted h value, indicated by $x = 0$ red dash line.

6. Uncertainty analysis

6.1 Measurement uncertainty

Measurement uncertainty (MU) is defined in the international vocabulary of metrology-basic and general concepts and associated terms (VIM 2.26) as a non-negative parameter characterising the dispersion of the quantity values being reasonably attributed to a measurand (the quantity being measured), based on the information used [1]. This parameter is used to define the interval limit around the measured value in which the true value of the measurand lies. All measurements are imperfect and have a certain degree of uncertainty, hence considered complete only when there is a quantitative statement of uncertainty accompanying the measurement result.

Uncertainties exist in measurements because there are effects causing them, these effects are known as sources of uncertainty or uncertainty contributors. These exist as a result of random effects and systematic effects in measurements [84]. The sources of uncertainty are responsible for the deviations in the measurement results and the magnitude of these deviations can only be estimated. The sources of uncertainty can be minimised if not eliminated by optimising the measurement instruments and procedures. The magnitude of the uncertainty may be estimated by statistical methods characterised by an experimental standard deviation. Other sources of uncertainty may be as a result of experience or other information which can be evaluated using the assumed probability distributions (refer to subsection 6.2.3) [85].

The statement of uncertainty says a lot about the quality of the measurement results. It is often used as a tool to report the measurement capability of a laboratory based on the instruments and procedures used. The uncertainty can be expressed as an absolute measurement uncertainty where the measurement uncertainty is expressed in similar units as that of the measured value. It can also be expressed as a relative uncertainty given by the ratio of the absolute uncertainty over the measurand which becomes a unitless quantity often expressed in percentages.

6.2 The GUM method

6.2.1 Origin of GUM

The International Committee for Weights and Measures (CIMP) in 1977 realised the lack of uniformity or consistency on how measurement uncertainties are evaluated and expressed internationally, hence placed an appeal to the International Bureau of Weights and Measures (BIPM) together with the national standards laboratories to address this issue [86]. It was then in 1993 and 1995 that the International Organization for Standardization (ISO) published the first version of the "Guide to the expression of Uncertainty of Measurements (GUM)" recommending a probabilistic approach for data analysis and interpretation of measurements. The recommendations were later adopted by many national standards bodies such as NIST, BIPM, IEC, IFCC, IUPAC, IUPAP and OIML adopted these recommendations [43], [87]. These standard bodies combined to form a committee known as the Joint Committee for Guides in Metrology (JCGM).A series of documents is available on the JCGM website known as the GUM series which supports the ISO-GUM with applicability and enhancement of the scope on the uncertainty in measurements [88]. The main purpose of these GUM publications is to ensure that the method used to evaluate and express uncertainties in measurements is recognised and adhered to globally. According to ISO (see page viii of GUM [43]), the ideal method was chosen on the basis that it should be:

- **Universal**: the method should be applicable to all kinds of measurements and to all types of input data used in measurements.

The actual quantity used to express uncertainty should be:

- **Internally consistent**: it should be directly derivable from the components that contribute to it, as well as independent of how these components are grouped and of the decomposition of the components into subcomponents.
- **Transferable**: it should be possible to use directly the uncertainty evaluated for one result as a component in evaluating the uncertainty of another measurement in which the first result is used.

6.2.2 **Description of the GUM method**

The GUM method uses metrological terminologies with definitions provided in VIM (International Vocabulary of Basic and General Terms in Metrology) [1] and statistical terms from the ISO publications on evaluation and expression of uncertainties [43]. According to the GUM, a measurand is described as a function of all the input parameters defining it. For example, if we have measurement result of a measurand y, there are some input parameters defining it denoted by $x_1, x_2, \ldots, x_n$ which act through a functional relation f given by:

$$y = f(x_1, x_2, \ldots, x_n) \text{ ; and} \tag{6.1}$$

$$u(y) = f\big(u\,(x_1), u\,(x_2), \ldots, u\,(x_n)\big). \tag{6.2}$$

Equation (6.2) states that the uncertainty of y is a combination of the standard uncertainties of all parameters defining the measurement result. The standard uncertainty of the input parameters may result from one or more other influences.

6.2.3 **Probability density/ distribution functions**

The GUM method is based on the probabilistic approach for data analysis. The mathematical functions are used to model the information available regarding the parameter under consideration. These mathematical functions are known as the probability density functions (pdfs). They are used to describe the probability of a measurand value lying between two values [87]. The procedures on how to evaluate various sources of uncertainties are based on these pdfs to determine the standard uncertainties. There are many types of pdfs that are useful for this purpose, but the common ones used in metrology are summarised in Table 6.1.

Table 6.1: Summary of probability density/distribution functions.

Type of probability distribution function		Standard uncertainty u is given by:
Normal/Gaussian pdf	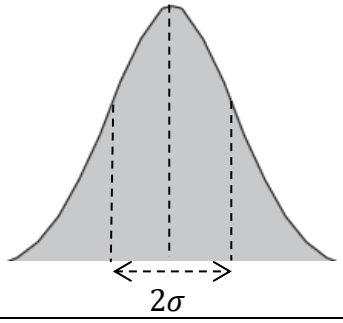	$u = \frac{\sigma}{\sqrt{n}}$ σ is the standard deviation & n is the number of readings in the set that are averaged.
Uniform /Rectangular pdf	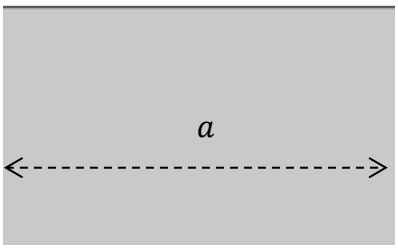	$u = \frac{a}{2\sqrt{3}}$
Triangular pdf	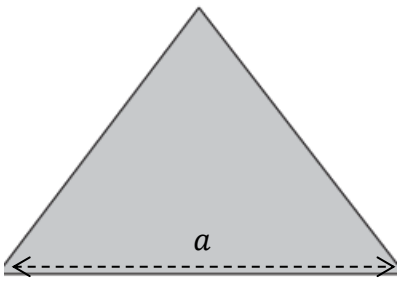	$u = \frac{a}{2\sqrt{6}}$

6.2.4 **Uncertainty classifications**

Uncertainties contributors or sources of uncertainty are evaluated differently based on their origination. The nature of uncertainty contributors is governed by the use made of the corresponding quantities which is basically how the quantities appear in the mathematical model of the measurement process. Regardless of the origin of the source of uncertainty, The GUM gives only two recommended standard ways of evaluating the sources of uncertainty known as Type A and Type B evaluations [89].

a) Type A uncertainty

Type A uncertainties are all sources of uncertainties that are analysed using statistical methods, which is usually from a series of repeated readings. These uncertainties are usually described by a Normal or Gaussian distribution function on a set of repeated readings n, where the standard uncertainty $u(x_i)$ is calculated from the mean $\bar{x}$ as the experimental standard deviation of the mean (ESDM) $s(\bar{x})$. In general, the experimental standard deviation (ESD) considers that only a limited number of measurements were taken, and that the data set may not include all possibilities of the full population. It describes the expected spread of the individual data points making up the data which is given by:

$$s(x) = \sqrt{\frac{\sum_{i=1}^{n}(x_i - \bar{x})^2}{n-1}}. \tag{6.3}$$

The ESD only helps determining the uncertainty of a single measurement. The experimental standard deviation of the mean (ESDM) $s(\bar{x})$ helps to determine the uncertainty of the mean value by describing the range within which the mean would be expected to be should a set of measurements be performed again. The ESDM is given by:

$$s(\bar{x}) = \frac{s(x)}{\sqrt{n}}. \tag{6.4}$$

b) Type B uncertainty

Type B uncertainties are all the sources of uncertainties from other any other information or where the values are obtained using means other than statistical. These uncertainties are characterised by the standard deviation based on the assumed probability distributions [90]. The Type B uncertainties are a result of evaluation based on the scientific judgement making use of all the available relevant information of the measurand subcomponent. This is usually from the manufacturer's specifications, previous published information, data from calibration certificates, calculations, etc.

A probability distribution can be assumed for the quantity based on the experience and knowledge about the quantity. The standard uncertainty $u(x_i)$ is calculated by applying an appropriate probability distribution, where the semi-rage or half-with interval is divided by a divisor of the distribution as follows:

$$u(x_i) = \frac{\text{semi} - \text{range}}{\text{divisor}} \tag{6.5}$$

where the divisor factor ($\sqrt{3}, \sqrt{6}$, etc.) is applied corresponding to the assumed probability distribution as summarised earlier in Table 6.1.

6.2.5 **Uncertainty evaluation using the GUM method**

Figure 6.1 shows a summary of the main steps to follow when evaluating uncertainties according to the GUM method. Consider a general mathematical model of the measurement result y from Eq.(6.1) given by:

$$y = f(x_1, x_2, \ldots, x_n). \tag{6.6}$$

To determine the uncertainty of the measurement result y, the uncertainties of the input parameters $x_1, x_2, \ldots, x_n$ are estimated and converted into standard uncertainties $u(x_1, x_2, \ldots, x_n)$ by using the appropriate distribution function. In a case where the uncertainty is from the calibration certificate, a normal distribution is applied to determine the standard uncertainty by dividing the value by a coverage factor that was used to report the uncertainty on the certificate.

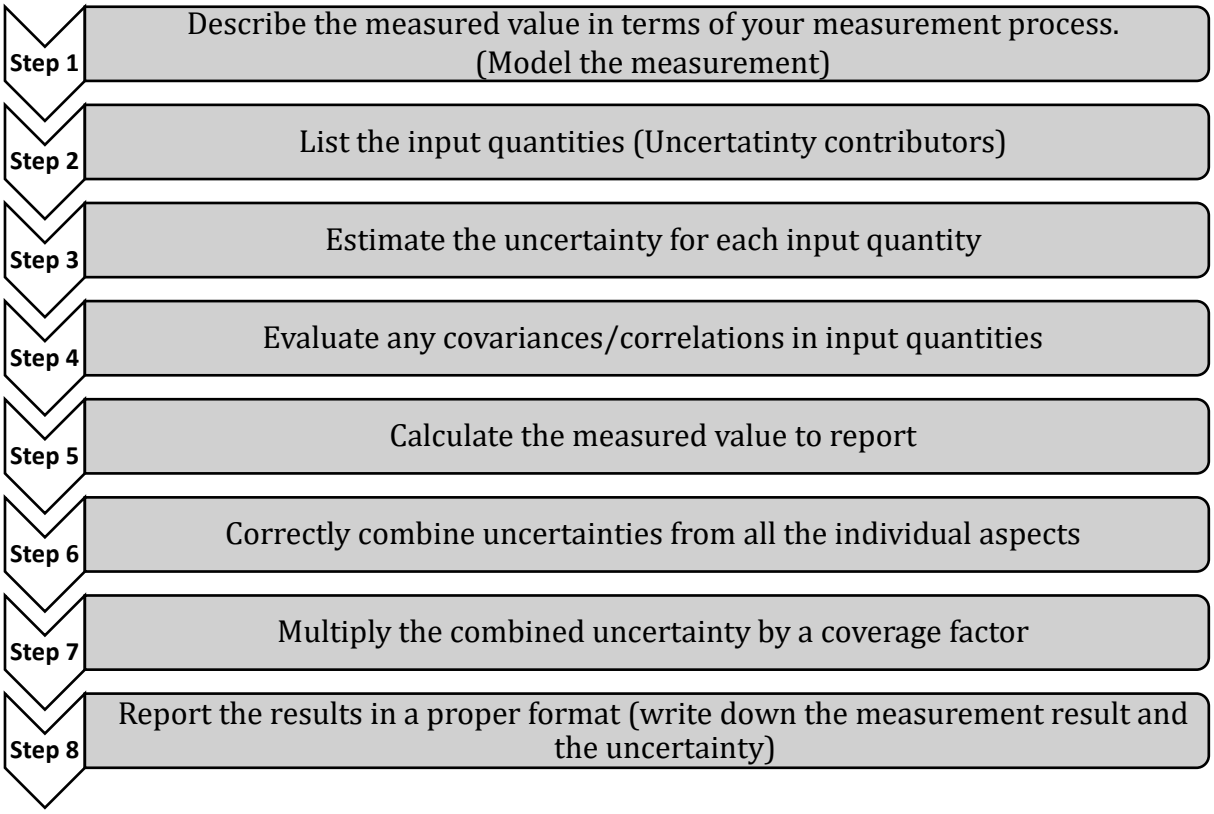

Figure 6.1: Eight main steps to follow when evaluating uncertainty according to the GUM method [43].

a) Sensitivity coefficient

The GUM recommends that the standard uncertainties $u(x_i)$ of the input parameters should be converted into the defining units of the measurand before combining them. The conversion is performed using the sensitivity coefficients c_i based on the analytical method and the numerical method. These coefficients are usually used in cases where the measurand is determined from indirect measurements. The sensitivity coefficient c_i can be calculated mathematically by determining the partial derivative of the function f with respect to the input parameters x_i given by:

$$c_i = \frac{\partial f}{\partial x_i}. \tag{6.7}$$

b) Combining uncertainties

After the uncertainties of the measurand input parameters have been individually estimated, evaluated using the probability distributions and converted to standard uncertainties of the same units as the measurand using the sensitivity coefficients, the standard uncertainties are combined to give a combined uncertainty value of the measurand $u_c(y)$. The combined uncertainty $u_c(y)$ is calculated by the root-sum-square formula (summation in quadrature) given by:

$$u_c(y) = \sqrt{{c_1}^2 u^2(x_1) + {c_2}^2 u^2(x_2) + \cdots + {c_n}^2 u^2(x_n)}. \tag{6.8}$$

Uncertainties may also be considered in terms of fractional or relative uncertainties. For example, considering a general function:

$$y = f(x_1, x_2, \ldots, x_n). \tag{6.9}$$

The standard uncertainty for y is given by:

$$\frac{u_c(y)}{y} = \sqrt{\left(\frac{u(x_1)}{x_1}\right)^2 + \left(\frac{u(x_2)}{x_2}\right)^2 + \cdots + \left(\frac{u(x_n)}{x_n}\right)^2} \text{ ; and} \tag{6.10}$$

$$u_{\,c}(y) = y\sqrt{\left(\frac{u(x_1)}{x_1}\right)^2 + \left(\frac{u(x_2)}{x_2}\right)^2 + \cdots + \left(\frac{u(x_n)}{x_n}\right)^2}. \tag{6.11}$$

c) Expanded uncertainty

The root-sum-square of all the standard uncertainty yields the combined uncertainty $u_c(y)$. According to the GUM, this is equivalent to one standard deviation which is about 68 % true uncertainty value of the measurand. The uncertainty of the measurand may be expanded to increase the level of confidence. The result is known as the expanded uncertainty U. It is calculated by multiplying the uncertainty of the measurand by the so-called coverage factor k. There are various values of k yielding different percentages of confidence level which can be found in a table known as the *student-t table,* but the most commonly used in the metrology labs is coverage factor $k = 2$ which is equivalent to a 95.45 % confidence level. The expanded uncertainty U is given by:

$$U(y) = ku_c(y). \tag{6.12}$$

d) Uncertainty budget

An uncertainty budget is a table listing all the sources of uncertainty, their contributions and how they were evaluated for a particular measurand. This table is a useful way to illustrate how a combined uncertainty $u_c(y)$ of the measurand was calculated. An example of the uncertainty budget is shown in Appendix D.

6.3 Uncertainty contributions for the Kibble balance

The required measurement results of the Kibble balance subcomponents have been presented in chapter 5. In this section, the measurement uncertainties of the Kibble balance subcomponents required for the successive operation are discussed. This is necessary to illustrate the measurement capability of the precursor Kibble balance discussed in this study and to highlight the factors limiting the measurement capability of this balance. From eq. (2.8), applying the ISO-GUM method, mass measurement results determined using the Kibble balance should be reported in the format:

$$m = X \pm u(m) \tag{6.13}$$

where X represents the best estimate value of mass m and $u(m)$ is the uncertainty of the mass measurement. The mass measurement result together with its standard uncertainty depends on the individual measurements of the subcomponents namely voltage V, current I(voltage and resistance), gravity g, velocity v (distance and time) and their uncertainties, so it follows that:

$$m = f(V, I, g, v); \text{ and} \tag{6.14}$$

$$u(m) = f\big(u\,(V), u\,(I), u\,(g), u\,(v)\big). \tag{6.15}$$

In detail:

- **Voltage**: $V = X \pm u\,(V)$, where X represents the best estimate value of V and $u(V)$ is the measurement standard uncertainty of the voltage measurement;
- **Current**: $I = X \pm u(I)$, where X represents the best estimate value of I and $u(I)$ is the measurement uncertainty involved with current measurement, and since $I = \frac{V}{R}$ we have $V = X \pm u(V)$; $R = X \pm u(R)$, where $u(d)$ *and* $u(t)$ represent the measurement uncertainties accompanying voltage and resistance measurements respectively;
- **Gravity**: $g = X \pm u(g)$, where X represents the best estimate value of g and $u(g)$ is the measurement uncertainty of gravity g measurement; and
- **Velocity**: $v = X \pm u(v)$, where X represents the best estimate value of v and $u(v)$ is the measurement uncertainty involved with velocity measurement, and since $v = \frac{d}{t}$ we have $d = X \pm u(d)$; $t = X \pm u(t)$, where $u(d)$ *and* $u(t)$ represent the measurement uncertainties accompanying displacement and time measurements respectively.

From the general equation of mass measurement with a Kibble balance, it can be realised that the measurand depends on the four parameters, but each parameter is measured individually with a suitable equipment or standard and method that may be direct or indirect. For example, the velocity measurement, it has been shown previously in section 4.5 that these measurements depend on a set of distance measurements and time measurements; and the current measurement which depends on the voltage and resistance measurements. This now further expand the formula for mass to a more detailed formula given as:

$$m = \frac{V\ V_R\ d\ Vss_i\ \Delta t}{g\ R\ x_i\ r_{eff} \Delta Vss_i}. \tag{6.16}$$

The measurement uncertainties of each parameter in the above equation are discussed in the subsections below and the factors that affect the measurements of these parameters. A 2 g test mass was considered in the discussions for the cases where the uncertainties are mass dependent, for example in the case of determining the value of Planck's constant h as presented in Chapters 4 & 5. For the sake of consistency and clarity, the subcomponents are classified into two categories of operation modes, i.e. force mode and velocity mode.

Force mode

6.3.1 Current

Current measurements required to hold the balance at the balancing position with the mass ON and OFF during the force mode operation were performed via the voltage drop method through the Ohm's law relation. According to the voltage drop method, current is a function of voltage and resistance which implies that the uncertainty of the current measurement $u(I)$ depends on the uncertainties of its subcomponents, voltage $u(V)$ and resistance $u(R)$. Table 6.2 shows the uncertainty budget for the current measurements with the sources of uncertainty coming from voltage measurements and resistance measurements. The origin of each subcomponent uncertainty is discussed in the subsections below.

Table 6.2: Uncertainty budget for the current measurements.

Source of uncertainty	Estimated uncertainty value	Probability distribution	Divisor factor	Sensitivity coefficient	Standard uncertainty contribution
Voltage drop	1.39×10^{-4} V	Normal	2	$6.63 \times 10^{-4}\ \Omega^{-1}$	4.61×10^{-5} mA
Resistance	1.26 Ω	Normal	2	$9.19 \times 10^{-7}\ V\Omega^{-2}$	5.79×10^{-4} mA
Repeatability (Estimated standard deviation of the mean)	4.71×10^{-4} mA	Normal	1	1	4.71×10^{-4} mA
Total combined uncertainty				Combined uncertainty	7.48×10^{-4} mA
				Expanded uncertainty	1.50×10^{-3} mA

a) Voltage drop measurements

The voltage difference was measured at the terminals of a resistor using one of the NI USB-6001 DAQ channel AI1. The channel was used in the 1 V range and calibrated against the 5720 A multifunctional calibrator voltage standard. The uncertainty of the channel at the 1 V from the calibration report has in it the accuracy of the 5720A standard at that specified range. The sources of uncertainty considered during the voltage drop measurement are the DAQ resolution, the DAQ channel accuracy at 1 V range (from the calibration report) and measurement repeatability described by 20 readings taken at 1 s sampling rate. The evaluation of these sources of resistance measurement uncertainty is presented in a form of an uncertainty budget shown in Table 6.3. The major contributor was found from the measurement repeatability, followed by the accuracy of the DAQ channel.

Table 6.3: Uncertainty budget for the voltage drop measurements.

Source of uncertainty	Estimated uncertainty value	Probability distribution	Divisor factor	Sensitivity coefficient	Standard uncertainty contribution
NI USB-6001 resolution	1.00×10^{-5} V	Rectangular	1.73	1	5.77×10^{-6} V
NI USB-6001 DAQ accuracy at 1 V	5.21×10^{-5} V	Normal	2	1	2.61×10^{-5} V
Repeatability (Experimental standard deviation of the mean)	6.42×10^{-5} V	Normal	1	1	6.42×10^{-5} V
Total combined uncertainty				Combined uncertainty	6.95×10^{-5} V
				Expanded uncertainty	1.39×10^{-4} V

b) Resistance

The colour coded resistor with a nominal value of 1.5 kΩ was used as a current shunt to measure the voltage drop across. The true measurement value of the resistor is required to calculate the current values through Ohm's Law. The resistance was measured using the 3458A digital multimeter found to be $1508.7 \pm 1.3\ \Omega$. This true value was found to be within the manufacture's specified tolerance range of 1 %. The measurement uncertainty of the resistance value comes from the following sources of uncertainty: the 3458A digital multimeter resolution, the 3458A digital multimeter accuracy at 1 kΩ range (from the calibration certificate), the temperature coefficient (from the manufacture's specifications) of the carbon film resistor and the measurement repeatability from a set of 10 readings. Table 6.4 shows an uncertainty budget for the resistance measurement.

Table 6.4: Uncertainty budget for the resistance measurements.

Source of uncertainty	Estimated uncertainty value	Probability distribution	Divisor factor	Sensitivity coefficient	Standard uncertainty contribution
3458 Digital multimeter resolution	$1.00 \times 10^{-8}\ \Omega$	Rectangular	1.73	1	$5.77 \times 10^{-9}\ \Omega$
3458 Digital multimeter accuracy at 1 kΩ range	$6.50 \times 10^{-6}\ \Omega$	Normal	2	1	$3.25 \times 10^{-6}\ \Omega$
Resistor temperature coefficient	$5.00 \times 10^{-4}\ \Omega$	Rectangular	1.73	1	$2.89 \times 10^{-4}\ \Omega$
Repeatability (Estimated standard deviation of the mean)	0.630 Ω	Normal	1	1	0.630 Ω
Total combined uncertainty					
			Combined uncertainty		0.630 Ω
			Expanded uncertainty		1.26 Ω

6.3.1 **Gravitational acceleration**

The gravitational acceleration measurement value 9.7860985 $\mathrm{m\,s^{-2}}$ was taken from the mapping report carried out in the year 2000 with an uncertainty value of $5 \times 10^{-7}\ \mathrm{m\,s^{-2}}$ reported at 95% confidence level. The mapping carried out again in the year 2012 at the Building opposite to the building with the Kibble balance reported a slightly changed value of 9.7860970 $\mathrm{m\,s^{-2}}$ ($1.5 \times 10^{-6}\ \mathrm{m\,s^{-2}}$ difference) with the same uncertainty. The reported uncertainty was determined by considering the following contributors: gravimeter drift, earth tidal effects, polar motion, ocean loading and atmospheric pressure.

Velocity mode

6.3.2 **Induced voltage**

The induced voltage is one of the parameters required to determine the electromagnetic property (BL factor) of the measurement coil carried out during the velocity mode. The induced voltage was measured at the terminals of the measurement coil with the NI USB-6001 channel, but with a different channel compared to the voltage drop measurement. The considered uncertainty contributors are still the same but now at different voltage measurement range (100 mV), because the induced voltage was found to be under 100 mV. Table 6.5 shows the evaluation of the sources of uncertainties considered during the induced voltage measurements.

Table 6.5: Uncertainty budget for the induced voltage measurements.

Source of uncertainty	Estimated uncertainty value	Probability distribution	Divisor factor	Sensitivity coefficient	Standard uncertainty contribution
NI USB-6001 resolution	1.00×10^{-5} V	Rectangular	1.73	1	5.77×10^{-6} V
NI USB-6001 DAQ accuracy at 100 mV	4.82×10^{-5} V	Normal	2	1	2.41×10^{-5} V
Repeatability (Experimental standard deviation of the mean)	5.17×10^{-5} V	Normal	1	1	5.17×10^{-5} V
Total combined uncertainty				Combined uncertainty	5.73×10^{-5} V
				Expanded uncertainty	1.15×10^{-4} V

6.3.3 **Velocity**

The measurement of the coil velocity during the velocity mode was not a direct measurement process, but indirect and a bit complex. The velocity was determined as a numerical derivative of the coil position measured using the optical method, which makes the velocity measurement together with its uncertainty to depend on two individual subcomponents namely: distance or change in coil position and change in time.

Table 6.6: Uncertainty budget for the velocity measurements.

Source of uncertainty	Estimated uncertainty	Probability distribution	Divisor factor	Sensitivity coefficient	Standard uncertainty contribution
Laser spot on the wall scale, x_i	3.13×10^{-1} %	Rectangular	1.73	1	1.81×10^{-1} %
Effective radius, r_{eff}	1.24×10^{-2} %	Rectangular	1.73	1	7.17×10^{-3} %
Distance from the balance to the wall, d	6.20×10^{-2} %	Normal	2	1	3.10×10^{-2} %
Calibration shadow sensor voltage, Vss_i	9.50×10^{-2} %	Normal	2	1	4.75×10^{-2} %
Change in coil position given in shadow sensor voltage, ΔVss	9.50×10^{-2} %	Normal	2	1	4.75×10^{-2} %
Sampling rate accuracy	5.88×10^{-2} %	Rectangular	1.73	1	3.40×10^{-2} %
synchronisation	5.88×10^{-2} %	Rectangular	1.73	1	3.40×10^{-2} %
Total combined uncertainty				Combined uncertainty	2.01×10^{-1} %
				Expanded uncertainty	4.02×10^{-1} %

a) Distance/ change in coil position

The coil position was measured using the optical sensor method described in chapters 4 and 5 which was a better choice to get the smallest uncertainty possible. The measurement uncertainty of the coil position depends on the shadow sensor output readings which in turn depends on uncertainties from the shadow sensor calibration. The mathematical model for the coil position measurement is given by:

$$z_i(Vss_i) = C(Vss_i - Vss_0) \tag{6.17}$$

where, $Vss_i - Vss_0$ is the change in position with reference to the balancing position Vss_0 given in terms of shadow sensor voltage Vss and C is the calibration factor used to convert the coil position from shadow sensor voltage scale to millimetre scale given by:

$$C = \frac{x_i}{Vss_i}\left(\frac{r_{eff}}{d}\right). \tag{6.18}$$

The mathematical model for the change in coil position can be re-written as:

$$\Delta z = \frac{x_i}{Vss_i}\left(\frac{r_{eff}}{d}\right)\Delta Vss_i. \tag{6.19}$$

According to the mathematical model given in equation (6.19), the uncertainty of the change in coil position $u(\Delta z)$ is given as a combination of its subcomponent's individual standard uncertainties. The components shown in eq. (6.19) are the building blocks of measuring the change in coil position. The uncertainties for the change in coil position measurement subcomponents are summarised in Table 6.6 . The following sources of uncertainty were considered for the measurement of coil position: During calibration of the shadow sensor, the movement focusable laser light spot at the wall scale which oscillates on $\pm$ 80 mm interval range was measured with a ruler with standard uncertainty of 0.5 mm resulting in 0.31 %

relative uncertainty. The shadow sensor voltage readings in the range $\pm$ 45 mV corresponding to light spot movements at the wall scale were measured using the NI USB-6001 DAQ channel with an uncertainty of 8.55×10^{-5} V with 0.1 % relative uncertainty of which the uncertainty of the shadow sensor voltage changes depends on the DAQ resolution and the DAQ accuracy at 100 mV range. The length from the pivoting point to the coil suspension point (effective radius = 80.50 mm) was measured with a digital Vernier calliper with an uncertainty of 0.01 mm resulting in 0.01 % relative uncertainty and the distance from the balance's pivoting point to the wall scale $d = 4840$ mm was measured repeatedly (10 times) using an electronic distance meter (EDM) with an uncertainty of 3 mm calibrated against the Zygo laser working standard resulting in 0.06 % relative uncertainty.

During operation, the change in coil position was measured with the calibrated shadow sensor connected to the NI USB-6001 DAQ in terms of voltage measurement scale, ΔVss. The relative uncertainty of the readings is given as 0.1 % as discussed before for the shadow sensor calibration. Most of the subcomponents are given normal probability distribution because their uncertainties come from combined uncertainty of individual measurements results that covers both Type A and Type B types of uncertainties. For example, shadow sensor readings Vss_i, its uncertainty comes from a combination of sources such as DAQ resolution (Type B), DAQ accuracy from calibration report (Type A) and repeatability (Type A).

b) Time interval

The time interval measurements were carried out for the trajectory of the measurement coil during velocity mode. A sampling rate of 100 ms has been chosen for the acquisition of both the coil position measurements and the induced voltage measurements. The period of one trajectory with stable measurement results was found to be 1.7 s. The sampling rate was sourced from the computer time stamp with an uncertainty of 1 ms. The period for one trajectory was determined with a relative uncertainty of 5.88×10^{-2} %. The uncertainty comes from the time stamp accuracy. Another source of uncertainty that is added to the time interval measurements is the synchronisation error or delay. During the velocity mode measurements, the induced voltage and the corresponding velocity need to be synchronised.

This was accomplished by performing simultaneous data acquisition of the two signals where the same sampling rate was used. The synchronisation error or delay is then described as the fraction of time where one parameter is being measured and not the other. This error was then assigned to 1.0 ms same as the accuracy of the sampling rate because of the same time stamp.

6.3.4 **Test masses**

During the Planck's constant h determination, the true value of the test mass m used in the force mode to calculate a value of the $(BL)_{frc}$ factor. The test masses were taken to mass laboratory for calibration to establish their true values and their measurement uncertainties are presented in the form of a calibration certificate attached in Appendix C. The following sources of uncertainty were considered during the calibration process: the accuracy of the mass standard, drift of the standard, buoyancy, resolution of the standard and the repeatability from 10 readings. The expanded uncertainty was reported to be 4.0×10^{-5} g for 2 g test mass which corresponds to 2.0×10^{-3} % relative uncertainty.

6.3.5 **Other uncertainties**

The following uncertainties did not contribute into the overall uncertainty, but it is necessary to discuss them as they could have an impact in the future measurements when other uncertainties have been reduced. The NMISA precursor Kibble balance uses a knife edge and flat for the pivoting of the balance beam. Although the use of knife edges in the balance is robust, the hysteresis on the knife edge can introduce uncertainties in the weighing process and affect the weighing measurement repeatability. The knife edge hysteresis affects the system equilibrium point resulting from systematic shifts of the mechanics. The hysteresis arises mostly due to factors such as the radius of the knife edge, the material properties, friction coefficient, surface roughness, etc. The test masses have magnetic susceptibility which needs to be corrected as it creates some magnetic force on the test masses, this is usually very low in mass standards. Another source of uncertainty is the buoyancy, which does not have a significant impact now, but will in future Kibble balances.

6.3.6 **Total uncertainty budget**

Table 6.7 shows the overall uncertainty budget illustrating the evaluation of the main Kibble balance subcomponents. Each subcomponent has been evaluated individually as discussed in the previous subsections. The estimated uncertainties are reported in relative expanded uncertainties from a combination of other sources of uncertainty. The Index column was added to give a clear picture of the subcomponents contribution percentages towards the total uncertainty. About 87 % of the overall uncertainty shows to be coming from the velocity mode measurements of which mostly it is coming from velocity measurements and the repeatability of the BL_v determination. If one would like to reduce the overall uncertainty, these two are the sources of uncertainty to reduce first before any other. Subsection 6.3.3 gives more detailed information about the origin of the velocity measurements uncertainty which can help to identify the of uncertainty contributor within the velocity measurements subcomponents needs attention.

The total uncertainty is reported in terms of relative uncertainty percentage, the expanded relative uncertainty could then be multiplied with the measurement value of the mass to get the expanded standard uncertainty in the units of the mass. For example, if we measure a gram nominal mass (1 g) and the value is found to be 0.9992 g, then the expanded standard uncertainty of this measurement will be $0.9992 \times 0.49\ \% = 0.0049$ g. The measurement is then reported finally as:

$Test\ mass\ m = 0.9992 \pm 0.0049$ g, *where the reported expanded uncertainty of measurement is stated as the standard uncertainty of measurement multiplied by a coverage factor of k=2, which for a normal distribution approximates a level of confidence of 95.45 %.*

Table 6.7: The overall uncertainty budget of the precursor Kibble balance.

Source of uncertainty	Estimated relative uncertainty value	Probability distribution	Divisor factor	Sensitivity coefficient	Standard uncertainty contribution	Index %
Force mode measurements						**12.8**
Current	1.08×10^{-1} %	Normal	2	1	5.40×10^{-2} %	**12.8**
Gravitational acceleration	5.11×10^{-6} %	Normal	2	1	2.56×10^{-6} %	**0**
mass m (considered for Planck's constant measurements)	2.00×10^{-3} %	Normal	2	1	1.00×10^{-3} %	**0.2 (for h value)**
Velocity mode measurements						**87.2**
Induced voltage	9.58×10^{-2} %	Normal	2	1	4.79×10^{-2} %	**11.3**
Velocity	4.02×10^{-1} %	Normal	2	1	2.01×10^{-1} %	**47.5**
BL_v value repeatability	1.20×10^{-1} %	Normal	1	1	1.20×10^{-1} %	**28.4**
Other uncertainties						**0**
Knife edge hysteresis	$< 1.0 \times 10^{-7}$ %	Rectangular	1.73	1	$< 5.78 \times 10^{-8}$ %	**0**
Buoyancy	$< 1.0 \times 10^{-7}$ %	Rectangular	1.73	1	$< 5.78 \times 10^{-8}$ %	**0**
Magnetic susceptibility	$< 1.0 \times 10^{-7}$ %	Rectangular	1.73	1	$< 5.78 \times 10^{-8}$ %	**0**
Total combined uncertainty			Combined uncertainty		0.25 %	
			Expanded uncertainty		0.49 %	

6.4 Traceability of measurements

This section describes the traceability of the sub-components (velocity, voltage, current and gravity) measurement results leading to the successive determination of the mass and the Planck's constant using the Kibble balance. Various individual equipment were used to perform sub-components measurements, below the traceability of these measurements is discussed. Figure 6.2 illustrates the traceability tree for the measurements results of NMISA's precursor Kibble balance, consisting of several individual traceability chains. The figure also shows the increase in uncertainties as we move from primary standards to the test equipment used in this work.

6.4.1 **Velocity measurements traceability**

The velocity of the measurement coil is defined as the change in coil position over a period of time. This definition clearly entails that the velocity measurements depends on the measurement of displacement and time. The measurement of coil displacement was performed using an optical method linked to a meter ruler scale, Vernier calliper and an electronic distance meter. These equipment were calibrated against the working standard (the Zygo laser) which is calibrated against the primary standard for length measurement known as the He-Ne iodine stabilised laser (Winters Model 200). The time it takes for the coil to move from one position to the other was measured as a sampling rate using the computer time stamp. The computer time is linked to the South African primary standard for time and frequency UTC(ZA), and the Universal coordinated time (UTC) via the network time protocol (NTP) server. The server is traceable to the master clock that can be linked to the UTC(ZA).

6.4.2 **Voltage measurements traceability**

Voltage measurements that were required for this work are the shadow sensor voltage measurements, induced voltage measurements during the velocity mode and the voltage drop measurement for the current measurements in the force mode. The measurements were carried out using different channels of the NI USB-6001 DAQ. The DAQ was calibrated against the 5730A multifunctional calibrator voltage working standard for all the DAQ channels at points $\pm$100 mV, $\pm$1 V and $\pm$10 V. The 5730A standard is traceable to the 732A or B voltage reference standard that is directly traceable to the South African primary voltage standard known as the Josephson voltage standard (JVS).

6.4.3 **Current measurements traceability**

The current measurements in this work as described previously were not measured directly, but indirectly as a function of voltage drop measurements and resistance measurements through the Ohm's Law relation. The voltage drop method is commonly used in the electrical measurement laboratories for the calibration of current measurement standards. Measuring current through this method basically depends on two main parameters, that is voltage and resistance. The voltage drop was measured using one of the NI USB-6001 DAQ channels, with the measurement traceable to the primary voltage standard as explained in the previous subsection. The resistance measurements were carried out on a colour coded resistor using the HP 3458A KEYSIGHT digital multimeter. The multimeter was calibrated against the working standard resistors. These working standard resistors were calibrated against the two 1 Ω primary resistance standard using the 6010 C automatic high resistance ratio bridge. The two 1 Ω resistance standards are traceable to the Quantum Hall Resistance Standard (QHRS) at the BIPM in France.

6.4.4 **Gravity measurements traceability**

The gravitational acceleration measurement value g was taken from a mapping report carried out by the Council of Geosciences earlier before the precursor Kibble balance construction. The work was carried out using relative gravimeters capable of relating the known gravitational acceleration at an established gravity station (Sil 1 at CGS) to a new site through a tie procedure. In this case, the new site was the Kibble balance lab at NMISA. According to this procedure, after applying the tidal effect, instrumental drift and other corrections the measurement result is then traceable to the g value at the Sil 1 Base station that is in turn tied to the international gravity base station at the Botanical gardens in Pretoria.

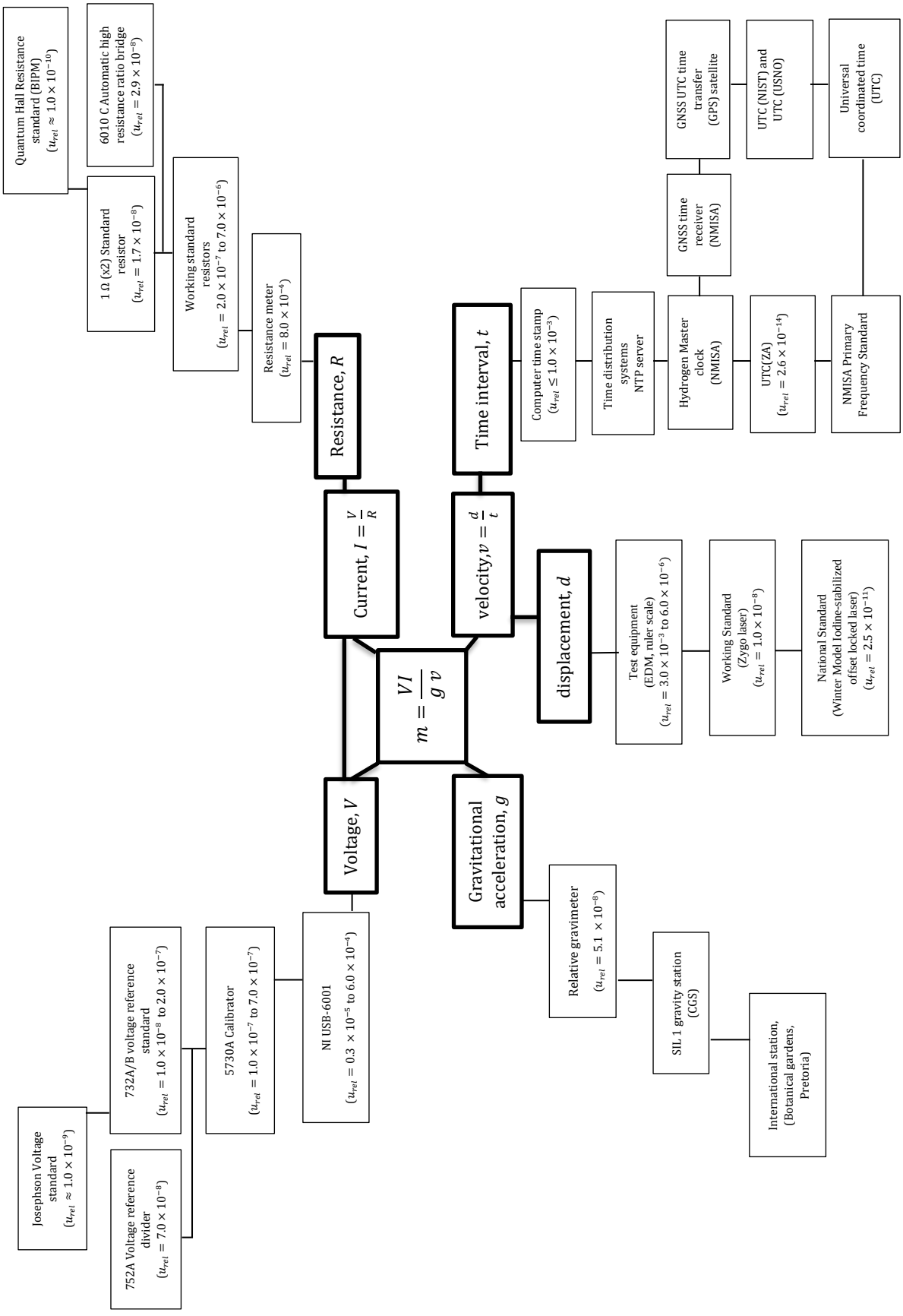

Figure 6.2: Traceability chain tree for the NMISA precursor Kibble balance measurements.

7. Conclusion and future work

7.1 Conclusion

The 26th General Conference on Weights and Measures (CGPM) held on the 16th November 2018 has adopted the revision of the International system of units (SI) to be based on fundamental physical constants. The changes will be in force starting from the international World Metrology day (20th May 2019). The revision of the kilogram definition took the spotlight as it was the last base unit to be based on a man-made physical object. The highlight of the revision and implication of the new international system has been presented in this study. The principle theory of the Kibble balance was proven to a satisfactory level of uncertainty for a precursor system.

Prototypes capable of measuring gram level masses have been developed mainly from Lego blocks, 3D printing and modifying an old equal arm balance. All the prototypes managed to perform the mass m and Planck constant h measurements but with the mechanical stability being a huge factor when it comes to the balance's accuracy. This showed that the Kibble balance measurements do not only depend on the four variables (voltage, current, gravitational acceleration and velocity), but also on the mechanical stability of the balance. This is supported by the drastic change in the repeatability of measurements (comparing the modified equal arm with the Lego and 3D printed prototypes Planck's constant h results).

Mass measurement results from all the prototypes were compared with the results from the calibration certificate of the test masses issued by the mass laboratory at NMISA. The Lego and 3D printed balance prototypes results agreed with calibration certificate results within $\leq$ 3 % difference on average, and the final prototype (modified equal-arm balance) agreed within $\leq$ 0.3 % difference. The ISO-GUM method has been successfully applied to evaluate the sub-components of the Kibble balance. It was found that the velocity subcomponent contributed most of the overall uncertainty, wherein the coil displacement measurements were the largest contributor.

The study has illustrated how the Kibble balance links various fields together. The traceability of the precursor Kibble balance measurements has been successfully established showing how the mass measurements performed with the Kibble balance are linked to respective primary standards. This was accomplished by assessing each parameter of the Kibble balance equation which are traceable to different primary standards. The main aim of developing a precursor Kibble balance was to implement the theory, evaluate the subcomponents and prepare for constructing the high accuracy primary mass standard for South Africa. After having gone through the process of constructing, operating and achieving the presented results with all the prototypes, this has shown that these prototypes can be great educational instruments to teach most aspects of science to schools and community in a more practical way. This will also make the general public more aware of the field of metrology and the importance of measurements reference standards.

7.2 Future improvements on the precursor Kibble balance

The NMISA precursor Kibble balance has shown the capabilities to measure the values of the test masses in the range 0.2-4 g with good repeatability for a prototype. The limiting factor on the test masses that the system can weigh is the electromagnetic force produced by the coil and magnetic system. The electromagnetic force depends on the strength of the magnets and current going through the coil. For the different Kibble balances described in this study, N42 grade Neodymium ring magnets were used. Although the operation of the precursor Kibble balance was a success with these magnets, they did not give enough field strength to measure heavier test masses. These magnets will in future be replaced with the N48 grade or N52 grade magnets of which can be able to generate an electromagnetic force that can balance mass pieces between 10 and 20 g. Structured light interferometer techniques will be introduced to the system replacing the shadow sensor optical method for velocity measurements thereby improving the measurement capability of the system because the velocity measurements have shown to contribute a substantial portion of the final uncertainty. The 3D printed Kibble balance will be modified to improve the structure mechanical stability. The current systems use laptops and desktops to evaluate measurement, but this is not an ideal way for mobility purposes. The RASPBERRY PI KIT will be introduced to replace the laptop in order to simplify the process of moving the system around schools.

7.3 Plans for the primary standard

This work was undertaken as a preparation for the primary standard Kibble balance that is currently under development in collaboration with NPL (UK). Upon completion, this system will be the primary reference standard for mass measurements in South Africa replacing copy no.56 of the IPK kept in the mass laboratory at NMISA. This study has illustrated how the sub-components measurements of the Kibble balance affects the mass and Planck's constant measurements. The main goal of the primary standard Kibble balance at NMISA is to reach the relative uncertainty of few parts in 10^8. This requires the uncertainty of the sub-components measurement results to be of the order 10^{-8} or less.

7.3.1 Proposed design

A table-top size design of the Kibble balance has been chosen at NMISA as the future primary standard for mass measurement in South Africa. The mechanical structure is under construction at National Physical Laboratory (NPL) in the United Kingdom as a collaboration between the two institutes. Figure 7.1 shows the design of this structure proposed by NPL to NMISA. Most of the existing Kibble balances like NMISA's precursor Kibble balance are of a classic design with pivot knife edges. Currently, the NMIs are busy trying to improve from the design to eliminate the coil horizontal movements during the velocity mode and reduce the mechanical complexity. The BIPM Kibble balance has already shown a distinct feature were the flexure pivots (with suspended springs) are used instead of the classic knife edges. Three equal arm beams are employed to support the mass pans. This design allows the coil to move in the z-direction by having the suspension of the coil-mass pan and the magnet circuit axially aligned.

The NMISA primary standard Kibble balance will use the same principle of axially aligned sub-systems, but the three equal arm beams are replaced with two flexure plates. Basically, this is a simpler design which eliminates the mechanical imbalances of the two balance beam sides of the classic design by having sub-systems vertically aligned. The size of the experiment is mostly determined by the magnetic circuit. Permanent magnets capable of delivering

magnetic field strength of around 1 tesla will be used. The use of permanent magnets to generate the magnetic field has been proven to be an efficient way from the existing systems [91].

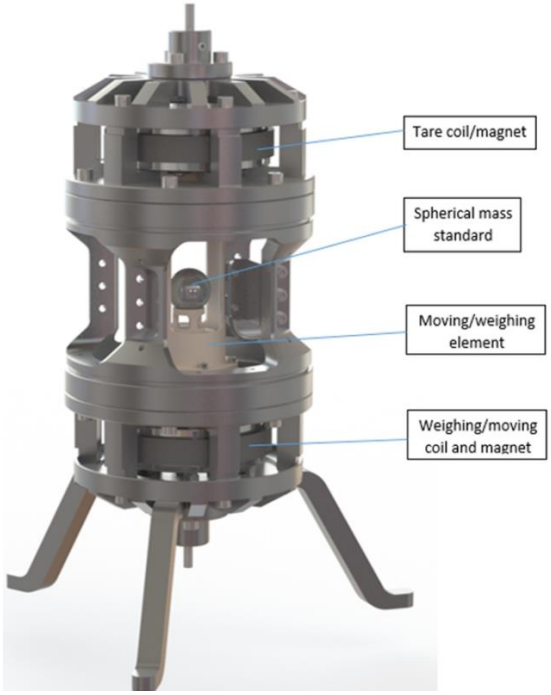

Figure 7.1: CAD model of the primary standard Kibble balance mechanical structure proposed by NPL.

7.3.2 **Current measurement**

a) Voltage measurements

The NMISA precursor Kibble balance uses the low-cost NI USB-6001 DAQ to measure voltages to a relative uncertainty order 10^{-4} . To lower this uncertainty to the order of 10^{-9}, the high-resolution voltmeters will be used together programmable Josephson Voltage Standard (JVS). The measurements will be acquired with high-resolution and high accuracy data acquisition cards. The equipment will be used to measure the voltage drop in the force mode for current measurements and also the induced voltage at the terminals of the coil in the velocity mode.

b) Resistance measurements

Accurate resistance measurements are necessary for determining the current measurements at a very low level of uncertainty. They have shown to contribute significantly to the measurements of current presented in this work. A temperature stabilised standard resistor is under development as shown in Figure 7.2. The resistor will be connected to the coil in series and a voltage drop will be measured across this resistor to determine the current going into the coil accurately through the Ohm's law. The standard resistor will be enclosed in an insulated chamber with the temperature controlled, this is to eliminate the fluctuations that might arise due to the resistor temperature coefficient. NMISA is currently procuring the Quantum Hall Resistance Standard (QHRS) that will be mainly based at the DCLF laboratory as the resistance measurement primary standard and the traceability of the resistance measurements in South Africa will no longer be linked to the BIPM. The standard resistor that will be used in the Kibble balance will then be periodically calibrated against the QHRS without any difficulties.

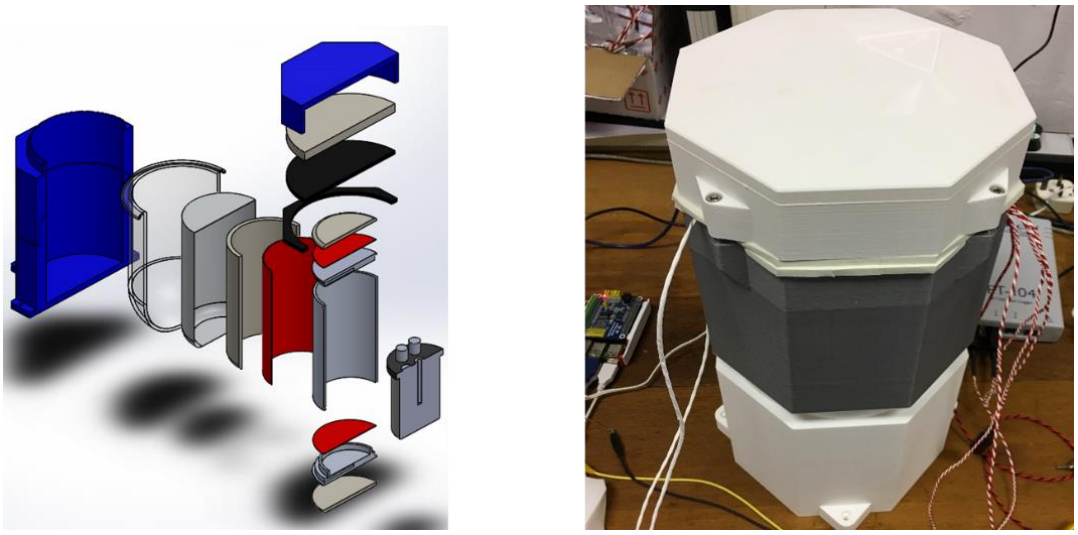

Figure 7.2: Temperature stabilised resistor under construction.

7.3.3 **Velocity and induced voltage measurements**

a) Velocity measurements

The velocity measurements have shown to be a major source of uncertainty from the precursor Kibble balance measurement uncertainty results presented in this study. As a result, a laser interferometry system is under development with the aim of decreasing the uncertainty to a satisfactory level. The interferometer uses the He-Ne iodine stabilised laser which is known as the primary standard for length measurements to measure the coil position and frequency oscillators known as the primary standard for time and frequency measurements to measure the time interval. This high accuracy of the coil displacement and time interval measurements will allow the interferometry system to perform velocity measurement accurately to a relative uncertainty of order of 10^{-9}.

b) Induced voltage measurements

The induced voltage is measured at the terminal of the coil depending on the velocity of the coil. The induced voltage will also be measured against the high accuracy programmable Josephson voltage standard. The induced voltage during the velocity mode needs to be measured simultaneously accurately and synchronised with the corresponding coil velocity measurements to determine the BL product of the coil. The target is to obtain the BL with a resolution of the order 10^{-9}. The vibration induced noise will influence the targeted resolution. If the integrals needed to measure the induced voltage and velocity are taken over the same time, the noise in the calculated BL product can be greatly reduced. By recording the time between triggers, it is then possible to calculate the average value of the input voltage. This will improve the accuracy of determining the BL product from the measured induced voltage and the corresponding velocity.

7.3.4 **Gravitational acceleration measurements**

The gravitational acceleration measurements g are vital for the successful operation of the Kibble balance. Although the gravitational acceleration value from a mapping report used in this work reported a satisfactory level of uncertainty and did not contribute significantly into the precursor Kibble balance measurement uncertainty, at the required level of order 10^{-8} the value is not the same within the room. The value changes at this level due to the following effects: The earth tides, polar motion, ocean loading, atmospheric pressure, season change and others. The g value needs to be measured at the exact location (height) where the weighing pan will be located. This requires the availability of a gravimeter on daily basis to monitor the value throughout.

NMISA will follow the measurement procedure already carried and proven to be feasible by other institutes at the required level of uncertainty. This procedure details that the gravitational acceleration should be mapped in the room where the Kibble balance will be located and again at the weighing location. An absolute gravimeter will be used to determine the gravitational acceleration value at the proposed weighing location. A relative gravimeter will be used to take measurements horizontally and vertically in the room to determine the change in gravity between separate locations within the room. The absolute value found at the proposed weighing location will be tied to another location within the room where the value can be easily monitored. NMISA has chosen to use the FG5-X micro-g LaCoste absolute gravimeter to monitor the local gravitational acceleration g value. This instrument is capable of monitoring the g value to a relative uncertainty of order 10^{-9}.

References

[1] Joint Committee For Guides In Metrology, "Vocabulaire international de métrologie," *VIM3 Int. Vocab. Metrol.*, vol. 3, no. third, p. 104, 2012.

[2] T. J. Quinn, "The Metre Convention," 2000.

[3] E. Göbel, I. M. Mills, and A. J. Wallard, "The International System of Units," *Report*, vol. 1, no. 2, 2006.

[4] H. P. Chester and P. Vigoureux, "The International Bureau of Weights and Measures 1875-1975," 1975.

[5] BIPM, "Member states." [Online]. Available: https://www.bipm.org/en/about-us/member-states/. [Accessed: 20-Aug-2018].

[6] BIPM, "BIPM, OIML, ILAC and ISO: Joint Declaration on Metrological Traceability," 2011.

[7] "The NMISA History." [Online]. Available: http://www.nmisa.org/the-nmisa/Pages/History.aspx. [Accessed: 17-Jun-2017].

[8] The Presidency, "Government Gazette: Measurement Units and Measurement Standards Act, 2006," 2007.

[9] SANAS, "South African National Accreditation System." [Online]. Available: http://www.sanas.co.za. [Accessed: 11-Dec-2017].

[10] SABS, "South African Bureau of Standards." [Online]. Available: https://www.sabs.co.za/. [Accessed: 11-Dec-2018].

[11] NRCS, "National Regulator for Compulsory Specifications." [Online]. Available: http://www.nrcs.org.za/. [Accessed: 11-Dec-2017].

[12] Dti, "Standardisation, Quality Assurance, Accreditation and Metrology Institutions." [Online]. Available: http://www.thedti.gov.za/agencies/ssa_agencies.jsp. [Accessed: 11-Dec-2017].

[13] D. B. Newell, "A more fundamental International System of Units," *Phys. Today*, vol. 67, no. 7, pp. 35–41, Jul. 2014.

[14] B. N. Taylor and A. Thompson, *The International System of Units*. 2008.

[15] BIPM, "Resolutions adopted by the 26th CGPM," 2018.

[16] Consultative Committees of the CIPM, "Information for users about the proposed revision of the SI," 2017.

[17] D. B. Newell *et al.*, "The CODATA 2017 values of h , e , k , and N A for the revision of the SI,"

Metrologia, vol. 55, no. 1, pp. L13–L16, 2018.

[18] BIPM, "The International System of Units (SI)," 2006.

[19] BIPM, "BIPM - Resolution of the 1st CGPM." [Online]. Available: https://www.bipm.org/en/CGPM/db/1/1/. [Accessed: 08-Apr-2017].

[20] C. F. Bruce and R. M. Hill, "WAVELENGTH OF KRYPTON 86, MERCURY 198 AND CADMIUM 114," *Aust. J. Phys.*, vol. 14, p. 64, 1960.

[21] P. Giacomo, "News from the BIPM," *Metrologia*, vol. 20, p. 25, 1984.

[22] NMISA, "NMISA: Physical Metrology (Length section)." [Online]. Available: http://www.nmisa.org/technical/physical-metrology/Pages/Length.aspx. [Accessed: 09-Mar-2018].

[23] T. J. Quinn, "Practical realization of the definition of the metre, including recommended radiations of other optical frequency standards (2001)," 2003.

[24] R. Davis, "The SI unit of mass," *Metrologia*, vol. 40, no. 6, pp. 299–305, 2003.

[25] BIPM, "BIPM - Resolution 9 of the 11th CGPM." [Online]. Available: https://www.bipm.org/en/CGPM/db/11/9/. [Accessed: 08-Mar-2018].

[26] B. Fellmuth *et al.*, "The kelvin redefinition and its mise en pratique," *Philos. Trans. R. Soc. A Math. Phys. Eng. Sci.*, vol. 374, no. 2064, 2016.

[27] O. W. van Assendelft, G. A. Mook, and W. G. Zijlstra, "International System of Units (SI) in physiology," *Pfl??gers Arch. Eur. J. Physiol.*, vol. 339, no. 4, pp. 265–272, 1973.

[28] D. Ghosh, "Illuminating the past: artificial lighting in America (1610-1930) and a guide to lighting historic house museums," The University of Georgia, 2004.

[29] A. C. Parr, "The Candela and Photometric and Radiometric Measurements," 2000.

[30] BIPM, "Draft 9th edition of the SI Brochure," 2018.

[31] BIPM, "A concise summary of the International System of Units, SI," 2018.

[32] M. Stock, "The Kibble balance: Determination of the Planck constant and redefinition of the kilogram," *Philos. Trans. R. Soc. A Math. Phys. Eng. Sci.*, vol. 369, no. 1953, pp. 3936–3953, 2011.

[33] BIPM, "International Prototype of the Kilogram." [Online]. Available: https://www.bipm.org/en/bipm/mass/ipk/. [Accessed: 16-Aug-2017].

[34] R. S. Davis, P. Barat, and M. Stock, "A brief history of the unit of mass: Continuity of successive definitions of the kilogram," *Metrologia*, vol. 53, no. 5, pp. A12–A18, 2016.

[35] M. Stock, P. Barat, R. S. Davis, A. Picard, and M. J. T. Milton, "Calibration campaign against the

international prototype of the kilogram in anticipation of the redefinition of the kilogram part I: Comparison of the international prototype with its official copies," *Metrologia*, vol. 52, no. 2, pp. 310–316, 2015.

[36] T. J. Quinn, "News from the BIPM," *Metrologia*, vol. 33, no. 1, pp. 81–89, Feb. 1996.

[37] P. Becker and H. Bettin, "The avogadro constant: Determining the number of atoms in a single-crystal 28Si sphere," *Philos. Trans. R. Soc. A Math. Phys. Eng. Sci.*, vol. 369, no. 1953, pp. 3925–3935, 2011.

[38] B. Andreas *et al.*, "Counting the atoms in a ^{28}Si crystal for a new kilogram definition," *Metrologia*, vol. 48, no. 2, pp. S1–S13, 2011.

[39] B. P. Kibble, "A measurement of the gyromagnetic ratio of the proton by the strong field method," *At. Masses Fundam. Constants*, vol. 5, pp. 545–551, 1976.

[40] BIPM, "Consultative Committee for Mass and Related Quantities (CCM))," 2013.

[41] H. Bettin and S. Schlamminger, "Realization, maintenance and dissemination of the kilogram in the revised SI," *Metrologia*, vol. 53, no. 5, pp. A1–A5, 2016.

[42] P. J. Abbott and Z. K. Kubarych, "The New Kilogram Definition and its Implications for High-Precision Mass Tolerance Classes," *J. Res. Natl. Inst. Stand. Technol.*, vol. 118, p. 353, 2013.

[43] JCGM, "Evaluation of measurement data — Guide to the expression of uncertainty in measurement," *Int. Organ. Stand. Geneva ISBN*, vol. 50, no. September, p. 134, 2008.

[44] D. Haddad *et al.*, "Measurement of the Planck constant at the National Institute of Standards and Technology from 2015 to 2017," *Metrologia*, vol. 54, no. 5, pp. 633–641, 2017.

[45] B. M. Wood, C. A. Sanchez, R. G. Green, and J. O. Liard, "A summary of the Planck constant determinations using the NRC Kibble balance," *Metrologia*, vol. 54, no. 3, pp. 399–409, 2017.

[46] G. Bartl *et al.*, "A new ^{28}Si single crystal: counting the atoms for the new kilogram definition," *Metrologia*, vol. 54, no. 5, pp. 693–715, Oct. 2017.

[47] P. J. Mohr, D. B. Newell, and B. N. Taylor, "{CODATA} {R}ecommended values of the fundamental physical constants 2014," 2016.

[48] S. S. Li, Z. H. Zhang, W. Zhao, Z. K. Li, and S. L. Huang, "Progress on accurate measurement of the Planck constant: Kibble balance and counting atoms," *Chinese Phys. B*, vol. 24, no. 1, 2015.

[49] Y. Azuma *et al.*, "Improved measurement results for the Avogadro constant using a ^{28}Si-enriched crystal," *Metrologia*, vol. 52, no. 2, pp. 360–375, Apr. 2015.

[50] B. D. Josephson, "Possible new effects in superconductive tunnelling," *Phys. Lett.*, vol. 1, no. 7, pp. 251–253, 1962.

[51] K. V. Klitzing, G. Dorda, and M. Pepper, “New method for high-accuracy determination of the fine-structure constant based on quantized hall resistance,” *Phys. Rev. Lett.*, vol. 45, no. 6, pp. 494–497, 1980.

[52] B. N. Taylor and T. J. Witt, “New international electrical reference standards based on the josephson and quantum hall effects,” *Metrologia*, vol. 26, no. 1, pp. 47–62, Jan. 1989.

[53] L. S. Chao *et al.*, “A LEGO Kibble balance : An apparatus to determine a mass based on the new SI,” *Am. J. Phys.*, vol. 83, no. 11, pp. 913–922, 2015.

[54] H. Fang, A. Kiss, A. Picard, and M. Stock, “A Kibble balance based on a simultaneous measurement scheme,” *Metrologia*, vol. 51, no. 2, pp. 80–87, 2014.

[55] M. Thomas *et al.*, “First determination of the Planck constant using the LNE Kibble balance,” *Metrologia*, vol. 52, no. 2, pp. 433–443, 2015.

[56] A. Eichenberger, H. Baumann, B. Jeanneret, B. Jeckelmann, P. Richard, and W. Beer, “Determination of the Planck constant with the METAS Kibble balance,” *Metrologia*, vol. 48, no. 3, pp. 133–141, 2011.

[57] H. Baumann *et al.*, “Design of the new METAS Kibble balance experiment Mark II,” *Metrologia*, vol. 50, no. 3, pp. 235–242, 2013.

[58] Z. Zhang *et al.*, “Coils and the Electromagnet Used in the Joule Balance at the NIM,” *IEEE Trans. Instrum. Meas.*, vol. 64, no. 6, pp. 1539–1545, 2015.

[59] S. Schlamminger *et al.*, “Determination of the Planck constant using a Kibble balance with a superconducting magnet system at the National Institute of Standards and Technology,” *Metrologia*, vol. 51, no. 2, pp. 1–22, 2014.

[60] D. Kim *et al.*, “Design of the KRISS Kibble balance,” *Metrologia*, vol. 51, no. 2, 2014.

[61] F. Hungwe and O. A. Kruger, “Tests on the new National Standard for Length,” 2016.

[62] R. E. Elmquist *et al.*, “The Ampere and Electrical Standards.,” *J. Res. Natl. Inst. Stand. Technol.*, vol. 106, no. 1, pp. 65–103, 2001.

[63] A. Hartland, K. Jones, J. M. Williams, B. L. Gallagher, and T. Galloway, “Direct comparison of the quantized Hall resistance in gallium arsenide and silicon,” *Phys. Rev. Lett.*, vol. 66, no. 8, pp. 969–973, Feb. 1991.

[64] B. N. Taylor, “History of the Present Value of 2e/h Commonly Used for Defining National Units of Voltage and Possible Changes in National Units of Voltage and Resistance,” *IEEE Trans. Instrum. Meas.*, vol. IM-36, no. 2, pp. 659–664, Jun. 1987.

[65] J. Clarke, “Experimental comparison of the Josephson voltage-frequency relation in different

superconductors," *Phys. Rev. Lett.*, vol. 21, no. 23, pp. 1566–1569, Dec. 1968.

[66] R. M. G. Jeff C. Gust Michael A. Lombardi, "Stopwatch and timer calibrations," *NIST Spec. Publ.*, vol. 960–12, p. 80, 2004.

[67] M. A. Lombardi, L. M. Nelson, A. N. Novick, and V. S. Zhang, "Time and Frequency Measurements Using the Global Positioning System," *Int. J. Metrol.*, vol. 8, no. 3, pp. 26–33, 2001.

[68] V. Zhang *et al.*, "Recent Calibrations of UTC(NIST) - UTC(USNO)," in *Proceedings of the 44th Annual Precise Time and Time Interval Systems and Applications Meeting*, 2012, pp. 35–42.

[69] M. Mihran, "UTC Dissemination to the Real-Time User: The Role of USNO," *Proc. 27th Annu. Precise Time Time Interval Syst. Appl. Meet.*, pp. 75–86, 1995.

[70] M. a Lombardi, "Traceability in Time and Frequency Metrology," *CalLab*, vol. p33, p. N-N, 1999.

[71] EndRun TECHNOLOGIES, "Establishing Traceability to," *White Pap.*, p. 6, 2008.

[72] C. Matthee, "Using GPS for establishing frequency traceability," 2013.

[73] Chris Matthee, "Improvements to time accuracy in South Africa - EE Publishers," *EE publishers*, 2017. [Online]. Available: http://www.ee.co.za/article/improvements-time-accuracy-south-africa.html. [Accessed: 04-Nov-2018].

[74] A. Germak, A. Prato, and M. Astrua, "Traceability of gravity acceleration measurement in calibration laboratories," *IMEKO*, no. September, pp. 1–4, 2018.

[75] Micro-g LaCoste, "FG5 Absolute Gravimeter User's Manual Micro-g LaCoste FG5 User's Manual," 2006.

[76] C. Morelli *et al.*, "The International Gravity Standardization NET 1971 (I.G.S.N.71)," 1971.

[77] U. Marti, P. Richard, A. Germak, L. Vitushkin, and H. Wilmes, "CCM – IAG Strategy for Metrology in Absolute Gravimetry Role of CCM and IAG," 2014.

[78] Ultimaker, "Ultimaker Cura: Advanced 3D printing software, made accessible." [Online]. Available: https://ultimaker.com/en/products/ultimaker-cura-software. [Accessed: 19-Apr-2017].

[79] L. S. Chao *et al.*, "An alternative circuit for the NIST LEGO Kibble Balance," *Am. J. Phys.*, vol. 83, no. 11, p. 917, 2015.

[80] National Instruments, "NI USB-6001 Specifications," 2014. [Online]. Available: http://www.ni.com/pdf/manuals/374369a.pdf. [Accessed: 02-Jul-2018].

[81] H. E. Swanson and S. Schlamminger, "Removal of zero-point drift from AB data and the statistical cost," *Meas. Sci. Technol.*, vol. 21, no. 11, p. 115104, Nov. 2010.

[82] R. . Stettler and B. . Beckett, "The establishment of a absolute gravity base in the force

laboratory," *Counc. Geosci.*, vol. Report No., 1999.

[83] R. . Stettler, "Tie in of the three gravity base stations at the national metrology institute of South Africa," *Counc. Geosci.*, vol. Report No., 2012.

[84] B. N. Taylor and C. E. Kuyatt, "Guidelines for Evaluating and Expressing the Uncertainty of NIST Measurement Results," *NIST Tech. Note*, vol. 1297, p. 20, 1994.

[85] JCGM, "Evaluation of measurement data — Supplement 1 to the 'Guide to the expression of uncertainty in measurement' — Propagation of distributions using a Monte Carlo method," *Evaluation*, vol. JCGM 101:2, p. 90, 2008.

[86] I. Farrance and R. Frenkel, "Uncertainty of measurement: A review of the rules for calculating Uncertainty components through functional relationships," *Clin. Biochem. Rev.*, vol. 33, no. 2, pp. 49–75, 2012.

[87] A. Buffler, S. Allie, F. Lubben, and B. Campbell, *Introduction to Measurement in the Physics Laboratory A probabilistic approach Introduction to Measurement in the Physics Laboratory*. Cape Town, 2009.

[88] JCGM - Joint Committee for Guides in Metrology, "JCGM 100 series – Guides to the expression of uncertainty in measurement (GUM series)." [Online]. Available: https://www.iso.org/sites/JCGM/GUM-introduction.htm. [Accessed: 17-May-2018].

[89] S. Bell, "A Beginner's Guide to Uncertainty of Measurement," *Meas. Good Pract. Guid.*, no. 2, p. 41, 1999.

[90] A. Ferrero and S. Salicone, "Measurement uncertainty," *IEEE Instrum. Meas. Mag.*, vol. 9, no. 3, pp. 44–51, 2006.

[91] I. A. Robinson and S. Schlamminger, "The Kibble or Kibble balance: A technique for implementing the new SI definition of the unit of mass," *Metrologia*, vol. 53, no. 5, pp. A46–A74, 2016.

Appendices

Appendix A: CSIR complex

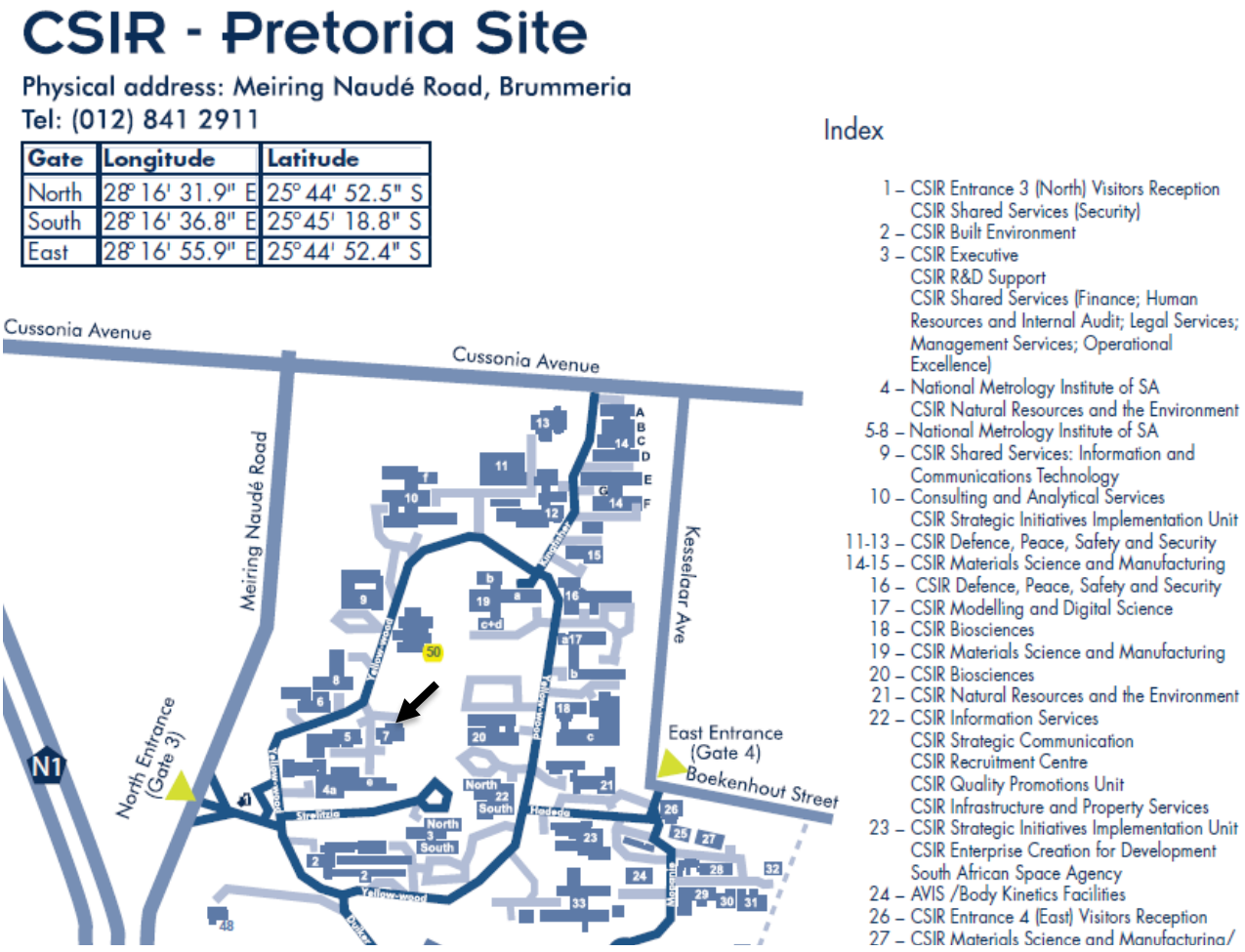

The Kibble balance lab is in building 7 indicated by the arrow on the map.

Appendix B: DAQ calibration results

Table of calibration results description:

- UUT- unit/device under test
- Mean- the average value of all the 5 measurement samples
- ESDM- the experimental standard deviation of the mean
- STD- the calibration voltage standard used, i.e. the Fluke 5720A multifunction calibrator for the input channel and the Wavetek 1281 self-calibrator digital multimeter for the output channel
- UoM- uncertainty of measurements

Input channel calibration results sample

UUT Range (V)	Applied Nominal (V)	Measured UUT Voltage (V)								STD Accuracy (V)	UUT Resolution (V)	Combined UoM (V)	Expanded UoM (V)
		1	2	3	4	5	Mean (V)	ESDM (V)					
0.1	0.1	0.09980	0.09950	0.09960	0.09940	0.09950	**0.099560**	1.52E-04		5.75E-07	2.89E-06	1.52E-04	3.03E-04
0.1	-0.1	-0.09975	-0.09975	-0.09970	-0.09940	-0.09960	**-0.099640**	1.47E-04		5.75E-07	2.89E-06	1.48E-04	2.95E-04
1	1	0.9988	0.9992	0.9992	0.9992	0.9987	**0.999020**	2.49E-04		2.85E-06	2.89E-05	2.51E-04	5.01E-04
1	-1	-0.9996	-1.0001	-1.0001	-1.0000	-0.9996	**-0.999880**	2.59E-04		2.85E-06	2.89E-05	2.60E-04	5.21E-04
10	10	9.995	9.998	9.995	9.992	9.999	**9.995800**	2.77E-03		1.88E-05	2.89E-04	2.79E-03	5.58E-03
10	-10	-9.990	-9.994	-9.998	-9.994	-9.997	**-9.994600**	3.13E-03		1.88E-05	2.89E-04	3.14E-03	6.29E-03

Output channel calibration results sample

UUT Range (V)	Applied Nominal (V)	Measured UUT Voltage (V)							STD Accuracy (V)	STD Resolution (V)	Combined UoM(V)	Expanded UoM (V)
		1	2	3	4	5	Mean (V)	ESDM(V)				
0.1	0.1	0.10032090	0.10031590	0.10032180	0.10032120	0.10032450	**0.100321**	3.12E-06	1.03E-06	2.89E-09	3.28E-06	6.56E-06
0.1	-0.1	-0.09961640	-0.09961490	-0.09962500	-0.09962850	-0.09963400	**-0.099624**	8.09E-06	1.03E-06	2.89E-09	8.15E-06	1.63E-05
1	1	1.0007170	1.0007250	1.000730	1.000725	1.000722	**1.000724**	4.76E-06	6.55E-06	2.89E-09	8.10E-06	1.62E-05
1	-1	-0.999362	-0.999349	-0.999354	-0.999359	-0.999355	**-0.999356**	4.97E-06	6.55E-06	2.89E-09	8.22E-06	1.64E-05
10	10	10.00357	10.00360	10.00359	10.00357	10.00356	**10.003578**	1.64E-05	5.50E-05	2.89E-09	5.74E-05	1.15E-04
10	-10	-10.00287	-10.00286	-10.00285	-10.00287	-10.00287	**-10.002864**	8.94E-06	5.50E-05	2.89E-09	5.57E-05	1.11E-04

Appendix C: Calibration certificate of the test masses

nmisa
National Metrology Institute of South Africa

Certificate of Calibration

Private Bag X34, Lynnwood Ridge, Pretoria, 0040
CSIR Campus, Meiring Naude Road, Brummeria, 0184
Calibration office: +27 12 841 4623
Reception: +27 12 841 4152
Fax: +27 12 841 4458
E-mail enquiries: info@nmisa.org

Calibration of:	A SET OF WEIGHTS
Manufacturer:	VOLAND
Model number:	UNKNOWN
Serial number:	MV-E-25
Calibrated for:	NMISA MASS LABORATORY – CSIR CAMPUS, MEIRING NAUDE ROAD, BRUMMERIA, PRETORIA
Location of calibration:	NMISA, BUILDING 5, BASEMENT
Calibration procedure:	MVM-0008
Period of calibration:	27 NOVEMBER 2018 TO 28 NOVEMBER 2018

1 PROCEDURE

These weights have been calibrated based on weighings made in air of density 1,003 kg/m³ against standards of known mass and density.
The results of the measurements are traceable to the National Standard of Mass, prototype No. 56 of the kilogram.
Should weighings being made require buoyancy corrections, a density of 8 000 kg/m³ should be assumed for these weights.

2 RESULTS

Nominal Mass (g)	True Mass (g)	Uncertainty of Measurement (g)
100	100,000 7	± 0,000 2
50	50,000 1	± 0,000 1
30	30,000 4	± 0,000 1
20	20,000 22	± 0,000 08
10	10,000 22	± 0,000 07
5	5,000 10	± 0,000 05
3	3,000 08	± 0,000 05
2	2,000 11	± 0,000 04

Calibrated by Signature Removed B Ndlovu **Metrologist (Technical Signatory)**	Checked by Signature Removed R Sleyn **Metrologist**	For Chief Executive Officer Signature removed
Date of Issue **04 December 2018**	**Page 1 of 2**	Certificate number **MVM-6356**

Your measure of excellence

CALIBRATION OF A SET OF WEIGHTS

Serial Number: MV-E-25

Nominal Mass (g)	True Mass (g)	Uncertainty of Measurement (g)
1	0,999 94	±0,000 03
0,5	0,500 01	±0,000 03
0,3	0,300 04	±0,000 03
0,2	0,200 01	±0,000 02
0,1	0,100 02	±0,000 02
0,05	0,050 06	±0,000 01
0,03	0,030 02	±0,000 01
0,02	0,019 95	±0,000 01
0,01	0,009 992	±0,000 008
0,005	0,004 998	±0,000 007
0,003	0,003 051	±0,000 007
0,002	0,002 041	±0,000 007
0,002.	0,001 904	±0,000 007
0,001	0,001 019	±0,000 007

3 REMARKS

3.1 The reported uncertainties of measurement were calculated and expressed in accordance with the BIPM, IEC, ISO, IUPAP, OIML document entitled "A Guide to the Expression of Uncertainty in Measurement" (International Organisation for Standardisation, Geneva, Switzerland).

3.2 The reported expanded uncertainty of measurement is stated as the standard uncertainty of measurement multiplied by a coverage factor of k=2, which for a normal distribution approximates a level of confidence of 95,45%.

3.3 Certain of the NMISA certificates are consistent with the capabilities that are included in appendix C of the MRA (Mutual Recognition Arrangement) drawn up by the CIPM. Under the MRA, all participating institutes recognise the validity of each other's calibration and measurement certificates for the quantities and ranges and measurement uncertainties specified in Appendix C. For details see http://www.bipm.org.

3.4 The calibrations were carried out at an ambient temperature of 23 °C ± 2 °C and a relative humidity of 50 %RH ± 10 %RH.

---------- *end of certificate* ----------

Calibrated by	Checked by	For Chief Executive Officer
Signature Removed B Ndovu **Metrologist (Technical Signatory)**	Signature Removed R Steyn **Metrologist**	Signature Removed
Date of Issue **04 December 2018**	**Page 2 of 2**	Certificate number **MVIM-6356**

Appendix D: Uncertainty budget spreadsheet

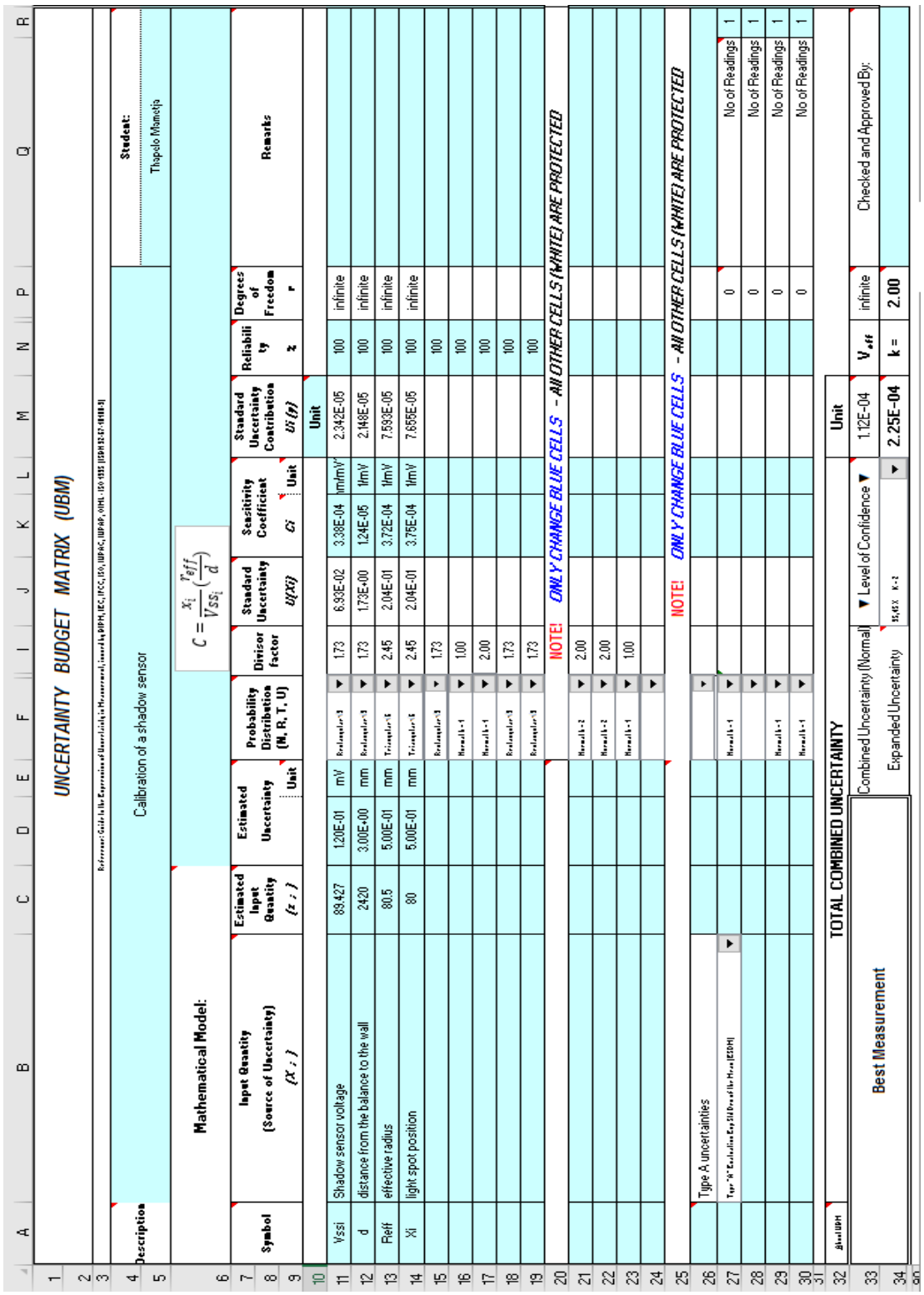

UNCERTAINTY BUDGET MATRIX (UBM)

Description: Calibration of a shadow sensor

Student: Thapelo Mamotja

Mathematical Model: $C = \frac{x_i}{Vss_i}\left(\frac{r_{eff}}{d}\right)$

Symbol	Input Quatity (Source of Uncertainty) {X_i}	Estimated Input Quatity {x_i}	Estimated Uncertainty	Unit	Probability Distribution (N, R, T, U)	Divisor Factor	Standard Uncertainty u(xi)	Sensitivity Coefficient Ci	Unit	Standard Uncertainty Contribution Ui(yi)	Unit	Reliability %	Degrees of Freedom r	Remarks
Vssi	Shadow sensor voltage	89.427	1.20E-01	mV	Rectangular	1.73	6.93E-02	3.38E-04	mm/mV	2.34E-05		100	infinite	
d	distance from the balance to the wall	2420	3.00E+00	mm	Rectangular	1.73	1.73E+00	1.24E-05	t/mV	2.14E-05		100	infinite	
Reff	effective radius	80.5	5.00E-01	mm	Triangular	2.45	2.04E-01	3.72E-04	t/mV	7.593E-05		100	infinite	
Xi	light spot position	80	5.00E-01	mm	Triangular	2.45	2.04E-01	3.75E-04	t/mV	7.655E-05		100	infinite	
					Rectangular	1.73						100		
					Normal	1.00						100		
					Normal	2.00						100		
					Rectangular	1.73						100		
					Rectangular	1.73						100		

NOTE! ONLY CHANGE BLUE CELLS - ALL OTHER CELLS (WHITE) ARE PROTECTED

					Normal	2.00								
					Normal	2.00								
					Normal	1.00								

NOTE! ONLY CHANGE BLUE CELLS - ALL OTHER CELLS (WHITE) ARE PROTECTED

	Type A uncertainties													
	Type "A" Evaluation Easy Std Deviation Mean (ESDM)				Normal							0	No of Readings	1
					Normal							0	No of Readings	1
					Normal							0	No of Readings	1
					Normal							0	No of Readings	1

Symbol	TOTAL COMBINED UNCERTAINTY		Unit					
	Best Measurement	Combined Uncertainty (Normal)	▼ Level of Confidence ▼	1.12E-04	V_{eff}	infinite	Checked and Approved By:	
		Expanded Uncertainty	95.45% k=2	2.25E-04	k =	2.00		